Reply to Reviewer Comment 1 (RC1)

Comment:
This manuscript describes a coupled via C-Coupler2 Arctic ocean sea ice configuration of MITgcm and Polar WRF atmosphere. The model is intended for high quality Arctic sea ice seasonal predictions. There is large demand for high quality regional climate models of the Arctic basin and such activity must be strongly appreciated. In the manuscript the setup has been validated for year 2012 because of a strong storm formed off the coast of Alaska on 5 August 2012. The role of sea ice-ocean-atmosphere interaction has been addressed. Although the authors demonstrate good modelling skills, good knowledge of the Arctic Ocean system and impressive level of model validation the paper in it's resent form failed to convince me that the new climate model is ready to use and that is better than any existing global climate model. My main criticism is that (1) the performance of the model on different HPC systems, regarding scalability and the costs of all individual components is not addressed, (2) the presented configuration is not properly tuned. I encourage this paper for resubmission after these weaknesses have been fixed.

Reply:
The authors thank the reviewer for the insightful comments, and we completely agree with the questions and comments raised by the reviewer, which have helped us to improve the quality of the manuscript. We have carefully considered the reviewer's comments. Some paragraphs are rewritten and figures are redrawn. Regarding to the two main criticisms, we have added a paragraph of model scalability and the costs of all individual components in the revised manuscript. We also tried different sea ice albedo parameters in the MITgcm to get a better sea ice simulation and re-written Section 4 with new results. To further adequately address the two main criticisms, our replies are as follows:

1. Following the comments on the model scalability and the costs, we run several experiments using different CPU numbers, each experiment runs for 7 model days, and we obtain the following results:

Table 1: Comparison of CPU time spent on coupled and stand-alone runs. The CPU time spent on two stand-alone simulations are presented to show the difference between coupled and stand-alone simulations. 'total_cpu_number' denotes the requested CPUs, 'total_run_time' denotes the total CPU elapsed time. 'wrf_interface', 'wrf_integration', 'mitgcm_interface' and 'mitgcm_integration' denote the CPU elapsed time used for coupling interface by the WRF, numerical integration by the WRF, coupling interface by the MITgcm, and numerical integration by the MITgcm, respectively. 'wrf_time_alone' denotes the CPU elapsed time of the stand-alone WRF runs. 'mitgcm_time_alone' denotes the CPU elapsed time of the stand-alone MITgcm runs. Each run is integrated for 7 model days.

total_cpu_number	cpu_number_on_each_component_model	total_run_time (unit: s)	wrf_interface (unit: s)	mitgcm_interface (unit: s)	wrf_integration (unit: s)	wrf_time_alone (unit: s)	mitgcm_integration (unit: s)	mitgcm_time_alone (unit: s)
28	14	12840	4.8	12131	12835.2	/	709	/
56	28	12000	4.74	11196	11995.26	7140	804	317
112	56	10440	5.16	6477	10434.84	3960	3963	154
224	112	3780	5.26	3550	3774.74	2160	230	96
448	224	2460	5.21	2116	2454.79	1560	344	68
896	448	1380	358	48	1022	1320	1332	84

In our model configuration, the requested total CPUs are assigned equally to the component models, that is, if we request 448 CPUs, then 224 CPUs are assigned to the WRF and 224 CPUs are assigned to the MITgcm. The total_run_time of the coupled model decreases from 12840 s to 1380 s when total_cpu_number increases from 28 to 896. Limited by computational resource of our center, we can not perform experiment which uses more than 1000 CPUs.

In the above table, the “wrf_interface” expresses time of coupling process implemented by the WRF, then the time of integration process implemented by the WRF, i. e. “wrf_integration” can be calculated as : “total_run_time” minus “wrf_interface”. The “mitgcm_interface” expresses time of coupling process implemented by the MITgcm, then the time of integration process implemented by the MITgcm, i. e. “mitgcm_integration” can be calculated as : “total_run_time” minus “mitgcm_interface”. The “wrf_time_alone” expresses runtime of the standalone WRF which implements 7 model days integration. The “mitgcm_time_alone” expresses runtime of the standalone MITgcm which implements 7 model days integration.

We find that, when total_cpu_number is not larger than 448, the “mitgcm_integration” is substantially smaller than the “wrf_integration”, meaning that the efficiency of the coupled model depends on the WRF component model. When total_cpu_number is larger than 448, the efficiency of the coupled model depends on the MITgcm component model. Additionally, both the integration efficiency of the component models in the coupled model are lower than those of the standalone model runs. The decrease in parallel efficiency results from the increase of communication time, load imbalance, and I/O (read and write) operation per CPU core (Christidis, 2015). By comparing the time cost of stand-alone WRF and MITgcm integration the parallel efficiency of the coupled model is higher than both ocean-alone or atmosphere-alone models with same numbers of grid points per CPU core.

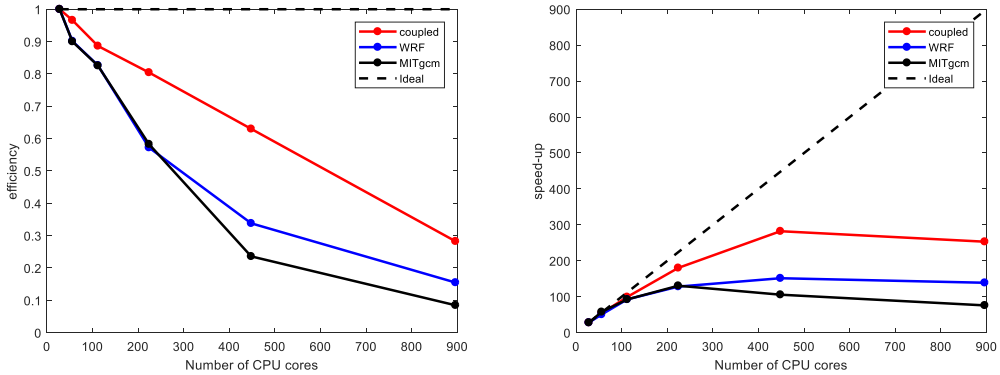

Fig.R1 The parallel efficiency (left) and speed-up (right) test of the coupled model, employing up to 896 CPU cores. The simulation using 28 CPU cores is regarded as the baseline case when computing the speed-up.

Table R1 added to Table 1 in the revised manuscript

Fig.R1 added to Figure 4 in the revised manuscript

Line 111 :"In section 3, a scalability test of the coupled model is performed to investigate its parallel capability." added

Line 206-229 :"In this section, the parallel efficiency of the ArcIOAM is investigated. Different numbers of CPU cores are used to evaluate the parallel speed-up of the coupled model. The CPU elapsed time spent on coupling interface of each component model in the coupled runs are detailed. Additionally, the parallel efficiency of each component model in the stand-alone runs are calculated for references. The parallel efficiency tests are performed on the High performance computing cluster at NMEFC. The High performance computing cluster is a Lenovo Blade Server system composed of 240 dual-socket compute nodes based on 14-core Intel Haswell processors running at 2.4 GHz. Each node has 128GB DDR4 memory running at 2133 MHz. Overall the system has a total of 6270 CPU cores (240 nodes x 2 x 14 CPU cores) and has a theoretical peak speed of 258 tetaflops. The parallel efficiency of the scalability test is Np0 tp0/ Npn tpn, where Np0 and Npn are the number of CPUs employed in the base case and the test case, respectively; tp0 and tpn represent the CPU elapsed time in the base case and the test case. The speed-up is defined as tp0 /tpn, which is the relative improvement of the CPU time. The scalability tests are performed by integrating 7 model days for the stand-alone Polar WRF, the stand-alone MITgcm and the coupled runs.

In the ArcIOAM runs, the requested CPUs are assigned equally to the component models. The minimum CPUs we use is 28, i. e. Np0 = 28. Limited by computational resource, the maximum CPUs we can use is 896. The total CPU elapsed time in the coupled runs decreases from 12840 s to 1380 s when the requested CPUs increases from 28 to 896 (Table 1). When the requested CPUs are not larger than 448, the CPU elapsed time used for numerical integration by the MITgcm is substantially smaller than that for numerical integration by the WRF, meaning that the efficiency of the coupled model depends on the WRF component model. When the requested CPUs are larger than 448, the efficiency of the coupled model depends on the MITgcm

component model.
The parallel efficiency of the coupled model remains more than 90% when employing less than 112 cores and is still as high as 80% when using 224 cores (Figure 4). The parallel efficiency of the stand-alone MITgcm is near to that of the stand-alone Polar WRF when the requested CPUs are less than 448, while both of them are substantially lower than the coupled model. The parallel speed-up of the coupled model is higher than the stand-alone component model. The decrease in parallel efficiency results from the increase of communication time, load imbalance, and I/O (read and write) operation per CPU core (Christidis, 2015). " added

2. In the MITgcm, sea ice albedo is a function of four kinds of ice/snow surface type: dry ice, wet ice, dry snow, wet snow. According the reference (Nguyen et al., 2011, Arctic ice ocean simulation with optimized model parameters: Approach and assessment, JGR-oceans), typical range of sea ice albedo in the AOMIP (Arctic Ocean Models Intercomparison Project) is: 0.6-0.75 for dry ice, 0.5-0.68 for wet ice, 0.8-0.84 for dry snow, 0.6-0.77 for wet snow. Typical sea ice albedo in the MITgcm under the JRA25 forcing is: (dry ice: 0.7, wet ice: 0.71, dry snow:0.87, wet snow: 0.81). They also found the optimized sea ice albedo parameters depend on the selected atmospheric forcing. In our previous studies (Liang et al., JGR-oceans, 2018, 2019), we use the sea ice albedo of (dry ice: 0.75, wet ice: 0.7, dry snow:0.86, wet snow: 0.8) when the JRA55 forcing is used. For this study using CFSR forcing, before manuscript submission, we tested the above albedo parameters for the coupled model and found that the model produced more sea ice than the observation. So we reduced the albedo parameters and tested the group of (dry ice: 0.65, wet ice: 0.55, dry snow:0.8, wet snow: 0.7) for the coupled model, and we found this group of albedo parameters is appropriate for the coupled model when the CFSR forcing is used.

Besides, we add the standalone MITgcm simulation in 2012 for the comparison. To keep consistency between the coupled model and standalone MITgcm model, the standalone MITgcm simulation is forced by surface variables derived from the CFSR data and uses the same albedo group of (dry ice: 0.65, wet ice: 0.55, dry snow:0.8, wet snow: 0.7). Results of the modeled sea ice show that the two-way coupled model generates more rational sea ice distribution than the standalone MITgcm run. The modeled and observed monthly sea ice concentration are shown as follows:

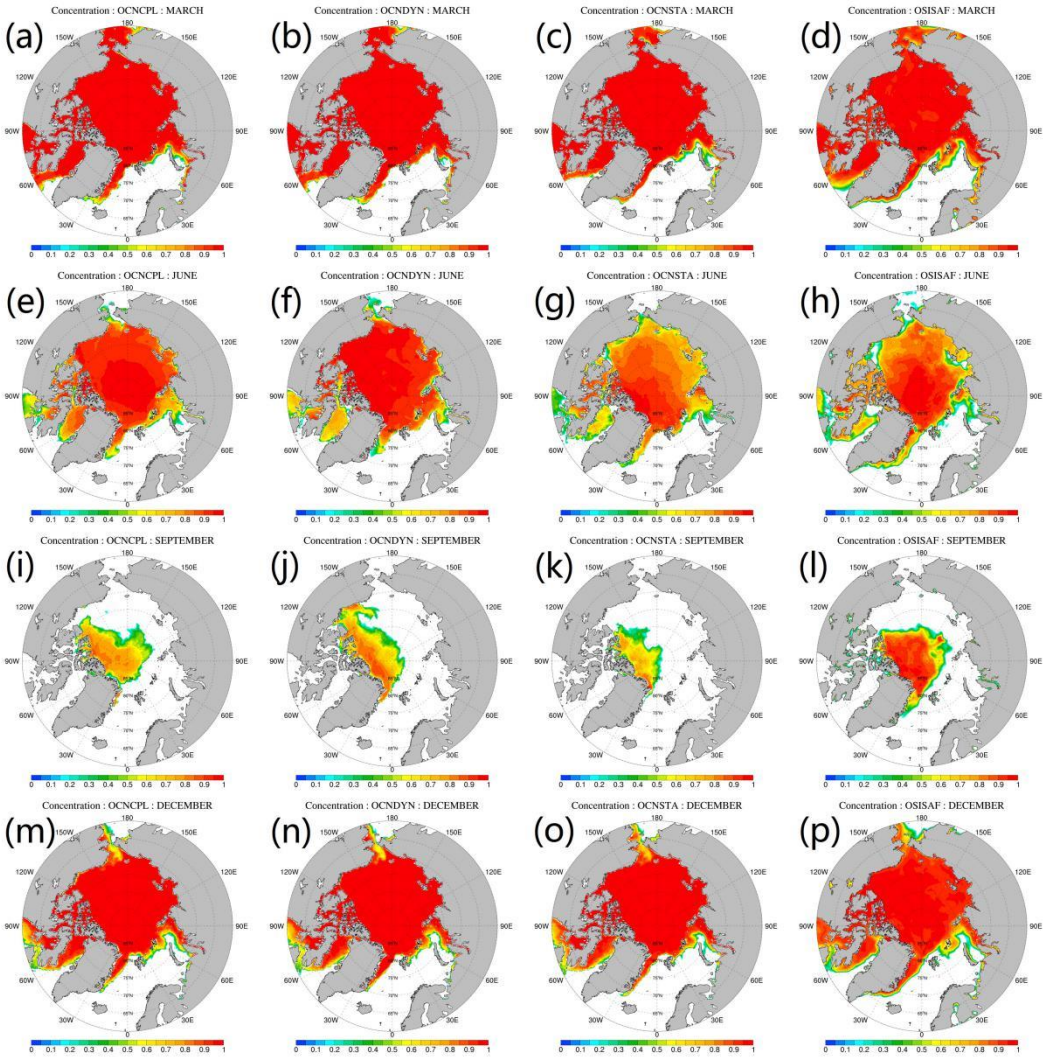

Fig.R2 Monthly mean sea ice concentration in 2012. The 1st, 2nd, 3rd, 4th row denotes March, June, September, December. The 1st, 2nd, 3rd, 4th column denotes the two-way coupled run (OCNCPL), the one-way coupled run (OCNDYN), the standalone MITgcm run (OCNSTA) and the observations (OSISAF).

We have re-drawed Figure4-10 by adding results of stand-alone experiment. And we also added three figures showing the deviation of three experiments minus observations.

Detailed replies to specific comments by the reviewer are presented below:

Comment :

In the model description, there need to be discussion on why fields and not fluxes are coupled. Do the authors guarantee the same bulk formulas are employed on the atmospheric and ocean sides? Which difference is expected if the fluxes are coupled? I guess that COSMO-CLM/NEMO group has some experience with it although not with the Arctic region. I find this aspect is more important than describing the computation of the corner geographic information for MITgcm. The latter piece I

would even omit due to its simplicity. A following chapter after the model description, which gives more information about the model scalability and cost is required.

Reply:

In the original manuscript, we have cited the paper from COSMO-CLM/NEMO group (Van Pham et al. 2014). For COSMO-CLM/NEMO model, the exchanged fields from COSMO-CLM to NEMO are the flux densities of water, momentum, solar radiation, non-solar energy and sea level pressure; and from NEMO to COSMO-CLM are SST and the fraction of sea ice. Regarding to the MITgcm model configuration we used, instead of forcing the model with heat flux data, the model calculates these fluxes using the changing sea surface temperature and ice surface temperature. We need to read in some atmospheric data: 2 m air temperature, 2 m air humidity, downward shortwave radiation, downward longwave radiation, precipitation, 10 m wind speed. This combination of setups have been used in our ocean-seaice model for several years and showed reasonable results in aspects of sea ice forecasts (Liang et al., JGR-oceans, 2018, 2019). Therefore when we build the coupled model, the same setups from the standalone ocean-seaice model are kept. We have checked the manual and source code from both the WRF and the MITgcm.

(1) The heat fluxes calculated in the MITgcm are shown below (https://mitgcm.readthedocs.io/en/latest/phys_pkgs/bulk_force.html):

Sensible heat flux (Qs):

$$Qs = \rho_{air} cp_{air} u^* T^*$$

Latent heat flux (Ql):

$$Q_l = \rho_{air} u^* q^*$$

Where

$$u^* = c_u u_s$$

$$T^* = c_T \Delta T$$

$$q^* = c_q \Delta q$$

$$c_u = c_T = c_q = \frac{\kappa}{\ln(z_{ref} / z_{rou})}$$

ρ_{air} : air density, cp_{air} : specific heat at constant pressure, u_s : wind speed, κ : Von Karman constant, z_{ref} : reference height and z_{rou} : roughness length scale which could be a function of type of surface.

(2) The heat fluxes calculated in the WRF are shown below (http://www2.mmm.ucar.edu/wrf/users/docs/user_guide_V3.8/contents.html) :

Sensible heat flux (H):

$$H = \rho c_p u_* \theta_*$$

Latent heat flux (E):

$$E = \rho u_* q_*$$

$$u_* = \frac{kV_r}{\ln(\frac{z_r}{z_0}) - \psi_m}$$

$$\theta_* = \frac{k\Delta\theta}{\ln(\frac{z_r}{z_{0h}}) - \psi_h}$$

$$q_* = \frac{k\Delta q}{\ln(\frac{z_r}{z_{0q}}) - \psi_h}$$

Where subscript r is reference level (the lowest model level, or 2 m or 10 m), Δ refers to difference between surface and reference level value, z_0 are the roughness lengths, k is the von Karman constant.

(3) The above calculations of bulk formula for sensible heat flux and latent heat flux are almost same. To further prove this, we also compare the sensible and latent flux from the WRF output and the MITgcm output within the coupled model based on the result on March 1, 2012. The results show very little discrepency, which mainly because that parameter setup is slightly different from atmosphere and ocean sides. In future work, we will use fluxes as exchange variables instead of fields, ensuring the energy balance.

Line 195-201 :"Normally in coupled models the coupler controls the exchange of heat and momentum fluxes among component models. In our model configuration, instead of coupling fluxes directly, we use the C-Coupler2 to control the exchange of fields between the Polar WRF and the MITgcm. Heat and momentum fluxes are calculated separately in each component model. Both the Polar WRF and the MITgcm use the same Bulk Formula and almost same parameters in calculating fluxes, which guarantees the quasi-conservation of heat and momentum transmission between the component models. The bilinear interpolation algorithm is involved in the transmission of model variables between the horizontal grid of the Polar WRF and that of the MITgcm." added

We agree with the reviewer that the computation of the corner geographic information for the MITgcm is more like a technical issue and with simplicity. So the part of the computation of corner information and Figure 3 are removed from the revised manuscript. We have already added a new chapter of model scalability and

cost analysis in the revised manuscript.

Line 229-243: removed
Figure 3 removed

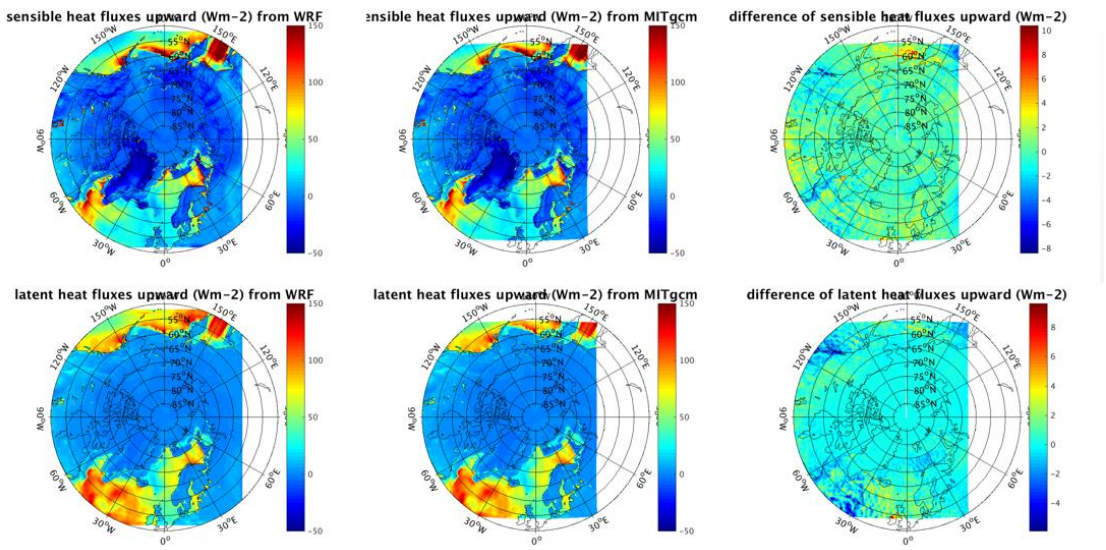

Fig.R3 Sensible and latent heat fluxes derived from WRF and MITgcm output on March 1, 2012. Differences (WRF - MITgcm) of heat fluxes are calculate by interpolation to the same grid.

Comment:
I believe that C-Coupler is a good tool to use but the statement that a model produces bitwise identical results with a different coupler means that the coupler just works. Is it better in terms of performance? Which interpolation option do you use (question is more relevant for the wind stress)? As an illustration it would be good to see the curl of the wind stress on the atmospheric and oceanic meshes (instead of Fig.3).

Reply:
The innovations of C-Coupler are flexible and automatic coupling configuration and 3-D coupling capability, which is easier for users to build coupled models. For the interpolation (remapping) from a source horizontal grid to a target horizontal grid, users can use the remapping weights that are either automatically generated by C-Coupler2 in parallel, or read from an existing remapping weight file produced by an external software tool such as SCRIP, ESMF, YAC, CoR, etc. Remapping configuration files enable to flexibly and conveniently specify how to remap coupling fields between grids. For our model, we used the default remapping configuration, the bilinear remapping algorithm is used for remapping the “state” fields between the horizontal grids.
The momentum variable transferred in our model is 10m-wind instead of wind stress. We have calculated the wind stress in WRF and made a comparison with MITgcm

output on March 1, 2012. The results show very little discrepency, which mainly because of parameter setup is slightly different from atmosphere and ocean sides.

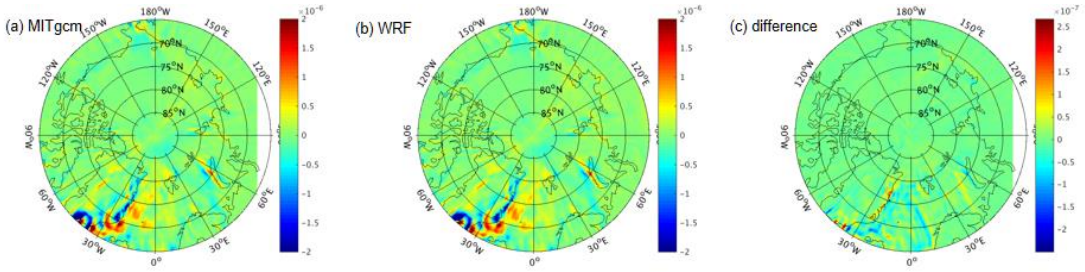

Fig.R4 Wind stress curl (unit: Nm^{-2}) derived from (a) MITgcm and (b) WRF output on March 1, 2012. Difference (WRF - MITgcm) of wind stress curl is calculate by interpolation to the same grid.

Line 200-203 :"Figure 3 shows wind stress curl derived from the Polar WRF output and the MITgcm output, as well as their difference on March 1, 2012. It can be seen that the Polar WRF and MITgcm model generate similar wind stress curl pattern, and the difference due to interpolation algorithm and momentum calculation accounts for less than 5% of the wind stress curl (Figure 3c)." added
Figure R4 added to Figure 3 in the revised manuscript

Comment:
In the OCNDYN run is it just setting alpha to 1.0? I believe that one year of coupled simulation is too short to validate the model. Either ensemble of runs or a longer simulation is desired here. I don't want to force the authors to do much of additional work but the cheapest way would be to add the stand-alone MITgcm run for the comparison here. The spin up with JRA55 has been already computed.

Reply:
For the OCNDYN run , we switch off the export interface of coupling in the code to close the variable transfer from ocean to atmosphere. The alpha in section of coupling strategy is a relax coefficient weight to combine the boundary variable, to diminish the abrupt value changes from two sources. We agree that one year is short to validate the model. So we add the standalone MITgcm runcase for the comparison. The results are shown in the revised manuscript.

Comment:
Section 4.1, which introduces Fig. 5 illustrates that the model has not been tuned properly yet. Although the authors (line 254) claim that OCNCPL is closer to observations, which might be true, but I see that both runs failed. Here it is important to give (at least visually) the measure of the error. A stand-alone MITgcm run, hence, would be a good choice. Provided the high skill of validation made in the following chapters I assume that the model has to be better tuned first.

Reply:

We have already tried different seaice parameters and tuned the model. The appropriate albedo of (dry ice: 0.65, wet ice: 0.55, dry snow: 0.8, wet snow: 0.7) in the coupled model for the CFSR forcing is used. Compared with the one-way coupled and standalone run, the OCNCPL case shows better results. We re-write the section 4 of validation with new results. The measure of the sea ice concentration error between the model and observation are shown as follows:

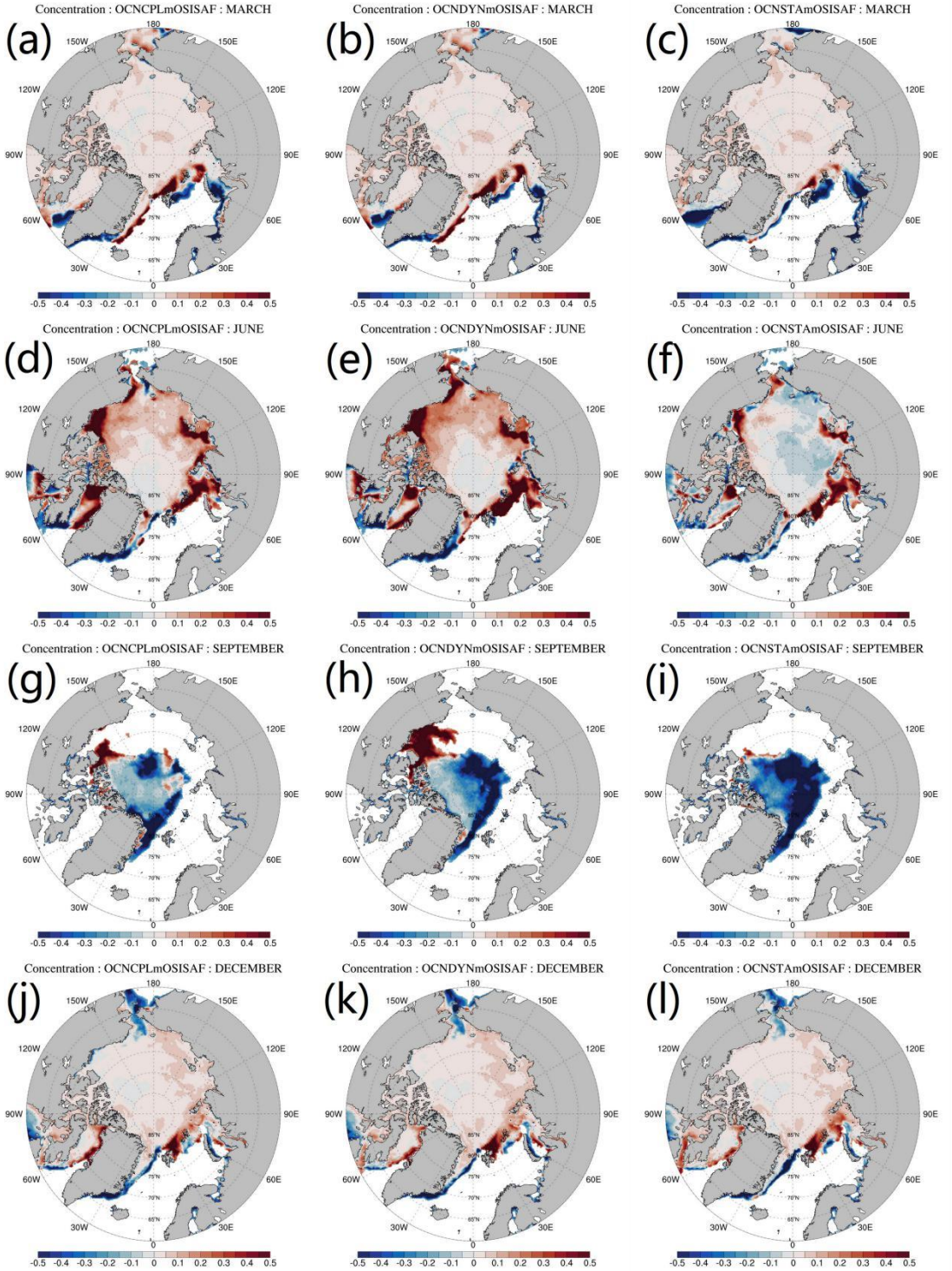

Fig.R5 Sea ice concentration bias between the model and the OSISAF observation in 2012. The 1st, 2nd, 3rd, 4th row denotes March, June, September, December. The 1st, 2nd, 3rd column denotes the two-way coupled model, the one-way coupled model, the standalone MITgcm run.

Figure R5 added to Figure 7 in the revised manuscript

Comment:
Minor things: line 181: "...without any data assimilation. . .". There was nothing said about new model is within an assimilation framework before or after. Why to mention this?

Reply:
In our institute, we have established an Arctic Ice Ocean Prediction System (ArcIOPS) based on the MITgcm and ensemble Kalman Filter data assimilation algorithm to carry out operational Arctic synoptic-scale sea ice forecast. Our future plan is to implement the coupled model with data assimilation algorithm to carry out Arctic seasonal sea ice prediction.

Line 246-247: "As a starting point, we need to evaluate the Arctic coupled model performance on seasonal timescale without any data assimilation." Revised to "As a starting point, we need to evaluate its performance on seasonal timescale."

Comment:
line 182: "...the coupled model free simulations..." what do you mean?

Reply:

Free simulation is aiming at the experiment with data assimilation in planning.

Line 248: "In this work, we perform the coupled model free simulations in the year of 2012 with special focuses on the summertime." Revised to "In this work, we perform the coupled model simulations in the year of 2012"

Comment:
line 188: indeed, nothing about atmosphere. Patterns of SLP although would be of interest.

Reply:
We have compared the patterns of atmospheric variable (2m temperature, SLP and wind fields) in OCNCPL run and OCNDYN run.

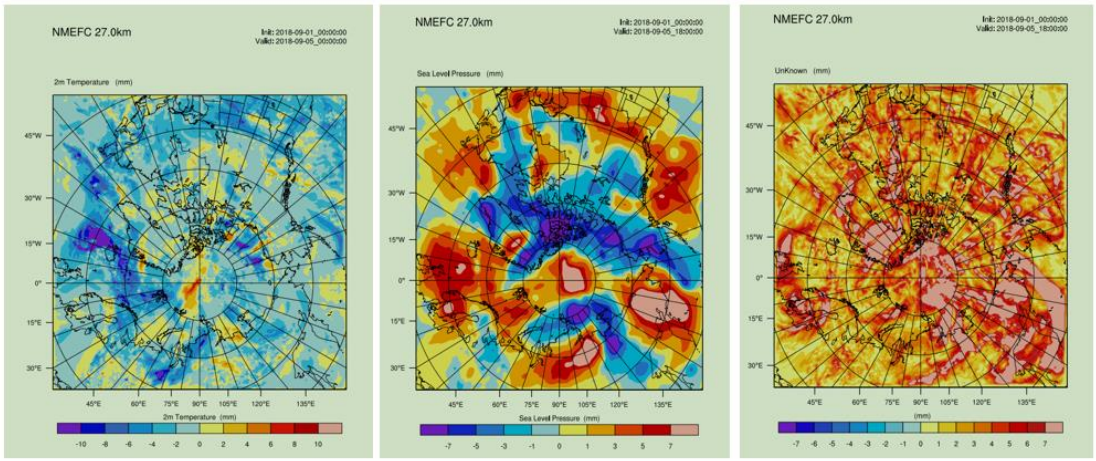

Fig.R6 Bias of 2m temperature, SLP and 10m wind speed from OCNCPL and OCNDYN on September 8, 2018.

Comment:
line 230: too speculative. did you do another run with different albedo?

Reply:
We have tried different sea ice albedo combinations and then chose a best albedo combination for the CFSR forcing. In our previous studies (Liang et al., JGR-oceans, 2018, 2019), we use the albedo combination of (dry ice: 0.75, wet ice: 0.7, dry snow:0.86, wet snow: 0.8) when JRA55 forcing is used. For this study using CFSR forcing, we tested the above albedo combination for the coupled model and found that the model produces more sea ice than the observation. So we reduced the albedo parameters and tested the combination of (dry ice: 0.65, wet ice: 0.55, dry snow:0.8, wet snow: 0.7) for the coupled model, and we found this group of albedo parameters is appropriate for the CFSR forcing.

Line 306-307: "A series of sensitivitiy experiments are performed to get an optimal combination of sea ice parameters (figures not shown)." Added

Comment:
line 290: I would elaborate more on this if possible.

Reply:
Line 385-390: "Day et al. (2014) pointed out that sea ice behaves long-term memory of melting-freezing processes. Notz and Bitz (2017) indicated that summertime sea ice thickness has an important influence on sea ice state in the following spring through the ice thickness-ice growth feedback. A negative anomaly of sea-ice area in late summer induces larger heat losses in autumn and winter from the ocean to the atmosphere due to enhanced outgoing long-wave radiation and turbulent heat fluxes, this causes thinner snow and ice due to later freeze-up and hence larger heat-

conduction fluxes through sea ice, eventually leading to larger ice-growth rates." Added

Comment:
line 366: not really or show that it is better than in other (global) models

Reply:
Indeed, we did not compare our results to other models. The motivation of our work is to enhance the operational sea ice seasonal prediction by coupling atmosphere, ocean and sea ice. Sea ice model intercomparison is a good index to weigh the performance of coupled models. In future, we hope that we can join such international project to evaluate and further improve our models.

Comment:
line 372: is it due to the albedo feedback? In OCECPL it is computed on the MITgcm side. What happens in OCEDYN? Again, figures 6c, 7 would have more value if the model is tuned. In the present form the model is not ready for this validation.

Reply:
We believe that two-way coupling between the WRF and the MITgcm provides a more rational representation of real air-ice-ocean physical processes, which includes the important ice-albedo feedback in early summer. In the MITgcm, sea ice albedo is calculated based on several variables, such as snow depth on ice, ice surface temperature. In the OCNCPL run, albedo is a coupling variable which affects both the WRF and the MITgcm. In the OCNDYN run, albedo used in the WRF are directly read from the CFSR forcing data.
In our original manuscript, we make a mistake when calculate sea ice extent in Figure 4a and 4b, which leads to the negative sea ice extent bias in Figure 4a. We confuse sea ice area with sea ice extent. Actually the blue and red curves in Figure 4a and 4b in the original manuscript are sea ice area. We redraw the modeled sea ice extent and add the standalone MITgcm run for the comparison (see the following figure). Compared with the standalone MITgcm run, the modeled sea ice extent in the coupled runs are more closer to the observation. With respect to the one-way coupled run, the spatial distribution of summertime sea ice concentration in the two-way coupled run is more closer to the OSISAF observation.
Line 499-503: "The two-way coupling between the Polar WRF and the MITgcm provides a more rational representation of real air-ice-ocean physical processes, which includes the important ice-albedo feedback in early summer. In the MITgcm, sea ice albedo is calculated based on several variables, such as snow depth on ice, ice surface temperature. In the OCNCPL run, albedo is a coupling variable which affects both the Polar WRF and the MITgcm. In the OCNDYN run, albedo used in the Polar WRF is directly read from the CFSR forcing data." Added

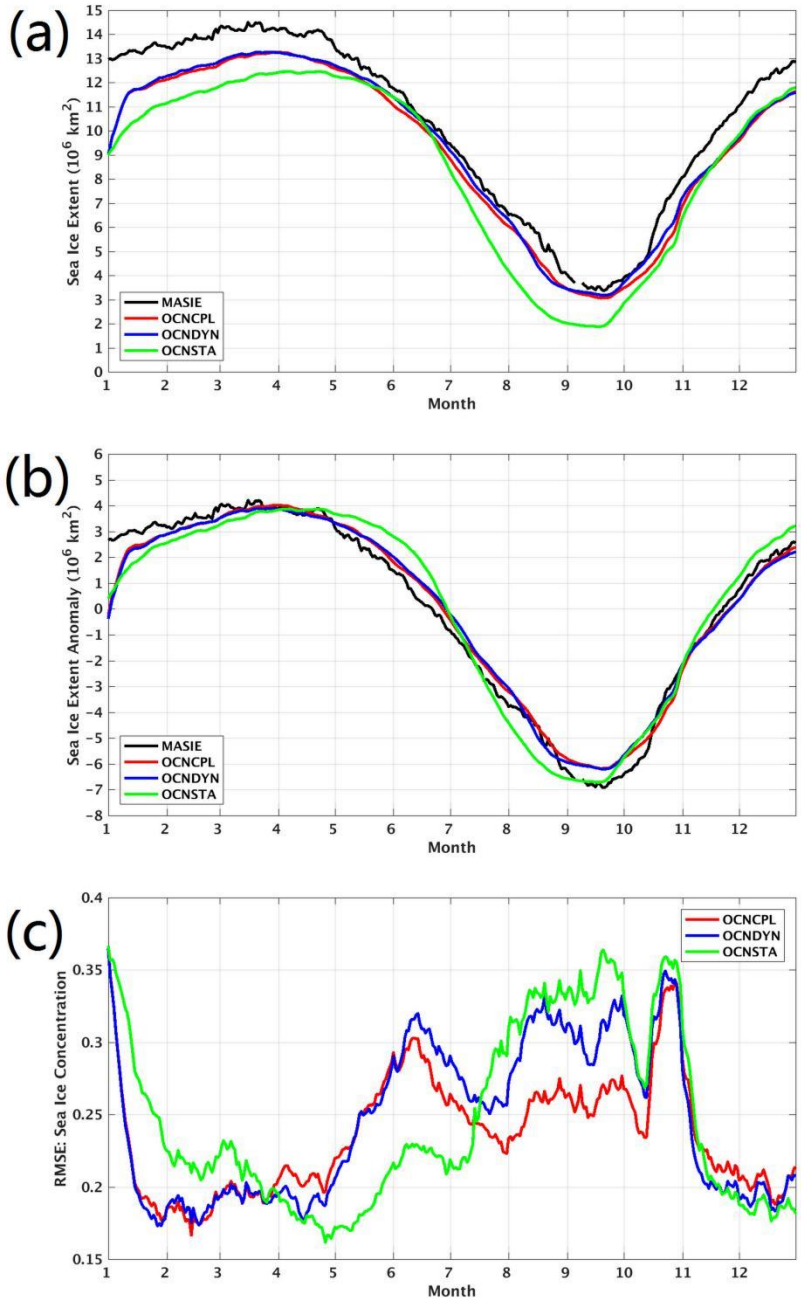

Fig.R7 Time series of (a) sea ice extent, (b) sea ice extent anomaly, and (c) root mean square error (RMSE) of modeled sea ice concentration with respect to the OSISAF observation in 2012. The black, red, blue and green lines in (a) denote sea ice extent of the MASIE observation, the OCNCPL run, the OCNDYN run, and the OCNSTA run respectively. The black, red, blue and green lines in (b) denote sea ice extent anomaly of the MASIE observation, the OCNCPL run, the OCNDYN run, and the OCNSTA run respectively. The red, blue and green lines in (c) denote the sea ice concentration RMSE of the OCNCPL run, the OCNDYN run, and the OCNSTA run, respectively.

Figure R7 added to Figure 7 in the revised manuscript

Reply to Reviewer Comment 2 (RC2)

Comment:
This manuscript describes a "new" regional coupled model for the Arctic intended for short-term forecasting and shows some preliminary simulation results. My main issue with this manuscript is that I do not see the novelty here. Similar regional models such as ARCSyM (Lynch et al. 1995), RASM (Cassano, Maslowski, others), Rinke et al. 2000 have not been mentioned here. The "novel" aspect seems only to be the coupling of the MITgcm to the Polar WRF model and perhaps the new C-Coupler. I nearly recommended reject for this manuscript. It seems more like a technical report. Also, the English usage here is confusing and there are a number of grammatical errors that I do not have time to go into here. Here are some specific suggestions that might make this worthy of publication in GMD.

Reply:
The authors thank the reviewer for the insightful comments. Thanks for pointing out that we omit similar works about regional coupled models. We have added these work as reference and re-written the introduction. The motivation of our work is to couple the Arctic ocean-seaice configuration of the MITgcm which is operationally running in our institute (ArcIOPS; Liang et al., 2020), to the Arctic atmospheric model (Polar WRF) in order to get a reasonable seasonal sea ice simulation. Beyond the scope of this work, our destination is operational sea ice seasonal prediction based on the coupled model and data assimilation algorithm. In my opinion, the novelty of our study is that we couple the Polar WRF and MITgcm which both featured with good performances in polar regions for the first time in the Arctic region and that we have solved some technical issues during the coupling process with a new coupler.
We have revised our manuscript by adding discussion on sea ice dynamic during coupling process. We have better motivated the manuscript in the introduction. We have proof-read the manuscript carefully to make it more readable.

Line 63-64: “The Arctic Region Climate System Model (ARCSyM) was developed to simulate coupled interactions among the atmosphere, sea ice, ocean, and land surface of the western Arctic (Lynch et al., 1995;Rinke et al., 2000).” Added
Line 68-73: “The Regional Arctic System Model (RASM) is a fully coupled, regional Earth system model covering the pan-Arctic domain (Maslowski et al., 2012;Cassano et al., 2017). The component models of RASM include the Weather Research and Forecasting (WRF) atmospheric model, the Variable Infiltration Capacity (VIC) land and hydrology model, and regionally configured versions of the ocean and sea ice models used in the Community Earth System Model (CESM): the CICE model and Parallel Ocean Program (POP).” Added
Line 81-84: “Since regional models can be run at higher resolution than global models, regional models can explicitly represent mesoscale features that may not be resolved in global models. Another potential advantage of the regional systems is that the

LBClateral boundary conditions can be controlled to get an optimal model input (Cassano et al., 2017)." Added

Comment :
1. There needs to be more on the novel aspects here. What does this model provide specifically that previous models did not? What time scales is this intended for? Short-term forecasting of weeks? Seasons?

Reply:
Sun et al. (2019) introduced a regional ocean-atmosphere coupled model covering the Red Sea based on the MITgcm and WRF. The novelty of our study is that we couple the Polar WRF and the MITgcm for the first time in the Arctic region and that we have solved some technical issues during the coupling process with a new coupler.
Both Polar WRF and MITgcm have specific features designed for polar regions, we speculate that coupling them will help us to improve seasonal sea ice prediction. We have used MITgcm model to make an operational Arctic synoptic-scale sea ice forecast for several years and showed reasonable results in aspects of sea-ice forecast in synoptic scale (ArcIOPS; Mu et al., 2019; Liang et al., 2020). This work is motivated by the need of a coupled Arctic sea ice-ocean-atmosphere model system for operational sea ice prediction of seasonal timescale (such as initialized at June and predict September sea ice).

Line 84-90: "This work is motivated by the need of a coupled Arctic sea ice-ocean-atmosphere model system for seasonal sea ice prediction in National Marine Environmental Forecasting Center of China." revised to "Aiming at operational seasonal sea ice prediction in the National Marine Environmental Forecasting Center (NMEFC) of China, the motivation of this work is to establish a fully coupled Arctic sea ice-ocean-atmosphere model with an capacity of reasonable sea ice simulation on seasonal timescale."

Comment:
2. There is no mention of the land component. Is this just the imbedded Polar WRF component? Why is this not important to the Arctic simulations?

Reply:
We apologize that we overlooked the description of land component in the section of Polar WRF. Yes, land component is embedded inside the Polar WRF. This Polar WRF incorporates many modifications to the standard version of the WRF. These adjustments are described by Bromwich et al. (2009), for example, adjustments to the surface parameterizations. The changes made in the Noah land surface model (LSM; Chen and Dudhia 2001) include using the latent heat of sublimation for calculating latent heat fluxes over ice surfaces, increasing the snow albedo and the emissivity value for snow, adjusting snow density, modifying thermal diffusivity and snow heat capacity for the subsurface layer, changing the calculation of skin temperature, and

assuming ice saturation in calculating the surface saturation mixing ratio over ice.
Land component is absolutely important to the Arctic simulation, however at current stage, our coupled model has not capacity of coupling an individual land model, instead, we use the embedded land component in the Polar WRF for technical simplicity. We have added the introduction of land component in the section of Polar WRF description.

Line 138-143: "The Noah land surface model is embedded inside the Polar WRF. The changes made in the Noah land surface model (LSM;(Chen and Dudhia, 2001)) include using the latent heat of sublimation for calculating latent heat flux over ice surface, increasing the snow albedo and the emissivity value for snow, adjusting snow density, modifying thermal diffusivity and snow heat capacity for the subsurface layer, changing the calculation of skin temperature, and assuming ice saturation in calculating the surface saturation mixing ratio over ice." Added
Line 504-506: "Land component is absolutely important to the Arctic simulation, however at current stage, our coupled model has not the capacity of coupling an individual land model, instead, we use the embedded land component in the Polar WRF for technical simplicity." Added

Comment:
3. The MITgcm sea ice component is quite old and simplistic. What is the albedo formulation on sea ice? What about on land? What about a sea ice thickness distribution?

Reply:
There are two calculations of surface albedo provided in the MITgcm.
1) from LANL CICE model:

$$\alpha = f_s\alpha_s + (1 - f_s)(\alpha_{i_{min}} + (\alpha_{i_{max}} - \alpha_{i_{min}})(1 - e^{-h_i/h_\alpha}))$$

where f_s is 1 if there is snow, 0 if not; the snow albedo, α_s has two values depending on whether T_s < 0 or not; $\alpha_{i\min}$ and $\alpha_{i\max}$ are ice albedo for thin melting ice, and thick bare ice respectively, h_i is snow depth, and h_α is a scale height.
2) From GISS model (Hansen et al 1983):

$$\alpha = \alpha_i e^{-h_s/h_a} + \alpha_s(1 - e^{-h_s/h_a})$$

where α_i is a constant albedo for bare ice, h_s is snow depth, h_a is a scale height and α_s is a variable snow albedo

$$\alpha_s = \alpha_1 + \alpha_2 e^{-\lambda_a a_s}$$

where α_1 is a constant, α_2 depends on T_s, α_s is the snow age, and λ_a is a scale frequency.

In our coupled model, surface albedo from LANL CICE model is used. Land component is from atmospheric component of Polar WRF mentioned in last reply.

Line 129-131: "In order to parameterize a sub-grid scale distribution for sea ice thickness, the mean sea ice thickness in each grid can be split into as many as 7 thickness categories in the MITgcm sea ice model. In our coupled model for simplicity, we use 2 thickness categories: open water and sea ice." Added

Comment:

4. The authors suggest that CMIP5 models represent sea ice in a simple way, but MITgcm is not any more complicated. A number of CMIP5 models used the Los Alamos Sea Ice Model (CICE) which is leading edge. What about CMIP6?

Reply:

We apologize for the improper statement about sea ice representation in the CMIP5 models in the original manuscript. The sea ice physical mechanism is rather complicate in the CICE. We have replaced the improper words in the manuscript. We have also gone through the entire manuscript to revise other improper words.

Line 40-44: "Climate models, such as those involved in the Coupled Model Intercomparison Project Phase 5 (CMIP5), normally incorporate sea ice model in a relatively simple way, thus can be used to generate long-term sea ice outlook with low confidence on spatial distribution." revised to "For climate model, the current generation of global climate models (GCMs) comprising phase 5 of the Coupled Model Intercomparison Project (CMIP5) show some biases in sea ice extent and thickness (Stroeve et al., 2012;Shu et al., 2015)."

Comment:

5. The grid staggering discussion and Figure 3 are really not necessary.

Reply:

We agree with the reviewer that the grid staggering discussion and Figure 3 are not necessary. So the part of computation of corner information and Fig. 3 are removed from the revised manuscript.

Line 229-243 deleted

Figure 3 deleted

Comment:

6. The case study they use is the year 2012. The boundary forcing for the atmosphere is from NCEP/NCAR re-analysis and for the ocean from the ECCO model. The sea ice extent is reasonable, but the sea ice volume is biased low compared to PIOMAS.
I believe the problem here is the simplicity of the sea ice thermodynamics and lack of a subgridscale thickness distribution. I feel like the model might be tuned for 2012 and want to see how it performs for other years. Some comparison to IceSAT data would also be beneficial here.

Reply:

We agree that one year is short to validate the model. So we add runcases of 2016 (for references, not shown in the manuscript), and add the standalone MITgcm run in 2012 for the comparison in the revised manuscript. To keep consistency between the coupled model and standalone MITgcm model, the standalone MITgcm simulation is forced by surface variables derived from the CFSR data and uses the same albedo parameters to the coupled model. As the IceSat data covers 2003-2008, we can not validate the sea ice thickness simulations of 2012 and 2016 with the IceSat data. Instead, we choose Cryosat2 and SMOS data to validate sea ice thickness.
In our original manuscript, we make a mistake when calculate sea ice extent in Figure 4a and 4b, which leads to the negative sea ice extent bias in Figure 4a. We confuse sea ice area with sea ice extent. Actually the blue and red curves in Figure 4a and 4b in the original manuscript are sea ice area. We redraw the modeled sea ice extent and add the standalone MITgcm run for the comparison (see the following figure). Compared with the standalone MITgcm run, the modeled sea ice extent in the coupled runs are more closer to the observation. With respect to the one-way coupled run, the spatial distribution of summertime sea ice concentration in the two-way coupled run is more closer to the OSISAF observation.

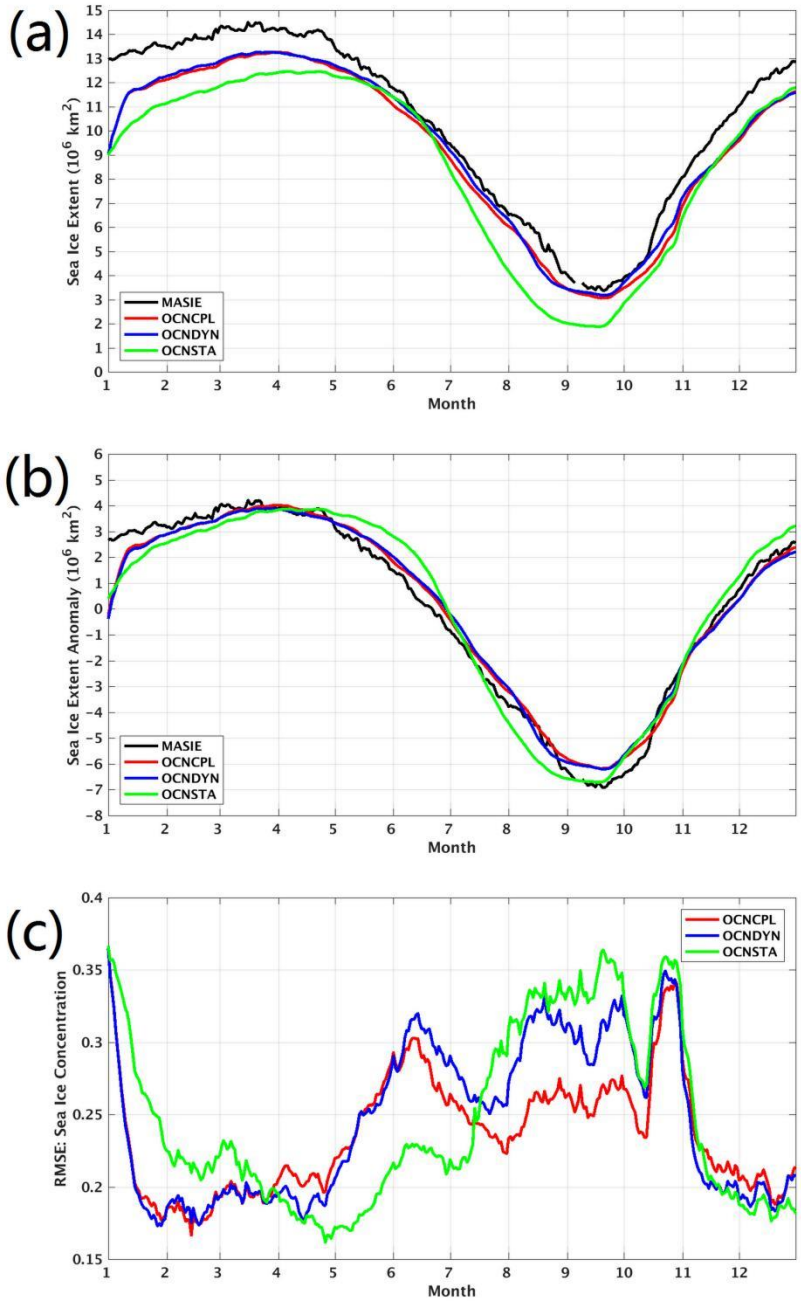

Fig.R8 Time series of (a) sea ice extent, (b) sea ice extent anomaly, and (c) root mean square error (RMSE) of modeled sea ice concentration with respect to the OSISAF observation in 2012. The black, red, blue and green lines in (a) denote sea ice extent of the MASIE observation, the OCNCPL run, the OCNDYN run, and the OCNSTA run respectively. The black, red, blue and green lines in (b) denote sea ice extent anomaly of the MASIE observation, the OCNCPL run, the OCNDYN run, and the OCNSTA run respectively. The red, blue and green lines in (c) denote the sea ice concentration RMSE of the OCNCPL run, the OCNDYN run, and the OCNSTA run, respectively.

Results of the modeled sea ice in 2016 are shown as follows:

The year of 2016 is selected because of the next anomalous sea ice extent minima event after 2012 appeared in 2016. We also conduct two-way coupled run, one-way coupled run, standalone MITgcm run for the year of 2016. The initial fields on 2016.1.1 of the MITgcm and the WRF model are derived from the standalone MITgcm simulation forced by JRA55 data and from the CFSR reanalysis data. Time evolution of modeled sea ice extent shows that the two-way coupled run produces more reasonable sea ice extent compared with the MASIE data, although the modeled September sea ice concentration of the two-way run in the Arctic Pacific section overmelts.

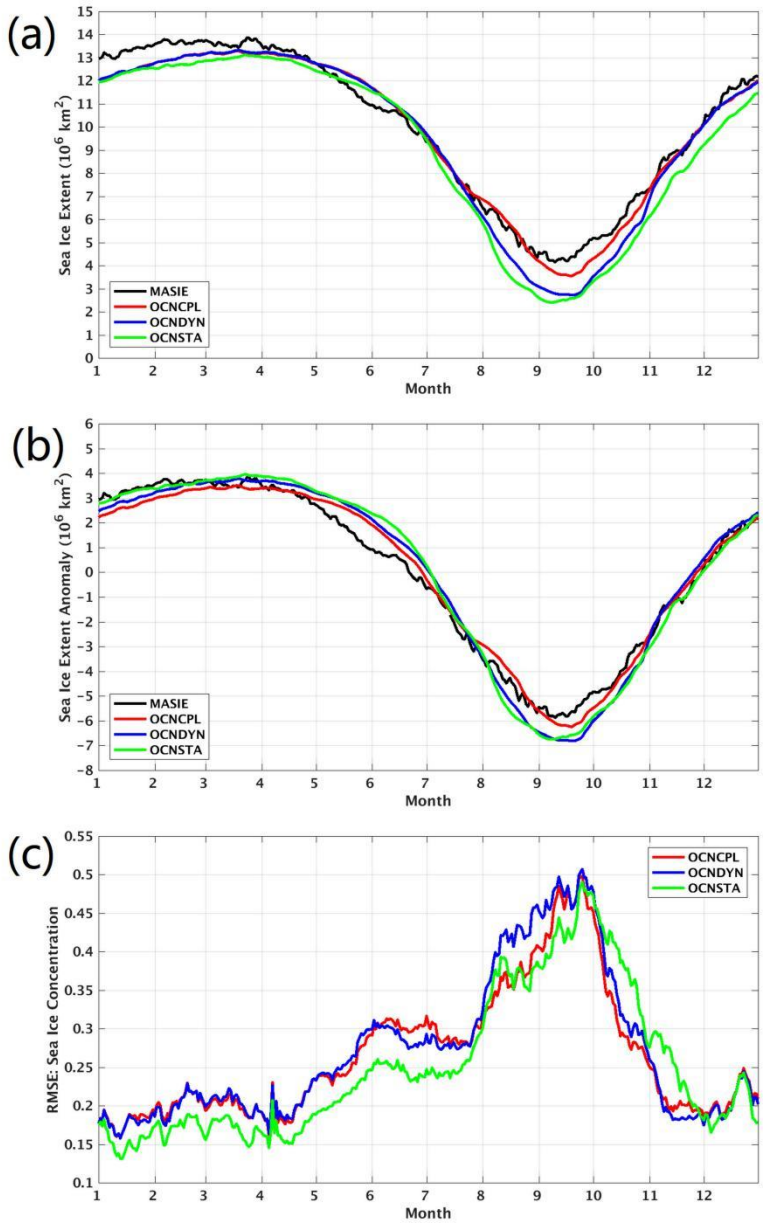

Fig.R9 Same to the above figure but for the year of 2016.

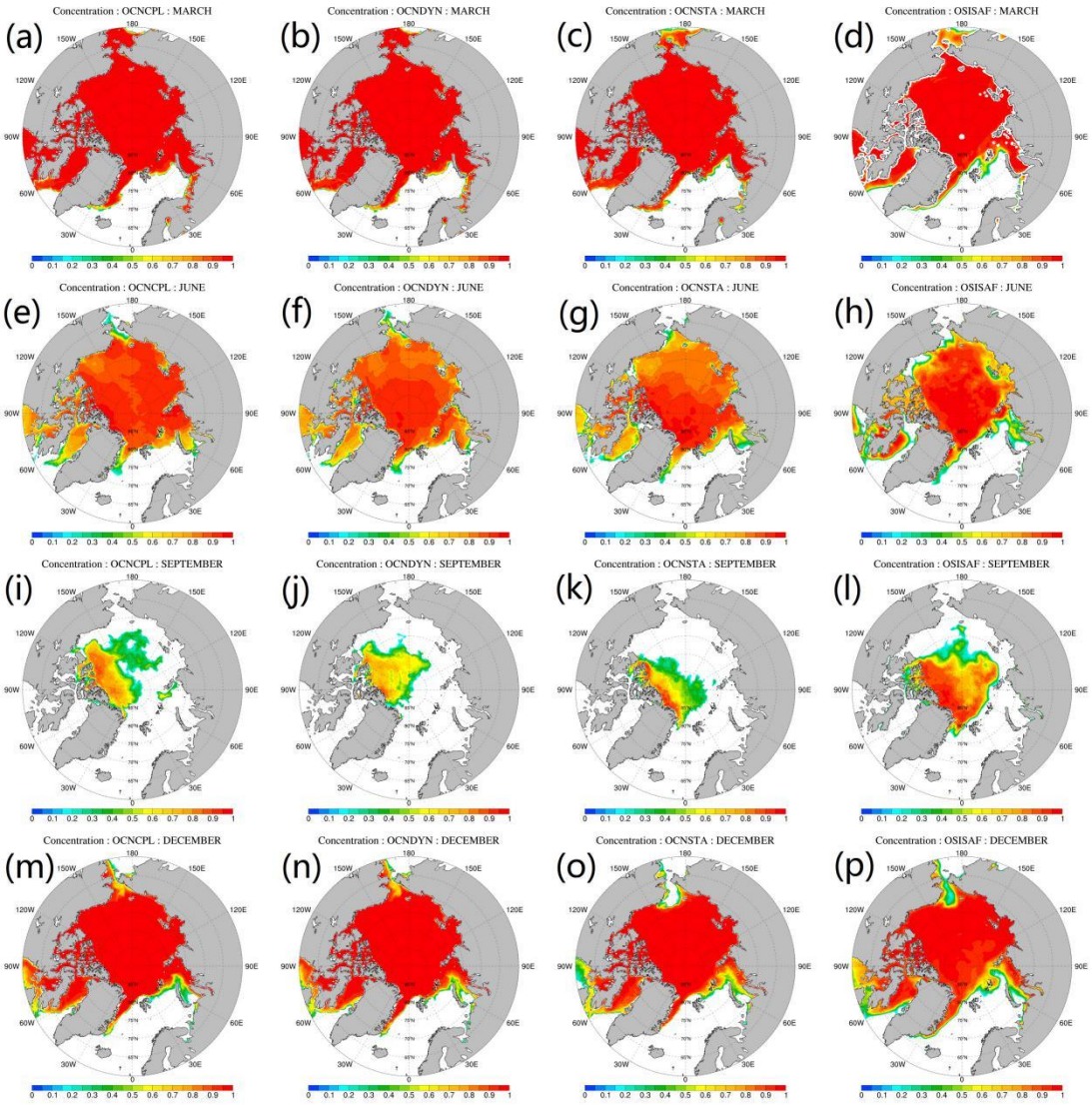

Fig.R10 Monthly mean sea ice concentration in 2016. The 1st, 2nd, 3rd, 4th row denotes March, June, September, December. The 1st, 2nd, 3rd, 4th column denotes the two-way coupled run (OCNCPL), the one-way coupled run (OCNDYN), the standalone MITgcm run (OCNSTA) and the observations (OSISAF).

Additional modifications

Line 4: “Bo Lin1” added
Line 13-14: “A newly developed coupler, C-Coupler2 (the Community Coupler 2),”revised to “In the ArcIOAM configuration, the Community Coupler 2 (C-Coupler2)”
Line 16-17 :“A scalability test is performed to investigate the parallelization of the coupled model.” added
Line 17-21: “ArcIOAM is demonstrated with focus on seasonal simulation of the Arctic sea ice and ocean state in the year of 2012. The results obtained by ArcIOAM, along with the experiment of one-way coupling strategy, are compared with available observational data and reanalysis products.” revised to “As the first step toward reliable Arctic seasonal sea ice prediction, the simulation results in the year of 2012 of the ArcIOAM implemented with two-way coupling strategy, along with one-way coupling strategy, are evaluated with respect to available observational data and reanalysis products.”
Line 21 :“Besides, the standalone MITgcm run with prescribed atmospheric forcing is performed for references.” added
Line 22-24: “From the comparison, results obtained from two experiments both realistically capture the sea ice and oceanic variables in the Arctic region over a 1-year simulation period.” revised to “From the comparison, all the experiments simulate rational evolution of sea ice and ocean states in the Arctic region over a one-year simulation period.”
Line 24: “The two-way coupled model” revised to “The two-way coupling strategy”
Line 25 : “result” added
Line 35: “can be” revised to “are”
Line 36 : “marginal seas” added
Line 47: “running operationally” revised to “operationally running”
Line 61: “process” revised to “processes”
Line 62: “study” revised to “studies”
Line 79-80: “the regional weather prediction system and wave prediction system” revised to “the regional weather and wave prediction system”
Line 101: “to this end,” removed
Line 102: “specific areas” revised to “lateral boundaries”; “developed” revised to “designed”
Line 103-106: “After implementing ArcIOAM, we run seasonal simulation of Arctic sea ice and ocean state in 2012. The simulated variables of the Arctic ocean and sea ice are examined and validated against available observational data and reanalysis products.” revised to “After implementing the ArcIOAM, we evaluate the model performance in the year of 2012 against available observational data. This year is selected because of the historical sea ice extent minimum record in the satellite era.”
Line 109 : “Besides, a stand-alone MITgcm simulation with prescribed atmospheric forcing is performed for references.” added
Line 111: “Section 3” revised to “Section 4”
Line 112: “Section 4” revised to “Section 5”

Line 133: “the” revised to “an”
Line 142-144: “Two key modifications for the Polar WRF are optimization of surface energy balance and heat transfer for the Noah land surface model over sea ice and permanent ice surfaces, and” revised to “Other modifications for the Polar WRF include”
Line 155: “The Coupler Component Model” revised to “The Coupler”
Line 156: “use” revised to “have implemented”
Line 181: “1)” removed; “there is” revised to “producing”
Line 245: “3 Numerical Experiments” revised to “4 Numerical Experiments”
Line 246: “Arctic coupled model” revised to “ArcIOAM”
Line 248-251: “The year of 2012 is chosen because an unusually strong storm formed off the coast of Alaska on 5 August 2012, and tracked into the center of the Arctic Basin where it lingered for several days and generated stronger sea ice-ocean-atmosphere interaction(Simmonds and Rudeva, 2012).” added
Line 254-256: “The year of 2012 is chosen because an unusually strong storm formed off the coast of Alaska on 5 August 2012, and tracked into the center of the Arctic Basin where it lingered for several days and generated stronger sea ice-ocean-atmosphere interaction(Simmonds and Rudeva, 2012).” removed
Line 257: “abilities” revised to “capabilities”
Line 258: “simulations” revised to “variables”
Line 259: “Two” revised to “Three”

Line 264-266: “α in Equ. 1 is set to 1 in the OCNDYN run. The third experiment of OCNSTA represents the stand-alone MITgcm simulation with the same sea ice albedo parameters to the coupled model but prescribed atmospheric forcing to keep consistency with previous two coupling experiments.” added
Line 266-267: “the two runs” revised to “these cases”; “on” revised to “in”; “and sea ice” removed
Line 269: “used in the OCNCPL and OCNDYN runs, and the prescribed atmospheric forcing used in the OCNSTA run” added
Line 275: “the ice is” revised to “the zones of sea ice are”
Line 275-276: “The ocean and sea ice initial condition” revised to “The initial condition of ocean and sea ice”
Line 276-277: “. The stand-alone MITgcm simulation was” removed
Line 279: “in our previous study” removed
Line 282: “coupled” removed; “and used in our analysis” removed
Line 283: “4” revised to “5”
Line 284: “4” revised to “5”
Line 285-286: “The lowest Arctic sea ice extent in the satellite-observed era occurred in the summer of 2012” revised to “The Arctic sea ice extent minimum value appeared in the summer of 2012 in the satellite era”
Line 287-288: “, obtained from http://nsidc.org/data/masie/, in the year of 2012” removed
Line 291-292: “Compared with the OCNSTA run, results from the experiments with

coupling (OCNCPL and OCNDYN) are closer to observations. It is noted that" added
Line 291-292: "Compared with the OCNSTA run, results from the experiments with coupling (OCNCPL and OCNDYN) are closer to observations. It is noted that" added
Line 293: "2" revised to "1.5"; "except" revised to "after"
Line 296: "Comparing" revised to "By comparing";
Line 297: "quite" removed
Line 300: "and phase" added; "of the two runs" revised to "in the OCNCPL and OCNDYN runs"
Line 301-303: "The sea ice extent bias between the model states and the observations likely arise from the sea ice model systematic bias which is induced by the choice of sea ice and snow albedo parameters in the two runs." revised to "While results of stand-alone run shows lag of sea ice melts and freezes in advance compared with the observations."
Line 305: "In the MITgcm sea ice model" revised to "In the sea ice model of MITgcm"
Line 308: "rationally amplifying albedo parameters or " removed ; "a" removed
Line 310: "We compare the modeled sea ice concentration" revised to "The modeled sea ice concentration is compared"
Line 311-312: ".; obtained from http://osisaf.met.no/; product identifier: OSI-409." removed
Line 315-316: "After 1 month of model state adjustment, three experiments shows similar patterns that RMSE is lower in winter and spring than in summer and autumn" added
Line 317: "January" revised to "November"; "(Figure 6)" added; "coupling" added
Line 321-347: "To further clarify sea ice spatial distribution, we show the modeled and observed monthly mean sea ice concentration in July, August and September (Figure 5). In July, the modeled sea ice extent of the OCNCPL run is similar to that of the OCNDYN run, but the modeled sea ice concentration of the OCNCPL run is much lower than that of the OCNDYN run in thick multiyear ice zone near the Canadian Arctic Archipelago and in the southern Beaufort Sea (Figure 5a and Figure 5b). The satellite observations show that the OCNCPL run still overestimates sea ice concentration in the southern Beaufort Sea and the Laptev Sea (Figure 5c). In August, the modeled sea ice melts quickly in the Eurasian marginal seas in the two runs. Compared with the satellite observations (Figure 5f), the OCNDYN run overestimates sea ice concentration in the southern Beaufort Sea while underestimates sea ice concentration in the center Arctic basin (Figure 5e). The OCNCPL run simulates similar sea ice extent to the satellite observations but with lower concentration in the center Arctic basin (Figure 5d). In September, the modeled sea ice in the marginal sea ice zone melts out in the two runs. Although the two runs simulate almost same sea ice extent, due to rational representation of sea ice-ocean-atmosphere interaction in the OCNCPL run, the modeled sea ice distribution of the OCNCPL run is closer to the observations (Figure 5g and Figure 5i)." revised to "To further clarify sea ice concentration spatial distribution, we show the modeled and observed monthly mean sea ice concentration (Figure 6) and deviation of model results and observation (Figure 7) in March, June, September and December In March when the Arctic Ocean is almost fully covered

by sea ice, the main source of discrepancy appears in sea ice edge zones in the Atlantic side (Figure 6a-c). In June, sea ice concentrations are overestimated in the Arctic marginal seas in the OCNCPL and OCNDYN runs (Figure 7d-e). The modeled sea ice concentration in the OCNSTA run is more closer to the observations (Figure 7f). In September, the modeled sea ice in the marginal sea ice zone melts out in all runs (Figure 6i-k). Compared with the satellite observations (Figure 6l), sea ice in the OCNSTA run overmelts in summertime which leads to an anomalous negative bias of sea ice concentration in the Arctic (Figure 7i), the two coupled runs overestimate sea ice concentration in the southern Beaufort Sea while underestimates sea ice concentration in the center Arctic basin (Figure 7g-h). Although the two coupled runs simulate similar sea ice extent patterns, due to rational representation of sea ice-ocean-atmosphere interaction in the OCNCPL run, the modeled sea ice distribution of the OCNCPL run is closer to the observations (Figure 6i and Figure 6l). In December, the situation is similar with that in March when sea ice dominates almost entire Arctic region."

Line 348: "4" revised to "5"

Line 353-355: "The OCNSTA run simulates more rational sea ice growth rate from January to May but systematic negative sea ice volume bias compared with the PIOMAS data. The sea ice volume in the OCNCPL and OCNDYN runs shows better results than that in the OCNSTA run from June to December." added

Line 356-358: "Both the two runs produce less sea ice volume than the PIOMAS data almost in a whole year of 2012, partly resulting from that our model underestimates sea ice extent (Figure 4a) without assimilating any observation." revised to "However, both the two coupled runs produce less sea ice volume than the PIOMAS data in most time of 2012, partly resulting from that our model underestimates sea ice extent (Figure 5a) without assimilating any observation."

Line 358: "However, it is" revised to "It"

Line 373: "mathematically" removed

Line 379-380: "Comparing with the CS2SMOS data, both runs produce rational sea ice thickness evolution" revised to "Comparing with the CS2SMOS data, both coupled runs produce more rational sea ice thickness evolution than stand-alone run"

Line 393: "two" revised to "three"; "the" revised to "mentioned";

Line 394-395: "Compared with the coupled runs, the sea ice thickness in the OCNSTA run shows larger bias in pack ice zone while smaller bias in marginal ice zone." added

Line 398-399: "OCNCPL run" revised to "coupled runs"; "model" revised to "the coupled runs";

Line 405: "(Figure 9)" added;

Line 406: "; obtained from http://www.whoi.edu/beaufortgyre/" removed;

Line 412-427: "Spatial distributions of monthly mean sea ice thickness in June, September, and December are shown in Figure 8. In June, almost the whole Arctic basin is still covered by thick ice, large sea ice thickness deviations between the two runs mainly appear around sea ice edge where sea ice-ocean-atmosphere interaction can impact significant influence on sea ice melting rate (Figure 8c). In September, accompanied by the change of sea ice concentration pattern when involving sea ice-

ocean-atmosphere interaction, the modeled sea ice becomes thicker in the central Arctic while thinner in the area near the Greenland Island and in the southern Beaufort Sea (Figure 8f). As summertime sea ice thickness has strong effect on preconditioning the following wintertime sea ice thickness (Day et al., 2014), the modeled sea ice of the OCNCPL run is universally thinner than that of the OCNDYN run in December (Figure 8i)." revised to "Spatial distributions of monthly mean sea ice thickness and its bias with respect to available CS2SMOS data in March, June, September, and December are shown in Figure 10 and Figure 11. In March and December, all three runs underestimate sea ice thickness in central Arctic, while overestimate sea ice thickness in marginal sea ice zone (Figure 11). In March, the OCNSTA run overestimates sea ice thickness in the Pacific sector of the Arctic Ocean and in the Baffin Bay (Figure 11e). The coupled runs overestimate sea ice thickness in the northern Barents Sea while underestimate sea ice thickness in the western Chukchi Sea (Figure 11a and Figure 11c). In December, compared with the OCNDYN run, the modeled sea ice thickness in marginal sea ice zone in the OCNCPL run is more closer to the CS2SMOS data (Figure 11b), partly due to the rational sea ice distribution at the beginning of freezing season, as summertime sea ice thickness has strong effect on preconditioning the following wintertime sea ice thickness (Day et al., 2014).";

Line 428: "4" revised to "5"

Line 438-451: "The SST RMSE of the two runs with respect to the GMPE data from July to September are shown in Figure 9. We do not show the time evolution of the SST RMSE in whole year because the two timeseries do not obviously diverge in the other months. In general, the SST RMSE of the OCNCPL run is smaller than that of the OCNDYN run in the summer of 2012, which means the SST simulation also improves when sea ice-ocean-atmosphere interaction is allowed in the model. Spatial patterns of modeled and observed SST in July, August and September are shown in Figure 10. The GMPE SST data is available in ice-free areas (Figure 10a, Figure 10e and Figure 10i). Comparing with the OCNDYN run, in July and August the modeled ocean surface of the OCNCPL run warms in Fram Strait, the Barents Sea, the Kara Sea and the Bering Strait while colds in the Baffin Bay, the Greenland Sea and the Laptev Sea (Figure 10d andFigure 10h). In September strong warming in the OCNCPL run appears in the southern Beaufort Sea (Figure 10l). These SST modifications induced by sea ice-ocean-atmosphere interaction not only lead to the reduction of the modeled ocean surface temperature bias, but also help to maintain a more rational sea ice spatial pattern." revised to "The SST RMSE of the three runs with respect to the GMPE data are shown in Figure 12. In general compared with the coupled runs, the SST RMSE in the OCNSTA run is smaller in the summertime but larger in the rest. Spatial patterns of the modeled and observed SST in March, June, September and December are shown in Figure 13. Deviation of the modeled SST and the GMPE SST observation is demonstrated in Figure 14. The GMPE SST data is available in ice-free areas (Figure 13d, Figure 13h, Figure 13l and Figure 13p). In March and June, the OCNSTA run produces a warmer sea surface in the Nordic Seas, which explains the positive SST bias from January to June in Figure 12 compared with the coupled runs. In September the SST RMSE in the OCNCPL run (Figure 12) arises from the strong negative bias in the southern Beaufort Sea and the

Baffin Bay (Figure 14g).";
Line 460: "Table 1" revised to "Table 2"
Line 467-469: "Figure 11" revised to "Figure 15"
Line 472: "5" revised to "6"
Line 475-478: "By coupling the Polar WRF and the MITgcm for the first time in Arctic region, a series of specific setup including data interpolation between different grids and relaxation algorithm in specific areas are designed." revised to "By coupling the Polar WRF and the MITgcm for the first time in Arctic region, a series of specific procedures including data interpolation between different grids and relaxation algorithm in lateral boundaries are designed. The parallel efficiency of the coupled model is also investigated."
Line 479: "new coupled model of" removed
Line 480: "coupled" revised to "coupling"; "and" removed
Line 481: "and stand-alone oceanic simulation (OCNSTA)" added
Line 482: "two" revised to "the two coupled";
Line 483-486: "From the comparison, results obtained from two experiments both realistically capture the sea ice and oceanic variables in the Arctic region over a 1-year simulation period. The two-way coupled experiment gives equal or better results compared with the one-way coupled experiment." revised to "From the comparison, results obtained from the two-way coupling experiment capture the sea ice and ocean evolution in the Arctic region over a 1-year simulation period. The two-way coupling experiment gives better results compared with the one-way coupling experiment and stand-alone oceanic simulation, especially in summertime."
Line 507-508: "seasonal scale simulation in" revised to "results for";
Line 521: "process understanding" revised to "better understanding of mechanism";
Line 533: "BL worked on the scalability test." added
Line 565-567: "Cassano, J. J., DuVivier, A., Roberts, A., Hughes, M., Seefeldt, M., Brunke, M., Craig, A., Fisel, B., Gutowski, W., Hamman, J., Higgins, M., Maslowski, W., Nijssen, B., Osinski, R., and Zeng, X.: Development of the Regional Arctic System Model (RASM): Near-Surface Atmospheric Climate Sensitivity, Journal of Climate, 30, 5729-5753, 10.1175/jcli-d-15-0775.1, 2017." Added
Line 573-574: "Christidis, Z.: Performance and Scaling of WRF on Three Different Parallel Supercomputers, High Performance Computing, Cham, 2015, 514-528," Added
Line 577-578: "Day, J. J., Hawkins, E., and Tietsche, S.: Will Arctic sea ice thickness initialization improve seasonal forecast skill?, Geophysical Research Letters, 41, 7566-7575, https://doi.org/10.1002/2014GL061694, 2014." Added
Line 582: "Dirk Notz, and Bitz, C. M.: Sea ice in Earth system models, in: Sea Ice, 304-325, 2017" Added
Line 626-627: "Liang, X., ZHAO, F., Li, C., ZHANG, L., and LI, B.: Evaluation of ArcIOPS sea ice forecasting products during the ninth CHINARE-Arctic in summer 2018, Advances in Polar ence, v.31;No.78, 19-30, 2020." Added
Line 636-637: "Lynch, A. H., Chapman, W. L., Walsh, J. E., and Weller, G.: Development of a Regional Climate Model of the Western Arctic, Journal of Climate, 8, 1555-1570, 10.1175/1520-0442(1995)008<1555:doarcm>2.0.co;2, 1995." Added

Line 663-664: “Rinke, A., Lynch, A. H., and Dethloff, K.: Intercomparison of Arctic regional climate simulations: Case studies of January and June 1990, Journal of Geophysical Research: Atmospheres, 105, 29669-29683, 10.1029/2000jd900325, 2000.” Added

Line 675-676: “Shu, Q., Song, Z., and Qiao, F.: Assessment of sea ice simulations in the CMIP5 models, The Cryosphere, 9, 399-409, 10.5194/tc-9-399-2015, 2015.” Added

Line 736-739: “Figure 3: Wind stress curl (unit: Nm-2) derived from (a) the MITgcm output, (b) the Polar WRF output, and (c) their difference on March 1, 2012. The difference of wind stress curl between the Polar WRF and MITgcm is calculated by interpolating the Polar WRF output onto the MITgcm grid.” added

Line 743-746: “Figure 4: The parallel efficiency (left) and speed-up (right) test of the coupled model and the stand-alone component models, employing up to 896 CPU cores. The simulation using 28 CPU cores is regarded as the baseline case when computing the speed-up. The tests are performed on a Lenovo Blade Server system composed of 240 dual-socket compute nodes based on 14-core Intel Haswell processors.” added

Line 750: “Figure 4” revised to “Figure 5”

Line 751: “green” added

Line 752: “the OCNSTA run” added

Line 753: “green” added

Line 754: “green” added; “the OCNSTA run” added

Line 755: “the OCNSTA run” added

Line 760-763: “Figure 5: Modeled and observed monthly mean sea ice concentration. The top, middle, and bottom panels show the July, August, and September sea ice concentration, respectively. The left, middle, and right panels show sea ice concentration of the OCNCPL run, the OCNDYN run, and the OSISAF observations. OSISAF = Ocean and Sea Ice Satellite Application Facility” revised to “Figure 6: Modeled and observed monthly mean sea ice concentration. From top to bottom panels show the March, June, September and December sea ice concentration, respectively. From left to right panels show sea ice concentration of the OCNCPL run, the OCNDYN run, the OCNSTA run and the OSISAF observations. OSISAF = Ocean and Sea Ice Satellite Application Facility.”

Line 766-770: “Figure 7: Deviation between the modeled and observed monthly mean sea ice concentration. From top to bottom panels show the March, June, September and December sea ice concentration deviation respect to the OSISAF observations, respectively. The left, middle, and right panels show results of the OCNCPL run, the OCNDYN run, and the OCNSTA run. OSISAF = Ocean and Sea Ice Satellite Application Facility.” added

Line 775-784: “Figure 6: Time series of (a) total sea ice volume, (b) spatial mean sea ice thickness, and (c) the RMSE of sea ice thickness with respect to the satellite-retrieved observations in 2012. The black, red, and blue lines in (a) denote total sea ice volume of the PIOMAS data, the OCNCPL run, and the OCNDYN run, respectively. The black, red, and blue dots in (b) denote sea ice thickness of the CS2SMOS observations, the OCNCPL run, and the OCNDYN run, respectively. The black bar in (b)

represents the observational uncertainties of the CS2SMOS data. The red and blue masks in (c) denote sea ice thickness RMSE of the OCNCPL run and the OCNDYN run with respect to the SMOS observations in thin ice (< 1 m) region (line), the Cryosat-2 observations (circle), the CS2SMOS observations (triangle), respectively. Model grid points without available observations are not taken into the sea ice thickness RMSE calculation. PIOMAS = Pan-Arctic Ice Ocean Modeling and Assimilation System; SMOS = Soil Moisture Ocean Salinity" revised to "Figure 8: Time series of (a) total sea ice volume, (b) spatial mean sea ice thickness, and (c) the RMSE of sea ice thickness with respect to the satellite-retrieved observations in 2012. The black, red, green and blue lines in (a) denote total sea ice volume of the PIOMAS data, the OCNCPL run, the OCNSTA run and the OCNDYN run, respectively. The black, red, green and blue dots in (b) denote sea ice thickness of the CS2SMOS observations, the OCNCPL run, the OCNSTA run and the OCNDYN run, respectively. The black bar in (b) represents the observational uncertainties of the CS2SMOS data. The red, green and blue masks in (c) denote sea ice thickness RMSE of the OCNCPL run, the OCNSTA run and the OCNDYN run with respect to the SMOS observations in thin ice (< 1 m) region (line), the Cryosat-2 observations (circle), the CS2SMOS observations (triangle), respectively. Model grid points without available observations are not taken into the sea ice thickness RMSE calculation. PIOMAS = Pan-Arctic Ice Ocean Modeling and Assimilation System; SMOS = Soil Moisture Ocean Salinity."

Line 788-790: "Figure 7: Time series of sea ice thickness at three positions: (a) (75 °N, 150 °W), (b) (78 °N, 150 °W), and (c) (74 °N, 140 °W). The red and blue lines denote sea ice thickness of the OCNCPL run and the OCNDYN run, respectively. The black solid and dashed lines denote sea ice thickness observations of the BGEP ULSs, which were deployed in the summers of 2011 and 2012. The black lines of the BGEP ULS observations have been smoothed with the gray bar representing the observational uncertainties. BGEP = Beaufort Gyre Exploration Project; ULS = upward-looking sonar." revised to "Figure 9: Time series of sea ice thickness at three positions: (a) (75 °N, 150 °W), (b) (78 °N, 150 °W), and (c) (74 °N, 140 °W). The red, blue and green lines denote sea ice thickness of the OCNCPL run, the OCNDYN run and the OCNSTA run, respectively. The black solid and dashed lines denote sea ice thickness observations of the BGEP ULSs"

Line 798-800: "Figure 8: Monthly mean sea ice thickness. The top, middle, and bottom panels show the June, September, and December sea ice thickness, respectively. The left, middle, and right panels show sea ice thickness of the OCNCPL run, the OCNDYN run, and the deviation between them." revised to "Figure 10: Monthly mean sea ice thickness. From top to bottom panels show the March, June, September, and December sea ice thickness, respectively. From left to right panels show sea ice thickness of the OCNCPL run, the OCNDYN run, the OCNSTA run and the CS2SMOS data."

Line 803-806: "Figure 11: Deviation of the modeled monthly mean sea ice thickness and the CS2SMOS data. The top, middle, and bottom panels show sea ice thickness deviation of the OCNCPL run, the OCNDYN run and the OCNSTA run, respectively. The left and right panels show results in March and December." added

Line 810-812: “Figure 9: Time series of the RMSE of modeled SST with respect to the GMPE observations in summer of 2012. The red and blue lines denote the SST RMSE of the OCNCPL run and the OCNDYN run, respectively. GMPE = Group for High-Resolution Sea Surface Temperature Multi-Product Ensemble.” revised to “Figure 12: Time series of the RMSE of modeled SST with respect to the GMPE observations in 2012. The red, blue and green lines denote the SST RMSE of the OCNCPL run, the OCNDYN run and the OCNSTA run, respectively. GMPE = Group for High-Resolution Sea Surface Temperature Multi-Product Ensemble.”

Line 815-820: “Figure 10: Modeled and observed monthly mean SST. Rows 1 to 3 show the July, August, and September SST, respectively. Columns 1 to 4 show the SST of the GMPE observations, the OCNCPL run, the OCNDYN run, and the deviation between the OCNCPL and OCNDYN runs, respectively. GMPE = Group for High-Resolution Sea Surface Temperature Multi-Product Ensemble” revised to “Figure 13: Modeled and observed monthly mean SST. From top to bottom panels show the March, June, September and December SST, respectively. From left to right panels show the SST of the OCNCPL run, the OCNDYN run, the OCNSTA run and the GMPE observations, respectively. GMPE = Group for High-Resolution Sea Surface Temperature Multi-Product Ensemble.”

Line 822-826: “Figure 14: Deviation of the modeled monthly mean SST and the GMPE SST data. From top to bottom panels show the March, June, September and December SST deviation, respectively. From left to right panels show the SST of the OCNCPL run, the OCNDYN run and the OCNSTA run, respectively. GMPE = Group for High-Resolution Sea Surface Temperature Multi-Product Ensemble.” added

Line 829: “Figure 11” revised to “Figure 15”

Line 833-840: Table 1 added

Line 843: “Table 1” revised to “Table 2”

Reference:

Day, J. J., et al., Will Arctic sea ice thickness initialization improve seasonal forecast skill? Geophys Res Lett, 2014, 41: 7566-7575.

Nguyen, A. T., et al., Arctic ice-ocean simulation with optimized model parameters: Approach and assessment. J. Geophys. Res., 2011, 116: C04025.

Notz, D. & Bitz, C. M. in *Sea Ice* (ed. Tomas, D. N.) (John Wiley & Sons, Chichester, 2017).

Van Pham, T., et al., New coupled atmosphere-ocean-ice system COSMO-CLM/NEMO: assessing air temperature sensitivity over the North and Baltic Seas. Oceanologia, 2014, 56(2): p. 167-189.

Christidis, Z., et al., Performance and Scaling of WRF on Three Different Parallel Supercomputers, in: International Conference on High Performance Computing, Springer, 514–528, 2015.

Bromwich, D. H., K. M.Hines, and L.-S.Bai, 2009: Development of Polar Weather Research and Forecasting Model: 2. Arctic Ocean. J. Geophys. Res., 114, D08122, doi:10.1029/2008JD010300.

Chen, F., and J.Dudhia, 2001: Coupling an advanced land surface-hydrology model with the Penn State–NCAR MM5 modeling system. Part I: Model implementation and sensitivity. Mon. Wea. Rev., 129, 569–585.

Hansen, J., G. Russell, D. Rind, P. Stone, A. Lacis, S. Lebedeff, R. Ruedy and L.Travis, 1983: Efficient Three-Dimensional Global Models for Climate Studies: Models I and II. Monthly Weather Review, 111, 609 – 662.

Liang, X. and M. Losch, On the Effects of Increased Vertical Mixing on the Arctic Ocean and Sea Ice. Journal of Geophysical Research: Oceans, 2018. 123(12): p. 9266-9282.

Liang, X., et al., Using Sea Surface Temperature Observations to Constrain Upper Ocean Properties in an Arctic Sea Ice-Ocean Data Assimilation System. Journal of Geophysical Research: Oceans, 2019. 124(7): p. 4727-4743.

Liang, X., et al., Evaluation of ArcIOPS sea ice forecasting products during the ninth CHINARE-Arctic in summer 2018. Adv. Polar. Sci., 2020, 31(1), 14-25.

Sun, R., Subramanian, A. C., Miller, A. J., Mazloff, M. R., Hoteit, I., and Cornuelle, B. D.: SKRIPS v1.0: a regional coupled ocean–atmosphere modeling framework (MITgcm–WRF) using SMF/NUOPC, description and preliminary results for the Red Sea, Geosci.

Model Dev., 12, 4221-4244, 10.5194/gmd-12-4221-2019, 2019

Mu, L., et al., Arctic Ice Ocean Prediction System: evaluating sea-ice forecasts during Xuelong's first trans-Arctic Passage in summer 2017. Journal of Glaciology, 2019. 65(253): p. 813-821.

Winton, M, 2000: A reformulated Three-layer Sea Ice Model. Journal of Atmospheric and Ocean Technology, 17, 525 – 531.

A fully coupled Arctic sea ice-ocean-atmosphere model (ArcIOAM v1.0) based on C-Coupler2: model description and preliminary results

Shihe Ren[1], Xi Liang[1], Qizhen Sun[1], Hao Yu[2], L. Bruno Tremblay[3], Bo Lin[1], Xiaoping Mai[1], Fu Zhao[1], Ming Li[1], Na Liu[1], Zhikun Chen[1], Yunfei Zhang[1]

[1]Key Laboratory of Research on Marine Hazards Forecasting, National Marine Environmental Forecasting Center, Ministry of Natural Resources, Beijing, China
[2]Ministry of Education Key Laboratory for Earth System Modelling, Department of Earth System Science, Tsinghua University, Beijing, China
[3]Department of Atmospheric and Oceanic Sciences, McGill University, Montreal, Canada

Correspondence to: Xi Liang (liangx@nmefc.cn)

Abstract. The implementation of a new Arctic regional coupled sea ice-ocean-atmosphere model (ArcIOAM) and its preliminary results in the year of 2012 are presented in this paper. In the ArcIOAM configuration, ~~A newly developed coupler, C-Coupler2 (the~~the Community Coupler 2 (C-Coupler2)~~,~~ is used to couple the Arctic sea ice-oceanic configuration of the MITgcm (Massachusetts Institute of Technology general circulation model) with the Arctic atmospheric configuration of the Polar WRF (Weather Research and Forecasting) model. A scalability test is performed to investigate the parallelization of the coupled model. As the first step toward reliable Arctic seasonal sea ice prediction, t~~ArcIOAM is demonstrated with focus on seasonal simulation of the Arctic sea ice and ocean state in the year of 2012. T~~he simulation results in the year of 2012 of~~btained by~~ the ArcIOAM implemented with two-way coupling strategy, along with ~~with the experiment of~~ one-way coupling strategy~~ and stand-alone oceanic simulations~~, are ~~compare~~evaluated with respect to available observational data and reanalysis products. Besides, the standalone MITgcm run with prescribed atmospheric forcing is performed for references. From the comparison, ~~results obtained from two these~~all the experiments simulate ~~both realistically capture the~~rational evolution of sea ice and ocean states~~ic variables~~ in the Arctic region over a one~~1~~-year simulation period. The two-way couplinged strategy ~~model~~ has better performance in terms of sea ice extent, concentration, thickness and SST, especially in summer. This result indicates that sea ice-ocean-atmosphere interaction takes a crucial role in controlling Arctic summertime sea ice distribution. The coupled model and documentation are available at https://doi.org/10.5281/zenodo.3742692 (last access: 9 June 2020), and the source code is maintained at https://github.com/cdmpbp123/Coupled_Atm_Ice_Oce (last access: 7 April 2020).

1 Introduction

It has been widely recognized that coupling between different earth system components (ocean, atmosphere, sea ice, and land) could provide improved forecasts of oceanic and atmospheric states on various timescales (Neelin et al., 1994). As an essential component in climate system, sea ice plays a crucial role in global energy and water budget, and has a substantial impact on local and remote atmospheric and oceanic circulations. In polar region, strong interactions between different interfaces disturb sea ice motion and affect sea ice growth-melt process (Jung et al., 2016). Due to the combined features of solid and fluid, sea ice thermodynamical and dynamical representations in coupled models ~~can be~~are complicated. In recent years, marine traffic through the Arctic marginal seas are projected to become increasingly feasible as climate change continues, which has amplified the demand for reliable polar sea ice and marine environmental predictions from synoptic timescale to seasonal and interannual timescales.

In the past decades, a number of coupled models have been developed with various sea ice prediction capacities on various time-scales (Pellerin et al., 2004;Williams et al., 2018;Chen et al., 2010;Skachko et al., 2019). For climate model, the current generation of global climate models (GCMs) comprising phase 5 of the Coupled Model Intercomparison Project (CMIP5) show ~~large~~some biases in sea ice extent and thickness (Stroeve et al., 2012;Shu et al., 2015). ~~Climate models, such as those involved in the Coupled Model Intercomparison Project Phase 5 (CMIP5), normally incorporate sea ice model in a relatively simple way, thus can be used to generate long-term sea ice outlook with low confidence on spatial distribution.~~ Recently within the GODAE (Global Ocean Data Assimilation Experiment) Oceanview community, there is an increasing interest of using coupled global models to predict sea ice on shorter time-scales (Brassington et al., 2015). In Canada, a coupled global forecasting system is now operationally running ~~operationally~~ at the Canadian Centre for Meteorological and Environmental Prediction (Smith et al., 2018), providing global 10 days forecasts of ocean and sea ice states. The ocean-sea ice component~~s~~ of this system, namely the Global Ice-Ocean Prediction System (GIOPS, runs in real time since March 2014) (Smith et al., 2016), are based on the Nucleus for European Modelling of the Ocean (NEMO) and the Community Ice CodE (CICE) model. The GIOPS is coupled to an operational global deterministic medium-range weather forecasting system, namely the Global Deterministic Prediction System (GDPS) (Smith et al., 2014), which is based on the Global Environmental Multiscale (GEM) atmosphere model. In the United Kingdom, Hadley Centre Global Environment Model version 3 (HadGEM3) is under development and is planning to service in seasonal sea ice prediction (Williams et al., 2018). The HadGEM3 is constitute of the UK Met Office Unified Model (UKMO UM) atmosphere model (Walters et al., 2011), the Joint UK Land Environment Simulator land-surface model (Brown et al., 2012), the NEMO model and the CICE model. In the United States, a coupled global sea ice-ocean-wave-land-atmosphere prediction system providing operational daily predictions out to 10 days and weekly predictions out to 30 days is being developed by the US Navy (Brassington et al., 2015;Posey et al., 2015).

Although global coupled models are now being implemented with increased horizontal resolution, higher-resolution regional coupled models can provide an affordable way to study interactive ocean-atmosphere and sea ice-atmosphere feedback~~s~~ for polar weather and sea ice process~~es~~, if properly forced by initial and boundary conditions. On the regional scale, there are

also a few coupled sea ice-ocean-atmosphere model systems for the Arctic climate studies and operational sea ice forecasts. The Arctic Region Climate System Model (ARCSyM) was developed to simulate coupled interactions among the atmosphere, sea ice, ocean, and land surface of the western Arctic (Lynch et al., 1995;Rinke et al., 2000). Schrum et al. (2003) introduced a coupled sea ice-ocean-atmosphere model for the North and Baltic Seas. In their work, the regional atmospheric model REgional MOdel (REMO) was coupled to the HAMburg Shelf Ocean Model (HAMSOM) with a sea ice module. Pellerin et al. (2004) demonstrated that significant sea ice forecasting improvements occurred when implemented the two-way coupling between the Gulf of St. Lawrence model with the GEM atmosphere model. The Regional Arctic System Model (RASM) is a fully coupled, regional Earth system model covering the pan-Arctic domain (Maslowski et al., 2012;Cassano et al., 2017). The component models of RASM include the Weather Research and Forecasting (WRF) atmospheric model, the Variable Infiltration Capacity (VIC) land and hydrology model, and regionally configured versions of the ocean and sea ice models used in the Community Earth System Model (CESM): the CICE model and Parallel Ocean Program (POP). Van Pham et al. (2014) compared basin-scale climate simulation in the regional coupled model COSMO-CLM-NEMO with that in the stand-alone COSMO-CLM model for the North and Baltic Seas, and found large improvement in the simulated atmospheric low boundary temperature. As part of the Canadian Operational Network of Coupled Environmental PredicTion Systems (CONCEPTS), a fully coupled sea ice-ocean-atmosphere forecasting system for the Gulf of St. Lawrence has been developed (Faucher et al., 2009) and running operationally at the Canadian Meteorological Centre since June 2011. The new model developing plan is to couple a high-resolution (1/12 degree) sea ice-ocean regional model which covering the North Atlantic and Arctic Ocean (Dupont et al., 2015) to the regional weather and wave prediction system and wave prediction system of Environment Canada and provides short-term sea ice and ocean predictions to users. Since regional models can be run at higher resolution than global models, regional models can explicitly represent mesoscale features that may not be resolved in global models. Another potential advantage of regional systems is that lateral boundary conditions can be controlled to get an optimal model input (Cassano et al., 2017).

Aiming at operational seasonal sea ice prediction in the National Marine Environmental Forecasting Center (NMEFC) of China, the This work is motivated by the need of a coupled The motivation of this work is to couple the Arctic ocean-seaice configuration of the MITgcm which is operationallyestablish a fully coupled Arctic sea ice-ocean-atmosphere model with an capacity of reasonable sea ice simulation on seasonal timescale. running in the National Marine Environmental Forecasting Center of China (ArcIOPS;(Liang et al., 2020), to the Arctic atmospheric model in order to get a reasonable seasonal sea ice prediction.Arctic sea ice-ocean-atmosphere model system for seasonal sea ice prediction in National Marine Environmental Forecasting Center of China. In coupled model systems, moisture, heat and momentum are often accomplished through the use of a separate coupling software like OASIS-MCT (Craig et al., 2017) or framework like the Earth System Model Framework (ESMF) (DeLuca et al., 2012) which links component models flexibly and controls the exchange and interpolation of coupling variables. The coupler, which can handle data interpolation and data transfer between different models and different grids, is the crucial part in the coupled systems. Using the ESMF and the National United Operational Prediction Capability (NUOPC), Sun et al. (2019) introduced a regional ocean-atmosphere coupled model covering the Red

Sea based on the ~~Massachusetts Institute of Technology general circulation model (~~MITgcm~~)~~ (Marshall et al., 1997) and the ~~Weather Research and Forecasting (~~WRF~~)~~ model (Skamarock et al., 2008).

In our study, we use a newly developed efficient coupling framework, the Community Coupler 2 (C-Coupler~~-~~2) (Liu et al., 2018), to couple the Arctic sea ice-oceanic configuration of the MITgcm (Nguyen et al., 2011;Liang and Losch, 2018) with the Arctic atmospheric configuration of the Polar WRF model (Hines and Bromwich, 2008) model. By coupling the Polar WRF and the MITgcm for the first time in Arctic region, ~~to this end, a~~ series of specific procedures including data interpolation between different grids and relaxation algorithm in ~~specific areas~~lateral boundaries are ~~developed~~designed. After implementing the ArcIOAM, we ~~run perform a seasonal simulation of Arctic sea ice and ocean state~~evaluate the model performance in the year of 2012 against available observational data. This year is selected because of the historical sea ice extent minimum record in the satellite era. ~~The simulated variables of the Arctic ocean and sea ice are examined and validated against available observational data and reanalysis products.~~ To evaluate the role of sea ice-ocean-atmosphere interaction ~~in of~~in Arctic sea ice seasonal cycle, we compare the simulation result of the two-way coupling experiment with that of the one-way coupling experiment in which the coupling variables are only transmitted from the Polar WRF to the MITgcm. Besides, a stand-alone MITgcm simulation with prescribed atmospheric forcing is performed for references.

The paper is organized as follows. The description of the component models and coupling strategy are detailed in Section 2. In section 3, a scalability test of the coupled model is performed to investigate its parallel capability. Section ~~3~~ 4 introduces the design of coupling experiments. Section ~~4~~ 5 discusses the preliminary results in the validation test. The last section concludes the paper and presents an outlook for future work.

2 Model Description

2.1 The Oceanic and Sea Ice Component Model

The ocean and sea ice component of ArcIOAM is an Arctic configuration of the MITgcm (Nguyen et al., 2011;Liang and Losch, 2018;Liang et al., 2019;Liang et al., 2020). The model has an average horizontal resolution of 18 km and covers the whole Arctic Ocean with open boundaries close to 55 °N in both the Atlantic and Pacific sectors (Losch et al., 2010). The ocean model includes 420x384 horizontal grid points and 50 vertical model layers based on Arakawa C grid and Z coordinates. The ocean model uses curvilinear coordinates and the model grid is locally orthogonal. Vertical resolution of the ocean model layers increases from 10 m near the surface to 456 m near the bottom. The K-profile parameterization (KPP) (Large et al., 1994) is used as the vertical mixing scheme. Time step is 1200 seconds.

The sea ice model shares the same horizontal grid with the ocean model and divides each model grid into two parts: ice and open ocean. In the open ocean area, ocean-atmosphere heat and momentum fluxes are calculated following the standard bulk formula (Doney et al., 1998). In the ice-covered area, the ice surface and bottom heat and momentum fluxes are calculated according to viscous-plastic dynamics and zero-layer thermodynamics (Hibler, 1980;Semtner, 1976). The so-called zero-layer thermodynamic model assumes one-layer ice underneath one-layer snow and ice does not store heat, therefore tends to

exaggerate the seasonal variability in ice thickness. Snow modifies ice surface albedo and conductivity. If enough snow accumulates on top of the ice, its weight submerges the ice and the snow is flooded. In order to parameterize a sub-grid scale distribution for sea ice thickness, the mean sea ice thickness in each grid can be split into as many as 7 thickness categories in the MITgcm sea ice model. In our coupled model for simplicity, we use 2 thickness categories: open water and sea ice.

2.2 The Atmospheric Component Model

The atmospheric component of ArcIOAM is based on ~~the~~an Arctic configuration of the Polar WRF (Bromwich et al., 2013;Hines and Bromwich, 2008) model, which is an optimized version of the WRF model (Skamarock et al., 2008) for use in polar region. The Polar WRF is developed and maintained by the Polar Meteorology Group at the Byrd Polar and Climate Research Center of the Ohio State University. In the Arctic configuration of the Polar WRF model, modifications for polar environments primarily encompass the land surface model and sea ice to adapt to the particular conditions in Arctic Regions. The Noah land surface model is embedded inside the Polar WRF. The changes made in the Noah land surface model (LSM;(Chen and Dudhia, 2001)) include using the latent heat of sublimation for calculating latent heat flux over ice surface, increasing the snow albedo and the emissivity value for snow, adjusting snow density, modifying thermal diffusivity and snow heat capacity for the subsurface layer, changing the calculation of skin temperature, and assuming ice saturation in calculating the surface saturation mixing ratio over ice. ~~Two key~~Other modifications for the Polar WRF ~~are optimization of surface energy balance and heat transfer for the Noah land surface model over sea ice and permanent ice surfaces, and~~include a fix to allow specified sea ice quantities and the land mask associated with sea ice to update during a simulation. These modifications improve model performance over the pan-Arctic for short-term forecasts.

The Arctic configuration of the Polar WRF model has been tested and evaluated by a set of simulations over several key surface categories, including large permanent ice sheets with the Greenland/North Atlantic grid and Arctic land (Hines et al., 2011;Hines and Bromwich, 2008) and the production of the Arctic System Reanalysis (ASR) (Bromwich et al., 2010). In this study, the Polar WRF model covers the Arctic regions with a horizontal resolution of 27 km. The model has 306x306 horizontal grid points and 60 vertical layers. The prognostic equations in the Polar WRF model are solved with a time step of 120 seconds. The Polar WRF model employed physics options that included the Mellor Yamada-Janjic boundary layer scheme in conjunction with the Janjic-Eta Monin Obukhov surface layer scheme (Janjić, 2002), the WRF single-moment 6-class microphysics scheme for microphysics, the Grell-Devenyi scheme for clouds (Grell and Dévényi, 2002), and the new version of the rapid radiative transfer model for both shortwave and longwave radiation.

2.3 The Coupler ~~Component Model~~

We ~~use~~ have implemented the C-Coupler~~-~~2 to couple the MITgcm and the Polar WRF model. The C-Coupler family was initiated from 2010 in China. The first version (C-Coupler1) includes features such as flexible coupling configuration and 3-D coupling capability (Liu et al., 2014). Two coupled models have been built using the C-Coupler1. The first is a coupled climate system model version FGOALS-gc at the Institute of Atmospheric Physics, Chinese Academy of Sciences. The

FGOALS-gc can achieve exactly the same (bitwise identical) simulation results as same model components with different coupler the CPL6 (Liu et al., 2014). The second is a regional coupled model FIO-AOW (Zhao et al., 2017) which includes an atmosphere model WRF, an ocean model POM (Princeton Ocean Model) , and a wave model MASNUM (Yang et al., 2005). The second version of the C-Coupler family, the C-Coupler-2 (Liu et al., 2018), is equipped with many advanced functions, including 1) a common, flexible, user-friendly coupling configuration interface, 2) the capability of coupling within one executable or the same subset of Message Passing Interface (MPI) processes, 3) flexible and automatic coupling procedure generation for any subset of component models, 4) dynamic 3-D coupling that enables convenient coupling of field on 3-D grids with time-evolving vertical coordinate values, 5) non-blocking data transfer, 6) facilitation for model nesting, 7) facilitation for increment coupling and 8) adaptive restart capability (Liu et al., 2018).

2.4 Coupling Strategy

The C-Coupler2 is employed as a library to achieve the two-way parallel coupling between the Polar WRF and the MITgcm (Figure 1~~Figure 1~~). The coupling interval is set to 20 minutes. At each coupling time step, the MITgcm is executed when the Polar WRF model is completed and vice versa. During coupling execution, the MITgcm sends SST, sea ice concentration, sea ice thickness, snow depth and ice surface albedo to the coupler, and these coupling variables are used directly as the bottom boundary conditions in the Polar WRF model. The Polar WRF model sends the atmospheric bottom boundary variables to the coupler, including downward longwave radiation, downward shortwave radiation, 10-m wind speed, 2-m air temperature, 2-m air specific humidity, and precipitation. The MITgcm uses these atmospheric variables to compute the open ocean and ice surface heat, freshwater and momentum forcing.

Model domain of the MITgcm and the Polar WRF model are shown in Figure 2~~Figure 2~~a. As the model domain and grid of the Polar WRF and the MITgcm are generally different, several important procedures have been carried out in conducting our coupled system.~~:~~

~~1)~~ The model domain of the Polar WRF is larger than that of the MITgcm, ~~there~~ producing ~~is~~ a non-overlapped area between the MITgcm domain and the Polar WRF domain. Besides, the MITgcm model only produces surface variables over ocean, and the Polar WRF model also needs bottom boundary conditions over land. Thus, the coupling variables received by the Polar WRF model need to be concatenated by value in the non-overlapped area and in the land area from an external forcing file, and value in the overlapped ocean area from the MITgcm model together. To diminish the abrupt value changes from two sources, a simple linear relax zone is designed near the open boundaries of the MITgcm model in both the Atlantic and Pacific sectors (Figure 2~~Figure 2~~b). The coupling variables ($VAR_{recbyWRF}$) received by the Polar WRF model can be expressed as:

$$VAR_{recbyWRF} = (1-\alpha)VAR_{sedbyMIT} + \alpha VAR_{extern} \quad (1)$$

where α is relaxation coefficient, which is equal to 0 in the overlapped ocean area away from the MITgcm open boundaries, and equal to 1 in the land area and in the non-overlapped area away from the MITgcm open boundaries. While in the relax

zone, α increases from 0 to 1 linearly from the overlapped side to the non-overlapped side. $VAR_{sedbyMIT}$ is the coupling variables which are send by the MITgcm model. VAR_{extern} is the bottom boundary variables of the Polar WRF model which are read from external forcing file.

Normally in coupled models the coupler controls the exchange of heat and momentum fluxes among component models. In our model configuration, instead of coupling fluxes directly, we use the C-Coupler2 to control the exchange of fields between the Polar WRF and the MITgcm. Heat and momentum fluxes are calculated separately in each component model. Both the Polar WRF and the MITgcm use the same Bulk Formula and almost same parameters in calculating fluxes, which guarantees the quasi-conservation of heat and momentum transmission between the component models. The bilinear interpolation algorithm is involved in the transmission of model variables between the horizontal grid of the Polar WRF and that of the MITgcm. Figure 3 shows wind stress curl derived from the Polar WRF output and the MITgcm output, as well as their difference on March 1, 2012. It can be seen that the Polar WRF and MITgcm model generate similar wind stress curl pattern, and the difference due to interpolation algorithm and momentum calculation accounts for less than 5% of the wind stress curl (Figure 3c).

3 Scalability test

In this section, the parallel efficiency of the ArcIOAM is investigated. Different numbers of CPU cores are used to evaluate the parallel speed-up of the coupled model. The CPU elapsed time spent on coupling interface of each component model in the coupled runs are detailed. Additionally, the parallel efficiency of each component model in the stand-alone runs are calculated for references. The parallel efficiency tests are performed on the High performance computing cluster at NMEFC. The High performance computing cluster is a Lenovo Blade Server system composed of 240 dual-socket compute nodes based on 14-core Intel Haswell processors running at 2.4 GHz. Each node has 128GB DDR4 memory running at 2133 MHz. Overall the system has a total of 6270 CPU cores (240 nodes x 2 x 14 CPU cores) and has a theoretical peak speed of 258 tetaflops. The parallel efficiency of the scalability test is $N_{p0}\ t_{p0}/\ N_{pn}\ t_{pn}$, where N_{p0} and N_{pn} are the number of CPUs employed in the base case and the test case, respectively; t_{p0} and t_{pn} represent the CPU elapsed time in the base case and the test case. The speed-up is defined as t_{p0} / t_{pn}, which is the relative improvement of the CPU time. The scalability tests are performed by integrating 7 model days for the stand-alone Polar WRF, the stand-alone MITgcm and the coupled runs.

In the ArcIOAM runs, the requested CPUs are assigned equally to the component models. The minimum CPUs we use is 28, i. e. N_{p0} = 28. Limited by computational resource, the maximum CPUs we can use is 896. The total CPU elapsed time in the coupled runs decreases from 12840 s to 1380 s when the requested CPUs increases from 28 to 896 (Table 1). When the requested CPUs are not larger than 448, the CPU elapsed time used for numerical integration by the MITgcm is substantially smaller than that for numerical integration by the WRF, meaning that the efficiency of the coupled model depends on the WRF component model. When the requested CPUs are larger than 448, the efficiency of the coupled model depends on the MITgcm component model.

The parallel efficiency of the coupled model remains more than 90% when employing less than 112 cores and is still as high as 80% when using 224 cores (Figure 4). The parallel efficiency of the stand-alone MITgcm is near to that of the stand-alone Polar WRF when the requested CPUs are less than 448, while both of them are substantially lower than the coupled model. The parallel speed-up of the coupled model is higher than the stand-alone component model. The decrease in parallel efficiency results from the increase of communication time, load imbalance, and I/O (read and write) operation per CPU core (Christidis, 2015).

~~2) The MITgcm model uses curvilinear grid whose horizontal resolution is variable. The Polar WRF model uses polar stereographic grid whose horizontal resolution is constant. Because the Polar WRF domain covers the MITgcm domain, the coupling interpolation from the Polar WRF grid to the MITgcm grid is straightforward, but the coupling interpolation from the MITgcm grid to the Polar WRF grid creates irregularities if the detailed geographic information of the MITgcm model grid is not specified. Meanwhile the MITgcm model is based on Arakawa C grid, geographic information of each grid cell is given at the center of the grid cell and at the four centers of the four boundaries of the grid cell. To correctly handle data interpolation between the different grids, the C-Coupler2 automatically calculates geographic information at the four corners of each grid cell (Figure 3) during the coupling initialization process. Take the left bottom corner (v1) of grid cell (i, j) as an example, the longitude (xv1) and latitude (yv1) are calculated as follows:~~

~~$$x_{v1} = \frac{x_{point(i-1,j)} + x_{point(i,j)} + x_{point(i-1,j-1)} + x_{point(i,j-1)}}{4} \quad (2)$$~~

~~$$y_{v1} = \frac{y_{point(i-1,j)} + y_{point(i,j)} + y_{point(i-1,j-1)} + y_{point(i,j-1)}}{4} \quad (3)$$~~

~~where the subscripts *point(i-1, j), point(i, j), point(i-1, j-1) and point(i, j-1)* denote the four centers of the four grid cells around the corner. In the following model execution or model restarting process, the C-Coupler2 uses the corner geographic information of the MITgcm grid to constrain interpolation domain from the MITgcm model to the Polar WRF model.~~

43 Numerical Experiments

The Arc~~tic coupled model~~IOAM will be used to conduct seasonal sea ice prediction in our future plan. As a starting point, we need to evaluate ~~the Arctic coupled model~~its performance on seasonal timescale ~~without any data assimilation~~. In this work, we perform the coupled model ~~free~~ simulations in the year of 2012 ~~with special focuses on the summertime~~. The year of 2012 is chosen because an unusually strong storm formed off the coast of Alaska on 5 August 2012, and tracked into the center of the Arctic Basin where it lingered for several days and generated stronger sea ice-ocean-atmosphere interaction (Simmonds and Rudeva, 2012). With more open ocean area be exposed to atmosphere, we expect that sea ice-ocean-atmosphere interaction processes are relatively more intensified in the summertime than that in the wintertime. In the Arctic region, demands of seasonal prediction for sea ice and ocean are also strong in summertime when more commercial and scientific activities of Arctic shipping occur. ~~Additionally, the year of 2012 is chosen because an unusually strong storm~~

formed off the coast of Alaska on 5 August 2012, and tracked into the center of the Arctic Basin where it lingered for several days and generated stronger sea ice ocean atmosphere interaction (Simmonds and Rudeva, 2012). The main aim of this paper is to assess the sea ice and ocean simulation capabilities of the coupled system. For this reason, less attention will be paid on the atmosphere simulation. Future work will emphasize atmospheric simulation variables and seasonal sea ice prediction skill with available observations be assimilated.

Two Three experiments using different coupling strategy are performed in this study. The first experiment which denoted by OCNCPL is a two-way coupled simulation that the MITgcm receives the coupled variables from the Polar WRF, and the Polar WRF also receives the coupled variables from the MITgcm. The second experiment which denoted by OCNDYN is a one-way coupled simulation that the MITgcm only receives the coupled variables from the Polar WRF, but without sending the coupled variables back to the Polar WRF. α in Equ. 1 is set to 1 in the OCNDYN run. The third experiment of OCNSTA represents the stand-alone MITgcm simulation with the same sea ice albedo parameters to the coupled model but prescribed atmospheric forcing to keep consistency with previous two coupling experiments. The model state deviation between the two runsthese cases represents the influences of sea ice-ocean-atmosphere interaction on in the Arctic Ocean and sea ice.

The atmospheric specific initial and lateral boundary conditions, as well as bottom boundary conditions in the external forcing file used in the OCNCPL and OCNDYN runs, and the prescribed atmospheric forcing used in the OCNSTA run are derived from the 6-hourly National Centers for Environmental Prediction (NCEP) Climate Forecast System Reanalysis (CFSR) data (Saha et al., 2010). The oceanic monthly lateral boundary condition of the coupled model is derived from the Estimating the Circulation and Climate of the Ocean phase II (ECCO2): high-resolution global-ocean and sea ice data synthesis (Menemenlis et al., 2008), including potential temperature, salinity, current, and sea surface elevation. The discrepancy of atmosphere and ocean boundary condition is less of an issue since the ocean does not vary much on shorter time scale and the zones of the sea ice areis far away from the lateral boundary. The ocean and sea ice initial condition of ocean and sea ice on 1 January 2012 are derived from a stand-alone MITgcm simulation. The stand-alone MITgcm simulation was initialized from climatological temperature and salinity field derived from the World Ocean Atlas 2005 (WOA05) (Locarnini et al., 2006;Antonov et al., 2006) and forced by the 3-hourly Japanese 55-year Reanalysis data (JRA55) (Harada et al., 2016;Kobayashi et al., 2015) from 1979 to 2011 in our previous study (Liang and Losch, 2018). After 33-year integration, the ocean and sea ice initial condition on 1 January 2012 used in the coupled model are retrieved from a quasi-equilibrium ocean-sea ice evolution period. River runoff is based on the Arctic Runoff Data Base (Nguyen et al., 2011). The coupled model states are outputted on daily basis and used in our analysis.

54 Preliminary Results

54.1 Sea Ice Extent and Concentration

The lowest Arctic sea ice extent minimum value appeared reached lowest in the summer of 2012 infromin the satellite observationeraed era occurred in the summer of 2012 (Francis, 2013). According to sea ice extent record derived from the

Multisensor Analyzed Sea Ice Extent-North Hemisphere (MASIE-NH) (NSIDC, 2010),~~, obtained from http://nsidc.org/data/masie/, in the year of 2012~~ Arctic sea ice extent grows to maximum value of 14.5 million km^2 in March and drops to minimum value of 3.5 million km^2 in September (Figure 5~~Figure 4~~a) ~~.~~in the year of 2012. The MASIE-NH data is provided daily by the National Ice Center Interactive Multisensor Snow and Ice Mapping System with a spatial resolution of 4 km. Compared with the OCNSTA run, results from the experiments with coupling (OCNCPL and OCNDYN) are closer to observations. It is noted that b~~B~~oth the OCNCPL and OCNDYN runs simulate lower sea ice extent than the observations by a bias of 1~~-2~~1.5 million km^2 (Figure 5~~Figure 4~~a) ~~except~~ after the first half month of January. Because sea ice initial field on 1 January 2012 is derived from a stand-alone MITgcm simulation which is forced by the JRA55 data, the change of atmospheric forcing data from the JRA55 to the NCEP CFSR induces a model state adjustment period which lasts about half month. By c~~C~~omparing the sea ice extent evolution of the OCNCPL and OCNDYN run, it seems that sea ice-ocean-atmosphere interaction generates ~~quite~~ slight sea ice extent change, but based on our following analysis related to sea ice spatial distribution, sea ice-ocean-atmosphere interaction plays a decisive role in summertime sea ice spatial distribution.

Figure 5~~Figure 45~~b shows the modeled and observed sea ice extent anomaly. After the model state adjustment period, both the amplitudes and phase of sea ice extent seasonal cycle ~~of~~in the ~~the two runs~~OCNCPL and OCNDYN runs are close to the observations. While results of stand-alone run shows lag~~melting~~ of sea ice ~~lag~~melts and freezes in advance compared with the observations. ~~The sea ice extent bias between the model states and the observations likely arise from the sea ice model systematic bias which is induced by the choice of sea ice and snow albedo parameters in the two runs.~~ Nguyen et al. (2011) pointed out that optimized parameters of sea ice and snow albedo depend on selected atmospheric forcing in the MITgcm. In the sea ice model of MITgcm~~ sea ice model~~, the actual surface albedo changes with time and is a function of four foundational albedo parameters (dry ice, dry snow, wet ice, wet snow), as well as ice surface temperature and snow depth. A series of sensitivitiy experiments are performed to get an optimal combination of sea ice parameters (figures not shown). The sea ice model systematic bias could also be reduced by ~~rationally amplifying albedo parameters or~~ involving ~~a~~ sea ice data assimilation module (Liang et al., 2019) when conducting seasonal sea ice prediction system.

~~We compare the~~ The modeled sea ice concentration is compared with the observations derived from the EUMETSAT Ocean and Sea Ice Satellite Application Facility (OSISAF) (Eastwood et al., 2011).~~; obtained from http://osisaf.met.no/; product identifier: OSI-409.~~ The observations are reprocessed daily sea ice concentration fields which are retrieved from the Scanning Multichannel Microwave Radiometer/Special Sensor Microwave Imager (SMMR/SSMI) data with a spatial resolution of 10 km. Figure 5~~Figure 45~~c shows the root mean square error (RMSE) evolution of the modeled sea ice concentration with respect to the OSISAF data. After 1 month of model state adjustment, three experiments shows similar patterns that RMSE is lower in winter and spring than in summer and autumn~~, because t~~. T~~T~~he Arctic basin is almost fully covered by sea ice from ~~January~~ November to May (Figure 6)~~., thus theT~~, thus the two coupling experiments do not produce substantial sea ice concentration differences. Along with more open ocean are exposed to atmosphere, from June to September the sea ice concentration RMSE of the OCNCPL run is significantly lower than that of the OCNDYN run. This

result indicates that sea ice-ocean-atmosphere interaction takes a crucial role in controlling Arctic summertime sea ice distribution.

To further clarify sea ice concentration spatial distribution, we show the modeled and observed monthly mean sea ice concentration (Figure 6) and deviation of model results and observation (Figure **7**) in ~~July~~March, June, September~~August~~ and December~~September~~ ~~(Figure 5 and Figure 6).~~ In March when ~~sea ice~~the Arctic Ocean~~e~~ is almost fully covered by sea ice, the main source of discrepancy appears in sea ice edge zones in the Atlantic side (Figure 6~~7~~a-~~d~~c). ~~Boreal summer is a transition season for sea ice melting. Sea ice begins to melt from the result of OSISAF (Figure 5h).~~In June, s~~S~~ea ice concentrations are overestimated in the Arctic marginal seas in the OCNCPL and OCNDYN runs (Figure **7**d-e)~~, which is in consistency with Figure 4c~~. The modeled sea ice concentration in the OCNSTA run is more closer to the observations (Figure 7f). In September, the modeled sea ice in the marginal sea ice zone melts out in all runs (Figure 6i-k). ~~Sea ice melts quickly in the Eurasian marginal seas in the two runs.~~ Compared with the satellite observations (Figure 6l), sea ice in the OCNSTA run overmelts in summertime which leads to an anomalous negative bias of sea ice concentration in the Arctic (Figure **7**i), the two coupled runs overestimate sea ice concentration in the southern Beaufort Sea while underestimates sea ice concentration in the center Arctic basin (Figure **7**g-h). Although the two coupled runs simulate similar sea ice extent patterns, due to rational representation of sea ice-ocean-atmosphere interaction in the OCNCPL run, the modeled sea ice distribution of the OCNCPL run is closer to the observations (Figure 6i and Figure 6l). In December, the situation is similar with that in March when sea ice dominates almost entire Arctic region.

~~In July, the modeled sea ice extent of the OCNCPL run is similar to that of the OCNDYN run, but the modeled sea ice concentration of the OCNCPL run is much lower than that of the OCNDYN run in thick multiyear ice zone near the Canadian Arctic Archipelago and in the southern Beaufort Sea (Figure 5a and Figure 5b). The satellite observations show that the OCNCPL run still overestimates sea ice concentration in the southern Beaufort Sea and the Laptev Sea (Figure 5c). In August, the modeled sea ice melts quickly in the Eurasian marginal seas in the two runs. Compared with the satellite observations (Figure 5f), the OCNDYN run overestimates sea ice concentration in the southern Beaufort Sea while underestimates sea ice concentration in the center Arctic basin (Figure 5e). The OCNCPL run simulates similar sea ice extent to the satellite observations but with lower concentration in the center Arctic basin (Figure 5d). In September, the modeled sea ice in the marginal sea ice zone melts out in the two runs. Although the two runs simulate almost same sea ice extent, due to rational representation of sea ice-ocean-atmosphere interaction in the OCNCPL run, the modeled sea ice distribution of the OCNCPL run is closer to the observations (Figure 5g and Figure 5i).~~

5~~4~~.2 Sea Ice Volume and Thickness

At current stage, satellite sea ice thickness data is not available in melting seasons from May to September. We compare the modeled sea ice volume with that from a widely used sea ice volume data source (Figure 8~~Figure 6~~a), the Pan-Arctic Ice Ocean Modeling and Assimilation System (PIOMAS) developed at the Applied Physics Laboratory of the University of Washington (Zhang and Rothrock, 2003). The PIOMAS assimilates sea ice concentration data from the National Snow and

Ice Data Center (NSIDC) and SST data from NCEP/NCAR Reanalysis. The OCNSTA run simulates more rational sea ice growth rate from January to May but systematic negative sea ice volume bias compared with the PIOMAS data. The sea ice volume in the OCNCPL and OCNDYN runs shows better results than that in the OCNSTA run from June to December. However, b~~B~~oth the two coupled runs produce less sea ice volume than the PIOMAS data ~~almost in~~in most time ~~a whole year~~ of 2012, partly resulting from that our model underestimates sea ice extent (Figure 5~~Figure 4~~a) without assimilating any observation. ~~However, i~~It is notable that the sea ice volume evolution of the OCNCPL run is closer to the PIOMAS data at the end of 2012.

Satellite sea ice thickness observations are usually retrieved from either ice surface brightness temperature or radar altimetric measurement of sea ice freeboard. We use three kinds of satellite sea ice thickness data to validate our model results (Figure 8~~8Figure 6~~b and Figure 8~~8Figure 6~~c). Daily sea ice thickness observations provided by the University of Hamburg are derived from the Soil Moisture Ocean Salinity (SMOS) brightness temperature combined with a sea ice thermodynamic model and a three-layer radiative transfer model (Kaleschke et al., 2012) obtained from http://icdc.cen.uni-hamburg.de/1/daten/cryosphere/l3c-smos-sit.html. Weekly sea ice thickness observations provided by the Alfred Wegener Institute, Helmholtz Centre for Polar and Marine Research are derived from the European Space Agency satellite mission CryoSat-2 radar altimetric data (Ricker et al., 2014) obtained from http://data.meereisportal.de/data/cryosat2/version2.0/. The SMOS observations retrieved from satellite brightness temperature data have promised qualities in marginal sea ice zone where ice thickness is thinner than 1 m (Tian-Kunze et al., 2014) while the CryoSat-2 observations retrieved from radar altimetric data have higher accuracies in pack sea ice zone than in marginal sea ice zone (Laxon et al., 2013;Wingham et al., 2006). Taking the spatial complementarity of the SMOS and CryoSat-2 data into consideration, Ricker et al. (2017) introduced a weekly sea ice thickness product covering the entire Arctic, the CS2SMOS sea ice thickness, which is generated by ~~mathematically~~ merging the SMOS sea ice thickness with the CryoSat-2 sea ice thickness (Ricker et al., 2017) obtained from https://data.meereisportal.de/data/cs2smos/version1.4/. The CS2SMOS data with observational uncertainty is also added in the comparison.

The weekly CryoSat-2 data is constitute of several banded sea ice thickness records which collected in one week when polar orbital satellite passes the Arctic region. The SMOS data used in this study are those in thin ice (< 1 m) region. Considering spatial coverage of the observations, we compare spatial-mean sea ice thickness evolution with the CS2SMOS data (Figure 8~~8Figure 6~~b). Comparing with the CS2SMOS data, both coupled runs produce more rational sea ice thickness evolution than stand-alone run from January to April. However, large sea ice thickness errors between the model and the observations exist in October and November. We attribute these large errors to the possibly observational uncertainties induced by radar altimetric measurement errors when ice surface starts to freeze up. The modeled sea ice in the OCNCPL run is thinner than that in the OCNDYN run, and the sea ice thickness deviations between the two runs amplify after the summer. Meanwhile the sea ice volume and thickness of the OCNCPL run are closer to the PIOMAS data and the CS2SMOS observations at the end of 2012. Day et al. (2014) pointed out that sea ice behaves long-term memory of melting-freezing processes. Notz and Bitz (2017) indicated that summertime sea ice thickness has an important influence on sea ice state in the following spring

through the ice thickness-ice growth feedback. A negative anomaly of sea-ice area in late summer induces larger heat losses in autumn and winter from the ocean to the atmosphere due to enhanced outgoing long-wave radiation and turbulent heat fluxes, this causes thinner snow and ice due to later freeze-up and hence larger heat-conduction fluxes through sea ice, eventually leading to larger ice-growth rates. We speculate that in the OCNCPL run sea ice-ocean-atmosphere interaction induces reasonable sea ice thickness distribution in the summer of 2012 which preconditions the sea ice thickness evolution in the following freezing season.

The sea ice thickness RMSEs of the ~~two~~ three runs with respect to ~~the~~ mentioned three kinds of satellite sea ice thickness data are shown in Figure 8~~8Figure 6~~c. Compared with the coupled runs, the sea ice thickness in the OCNSTA run shows larger bias in pack ice zone while smaller bias in marginal ice zone. The sea ice thickness RMSE between the OCNCPL run and the SMOS data is smaller than that between the OCNDYN run and the SMOS data, indicating that sea ice-ocean-atmosphere interaction substantially improves the sea ice thickness simulation in the marginal sea ice zone in the coupled~~OCNCPL~~ runs. The sea ice thickness RMSEs between ~~model~~the coupled runs and the CryoSat-2 data are generally larger than those between the coupled runs~~model~~ and the CS2SMOS data especially in October and November, which is partly due to the large uncertainty of radar altimetric measurement when ice surface starts to freeze up, and partly due to the low spatial coverage of the CryoSat-2 data.

Normally satellite sea ice thickness data has large uncertainty due to limitation of retrieval algorithm. In situ sea ice thickness observations with higher accuracy can provide a direct reference for the model. To further evaluate the modeled sea ice thickness, we compare the time evolution of modeled and observed sea ice thickness at three locations in the Beaufort Sea in 2012 (Figure 9). The observations are derived from moored upward-looking sonar (ULS) ice draft data from the Beaufort Gyre Exploration Project (BGEP) (Proshutinsky et al., 2005)~~; obtained from http://www.whoi.edu/beaufortgyre/~~. The ULS samples the ice draft with a precision of 0.1 m (Melling and Riedel, 1995)~~-~~, and the ice draft can be converted to ice thickness following the law of hydrostatic equilibrium (Nguyen et al., 2011). Generally speaking, at all three locations in the Beaufort Sea, when the modeled sea ice is thinner than 1 m, the sea ice thickness evolution improves in the OCNCPL run comparing with those in the OCNDYN run. This result further demonstrates that sea ice-ocean-atmosphere interaction plays an important role in marginal sea ice evolution.

Spatial distributions of monthly mean sea ice thickness and its bias with respect to available CS2SMOS data in March, June, September, and December are shown in Figure 10 and Figure 11. In March and December, all three runs underestimate sea ice thickness in central Arctic, while overestimate sea ice thickness in marginal sea ice zone (Figure 11). In March ~~and June~~, ~~almost the whole Arctic basin is still covered by thick ice,~~ the OCNSTA run overestimates sea ice thickness in the Pacific sector of the Arctic Ocean and in the Baffin Bay (Figure 11e). The coupled runs overestimate sea ice thickness in the northern Barents Sea while underestimate sea ice thickness in the western Chukchi Sea (Figure 11a and Figure 11c).~~large sea ice thickness deviations between the two runs mainly appear around sea ice edge where sea ice-ocean-atmosphere interaction can impact significant influence on sea ice melting rate. (Figure 8c).~~ In December ~~September~~, compared with the OCNDYN run, the modeled sea ice thickness in marginal sea ice zone in the OCNCPL run is more closer to the CS2SMOS data (Figure

11b), partly due to the rational sea ice distribution at the beginning of freezing season, as summertime sea ice thickness has strong effect on preconditioning the following wintertime sea ice thickness (Day et al., 2014)~~, the modeled sea ice of the OCNCPL run is universally thinner than that of the OCNDYN run in December (Figure 9Figure 8i). Figure 10. shows sea ice thickness deviation between modeled results and CS2SMOS observation in March and December when data is available. In March and December, all three runs underestimate sea ice thickness in central Arctic, while overestimate sea ice thickness in area near the Greenland Island and in the southern Beaufort Sea.OCNCPL run perform best results in these three runs in general.~~

54.3 Ocean Temperature and Current

Sea ice states are intimately linked to ocean states, both dynamically and thermodynamically. The modeled spatial distribution of sea ice concentration in the OCNCPL run exhibits great improvement comparing with the OCNDYN run. Since sea ice in marginal ice zone is strongly affected by SST through lateral heat transport, we suspect that sea ice-ocean-atmosphere interaction should impose positive influence on the modeled ocean temperature in the marginal sea ice zone.

The modeled SST is validated against the Group for High-Resolution SST Multi-Product Ensemble (GMPE) data (obtained from http://marine.copernicus.eu/, product identifier: SST_GLO_SST_L4_NRT_OBSERVATIONS_010_005). The GMPE SST data provided by the UKMO is a reanalysis daily global SST product that computed as the median of a large number of SST products by various institutes around the world. Each product contributing to the GMPE product uses different observational data sets or different retrieval algorithms. As a median product of multiproduct ensemble, the GMPE SST data greatly reduces observational uncertainties. The SST RMSE of the ~~two~~ three runs with respect to the GMPE data ~~from July to September~~ are shown in Figure 12~~2Figure 9~~. ~~We do not show the time evolution of the SST RMSE in whole year because the two timeseries do not obviously diverge in the other months.~~ In general compared with the coupled runs, the SST RMSE in~~of~~ the OCN~~CPL~~STA run is smaller ~~than that of the OCNDYN run i~~in the summertime but larger in the rest ~~of 2012, which means the SST simulation also improves when sea ice-ocean-atmosphere interaction is allowed in the model. S~~. Spatial patterns of the modeled and observed SST in ~~July~~March, June,~~August~~ ~~and~~ September and December are shown in Figure 13~~3Figure 10~~. Deviation of the modeled SST and the GMPE SST observation is demonstrated in Figure 14. The GMPE SST data is available in ice-free areas (Figure 13~~3Figure 10~~d~~a~~, Figure 13~~3Figure 10~~h~~e~~, Figure 13l ~~-~~and Figure 13~~3Figure 10~~p~~i~~). In March and June, the OCNSTA run produces a warmer sea surface in the Nordic Seas, which explains the positive SST bias from January to June in Figure 12 compared with the coupled runs. ~~Comparing with the OCNDYN run, in July and August the modeled ocean surface of the OCNCPL run warms in Fram Strait, the Barents Sea, the Kara Sea and the Bering Strait while colds in the Baffin Bay, the Greenland Sea and the Laptev Sea (Figure 10d andFigure 10h).~~ In September the SST RMSE in the OCNCPL run (Figure 12) arises from the strong negative bias in the southern Beaufort Sea and the Baffin Bay (Figure 14g).

Ocean current observations in the Arctic Ocean are quite sparse, we evaluate the modeled ocean velocity and temperature with climatological observation generated from the 1998-2003 mooring data in Fram Strait. Under the framework of the

European Union projects Variability of Exchanges In the Northern Seas (VEINS) and Arctic Subarctic Ocean Fluxes - North (ASOF-N), a series of moorings in Fram Strait had been deployed to record ocean properties since September 1997 to 2004 (obtained from https://www.whoi.edu/page.do?pid=30914). The observation covers water column from 10 m above the seabed to about 50 m below the surface. Although the observations were conducted at least one decade earlier than 2012, we believe that the comparison between the modeled and observed monthly mean value would likely still make sense since the phase of the Atlantic Multidecadal Oscillation does not reverse between 1995 and 2012. The modeled and observed northward cross-section velocity and temperature averaged between 5°E and 8°40'E at 78°50'N are listed in~~-~~ Table 2~~Table 1~~. Basically, the observations show that the northward velocity of the West Spitsbergen Current (WSC) increases from July to September, and the mean temperature of the section of 78°50'N also increases from July to December. It is notable that the modeled velocity and temperature of the OCNCPL run in Fram Strait are closer to the observations comparing with those of the OCNDYN run, although there are still large biases of the modeled velocity between the OCNCPL run and the observations. Vertical temperature distribution in the section averaged between July and September shows that sea ice-ocean-atmosphere interaction induces warming of the WSC until 700 m depth accompanied with strong cooling beside the WSC (Figure 15~~Figure 11~~c). The cross-section velocity deviation between the OCNCPL and OCNDYN run is characterized by enhanced northward velocity over the whole water column around 0 °E and east of 6 °E, while reduced northward velocity between them (Figure 15~~Figure 11~~f).

6~~5~~ Conclusion and Discussion

This paper describes the implementation of an Arctic regional sea ice-ocean-atmosphere coupled model (ArcIOAM). To connect the component models, a newly developed coupler, C-Coupler2 is implemented to couple the Arctic sea ice-oceanic configuration of the MITgcm model with the Arctic atmospheric configuration of the Polar WRF model. By coupling the Polar WRF and the MITgcm for the first time in Arctic region, a series of specific procedures including data interpolation between different grids and relaxation algorithm in lateral boundaries are designed. T~~t~~he parallel efficiency of~~in~~ the coupled model~~simulations~~ is also investigated~~a series of specific setup including data interpolation between different grids and relaxation algorithm in specific areas are designed~~.

After implementing the~~ new coupled model of~~ ArcIOAM, we demonstrate it on seasonal simulation of the Arctic sea ice and ocean states in 2012. Results from the two-way coupl~~ed~~ing simulation (OCNCPL), ~~and~~ the one-way coupling~~ed~~ simulation (OCNDYN) and stand-alone oceanic simulation (OCNSTA) are compared to a wide variety of available observational and reanalysis products. The model state deviation between the two coupled experiments represents the influences of sea ice-ocean-atmosphere interaction on the Arctic Ocean and sea ice. From the comparison, results obtained from the two-way ~~two~~ coupling~~ed~~ experiment~~s both realistically~~ capture the sea ice and ocean~~ic~~ evolution~~variables~~ in the Arctic region over a 1-

year simulation period. The two-way coupled~~ed~~ing experiment gives ~~equal or~~ better results compared with the one-way coupled~~ed~~ing experiment and stand-alone oceanic simulation, especially in summertime.~~.~~

Both the amplitudes of sea ice extent seasonal cycle of the two coupled runs are close to the observations. The spatial distribution of sea ice concentration in the OCNCPL run is similar to that in the OCNDYN run from January to May. From June to September the sea ice concentration RMSE of the OCNCPL run with respect to the observations is significantly lower than that of the OCNDYN run, indicating that sea ice-ocean-atmosphere interaction takes a crucial role in controlling Arctic summertime sea ice distribution. The sea ice thickness RMSE of the OCNCPL run with respect to the SMOS data in thin ice areas is smaller than that of the OCNDYN run. Meanwhile, the evolution of the modeled and observed sea ice thickness at three locations in the Beaufort Sea show that the modeled sea ice thickness evolution improves in the OCNCPL run when the ice is thinner than 1m. This result means that sea ice-ocean-atmosphere interaction is very likely to improve the sea ice thickness simulation in the marginal sea ice zone when considering feedback of ocean to atmosphere. Based on comparison with a series of mooring data in Fram Strait, the modeled velocity and temperature in the OCNCPL run are closer to the observations than those in the OCNDYN run, although large biases of the modeled velocity still exist. Comparing with the satellite data, the SST obtained in the OCNCPL run is also better than that in the OCNDYN run in summer 2012. The two-way coupling between the Polar WRF and the MITgcm provides a more rational representation of real air-ice-ocean physical processes, which includes the important ice-albedo feedback in early summer. In the MITgcm, sea ice albedo is calculated based on several variables, such as snow depth on ice, ice surface temperature. In the OCNCPL run, albedo is a coupling variable which affects both the Polar WRF and the MITgcm. In the OCNDYN run, albedo used in the Polar WRF is directly read from the CFSR forcing data. Due to strong sea ice-ocean-atmosphere interaction in summertime, the two-way coupling strategy ~~.~~not only improves the sea ice simulation, but also benefit the modeled ocean states.

Land component is absolutely important to the Arctic simulation, however at current stage, our coupled model has not the capacity of coupling an individual land model, instead, we use the embedded land component in the Polar WRF for technical simplicity. It is noticed that the simulation presented in this paper only covers one year, more ~~seasonal scale simulations~~results ~~in~~ for different years should be carried out to further assess the coupled model. However, given the encouraging results in 2012, this new developed Arctic regional coupled model exhibits its potential capacity of seasonal sea ice prediction and provides a reliable basis for investigating both thermodynamic and dynamic process and forecasting applications in the Arctic sea ice scope. Meanwhile, bias in the modeled sea ice extent and summertime sea ice thickness still exist, although satellite sea thickness data normally has large uncertainty in summertime, which partly contributes to the large sea ice thickness bias in October-November between the model and CS2SMOS data (Figure 8~~8Figure 6~~b), the foundational sea ice albedo parameters in our current model configuration seem to be underestimated, which allows more heat into the ice and causes thinner sea ice thickness, as well as lower sea ice extent. The choice of sea ice albedo parameters also contributes to the large sea ice thickness bias in October-November between the model and CS2SMOS data. On the way to operational seasonal sea ice prediction, the model physics and model uncertainty representation in the coupled model can be enhanced using advanced techniques, such as stochastic physics parameterizations and ensemble approaches. The

regional coupled forecasting system also can be improved by involving data assimilation capabilities for initializing the forecasts. Future work will involve exploring these and other aspects for a regional coupled modeling system suited for forecasting and ~~process~~ better understanding of mechanism.

Code and data availability. The latest version and future updates of the source code, user guide, and examples can be downloaded from https://github.com/cdmpbp123/Coupled_Atm_Ice_Oce (last access: 7 April 2020). The current version of this coupled model (ArcIOAM v1.0) used to produce the results in this paper can be accessed via https://doi.org/10.5281/zenodo.3742692.

Author contribution. SR and HY worked on the coding tasks for coupling the Polar WRF with the MITgcm using C-Coupler2. SR and XL designed and performed the simulations for the numerical experiments. SR, HY and XM worked on the technical details for debugging the model and wrote the code documentation. XL worked on the MITgcm model setup and performed sea ice analysis and validation. QS worked on the Polar WRF model setup. BL worked on the scalability test. All authors contributed to the writing of the final article.

Competing interests. The authors declare that they have no conflict of interest.

Acknowledgments. This work is supported by the National Key R&D Program of China (2016YFC1402700, 2018YFC1407200) and the National Natural Science Foundation of China (41806003). The authors thank the University of Hamburg for providing the SMOS sea ice thickness data, the Alfred-Wegener-Institut, Helmholtz Zentrum für Polar- und Meeresforschung for providing the CryoSat-2, CS2SMOS sea ice thickness data and Fram Strait mooring data, the Norwegian Meteorological Institute for the OSISAF sea ice concentration data, the University of Washington for providing the PIOMAS sea ice volume data, the National Snow and Ice Data Center for providing the MASIE-NH data (http://nsidc.org/data/masie/), the Woods Hole Oceanographic Institution for providing the BGEP ULS data (http://www.whoi.edu/beaufortgyre), and the Copernicus Marine Environment Monitoring Service for providing the GMPE SST data (http://marine.copernicus.eu/).

References

Antonov, J. I., Locarnini, R., Boyer, T., Mishonov, A., Garcia, H., and Levitus, S.: World Ocean Atlas 2005 Volume 2: Salinity, NOAA Atlas NESDIS, 62, 2006.

Brassington, G. B., Martin, M. J., Tolman, H. L., Akella, S., Balmeseda, M., Chambers, C. R. S., Chassignet, E., Cummings, J. A., Drillet, Y., Jansen, P. A. E. M., Laloyaux, P., Lea, D., Mehra, A., Mirouze, I., Ritchie, H., Samson, G., Sandery, P. A., Smith, G. C., Suarez, M., and Todling, R.: Progress and challenges in short- to medium-range coupled prediction, Journal of Operational Oceanography, 8, s239-s258, 10.1080/1755876X.2015.1049875, 2015.

Bromwich, D., Kuo, Y.-H., Serreze, M., Walsh, J., Bai, L.-S., Barlage, M., Hines, K., and Slater, A.: Arctic System Reanalysis: Call for Community Involvement, Eos, Transactions American Geophysical Union, 91, 13-14, 10.1029/2010EO020001, 2010.

Bromwich, D. H., Otieno, F. O., Hines, K. M., Manning, K. W., and Shilo, E.: Comprehensive evaluation of polar weather research and forecasting model performance in the Antarctic, Journal of Geophysical Research: Atmospheres, 118, 274-292, 10.1029/2012JD018139, 2013.

Brown, A., Milton, S., Cullen, M., Golding, B., Mitchell, J., and Shelly, A.: Unified Modeling and Prediction of Weather and Climate: A 25-Year Journey, Bulletin of the American Meteorological Society, 93, 1865-1877, 10.1175/BAMS-D-12-00018.1, 2012.

Cassano, J. J., DuVivier, A., Roberts, A., Hughes, M., Seefeldt, M., Brunke, M., Craig, A., Fisel, B., Gutowski, W., Hamman, J., Higgins, M., Maslowski, W., Nijssen, B., Osinski, R., and Zeng, X.: Development of the Regional Arctic System Model (RASM): Near-Surface Atmospheric Climate Sensitivity, Journal of Climate, 30, 5729-5753, 10.1175/jcli-d-15-0775.1, 2017.

Chen, F., and Dudhia, J.: Coupling an Advanced Land Surface–Hydrology Model with the Penn State–NCAR MM5 Modeling System. Part I: Model Implementation and Sensitivity, Monthly Weather Review, 129, 569-585, 10.1175/1520-0493(2001)129<0569:caalsh>2.0.co;2, 2001.

Chen, S., Campbell, T. J., Jin, H., Gaberšek, S., Hodur, R. M., and Martin, P.: Effect of Two-Way Air–Sea Coupling in High and Low Wind Speed Regimes, Monthly Weather Review, 138, 3579-3602, 10.1175/2009mwr3119.1, 2010.

Christidis, Z.: Performance and Scaling of WRF on Three Different Parallel Supercomputers, High Performance Computing, Cham, 2015, 514-528,

Craig, A., Valcke, S., and Coquart, L.: Development and performance of a new version of the OASIS coupler, OASIS3-MCT_3.0, Geosci. Model Dev., 10, 3297-3308, 10.5194/gmd-10-3297-2017, 2017.

Day, J. J., Hawkins, E., and Tietsche, S.: Will Arctic sea ice thickness initialization improve seasonal forecast skill?, Geophysical Research Letters, 41, 7566-7575, https://doi.org/10.1002/2014GL061694, 2014.

DeLuca, C., Theurich, G., and Balaji, V.: The Earth System Modeling Framework, in: Earth System Modelling - Volume 3: Coupling Software and Strategies, edited by: Valcke, S., Redler, R., and Budich, R., Springer Berlin Heidelberg, Berlin, Heidelberg, 43-54, 2012.

Dirk Notz, and Bitz, C. M.: Sea ice in Earth system models, in: Sea Ice, 304-325, 2017.

Doney, S. C., Large, W. G., and Bryan, F. O.: Surface Ocean Fluxes and Water-Mass Transformation Rates in the Coupled NCAR Climate System Model, Journal of Climate, 11, 1420-1441, 10.1175/1520-0442(1998)011<1420:sofawm>2.0.co;2, 1998.

Dupont, F., Higginson, S., Bourdallé-Badie, R., Lu, Y., Roy, F., Smith, G. C., Lemieux, J. F., Garric, G., and Davidson, F.: A high-resolution ocean and sea-ice modelling system for the Arctic and North Atlantic oceans, Geosci. Model Dev., 8, 1577-1594, 10.5194/gmd-8-1577-2015, 2015.

Eastwood, S., Larsen, K. R., Lavergne, T., Nielsen, E., and Tonboe, R.: Global sea ice concentration reprocessing Product User Manual, EUMETSAT OSISAF, 2011.

Faucher, M., Roy, F., Desjardins, S., Fogarty, C., Pellerin, P., Ritchie, H., and Denis, B.: Operational coupled atmosphere - ocean - ice forecast system for the Gulf of St. Lawrence, Canada, 9th EMS Annual Meeting, 2009,

Francis, J. A.: The where and when of wetter and drier: disappearing Arctic sea ice plays a role, Environmental Research Letters, 8, 041002, 10.1088/1748-9326/8/4/041002, 2013.

Grell, G. A., and Dévényi, D.: A generalized approach to parameterizing convection combining ensemble and data assimilation techniques, Geophysical Research Letters, 29, 38-31-38-34, 10.1029/2002gl015311, 2002.

Harada, Y., Kamahori, H., Kobayashi, C., Endo, H., Kobayashi, S., Ota, Y., Onoda, H., Onogi, K., Miyaoka, K., and Takahashi, K.: The JRA-55 Reanalysis: Representation of Atmospheric Circulation and Climate Variability, Journal of the Meteorological Society of Japan. Ser. II, 94, 269-302, 10.2151/jmsj.2016-015, 2016.

Hibler, W. D.: Modeling a Variable Thickness Sea Ice Cover, Monthly Weather Review, 108, 1943-1973, 10.1175/1520-0493(1980)108<1943:MAVTSI>2.0.CO;2, 1980.

Hines, K. M., and Bromwich, D. H.: Development and Testing of Polar Weather Research and Forecasting (WRF) Model. Part I: Greenland Ice Sheet Meteorology, Monthly Weather Review, 136, 1971-1989, 10.1175/2007mwr2112.1, 2008.

Hines, K. M., Bromwich, D. H., Bai, L.-S., Barlage, M., and Slater, A. G.: Development and Testing of Polar WRF. Part III: Arctic Land, Journal of Climate, 24, 26-48, 10.1175/2010JCLI3460.1, 2011.

Janjić, Z.: Nonsingular Implementation of the Mellor-Yamada Level 2.5 Scheme in the NCEP Meso model (NCEP Office Note No. 437), NCEP, Camp Springs, Md, 2002.

Jung, T., Gordon, N. D., Bauer, P., Bromwich, D. H., Chevallier, M., Day, J. J., Dawson, J., Doblas-Reyes, F., Fairall, C., Goessling, H. F., Holland, M., Inoue, J., Iversen, T., Klebe, S., Lemke, P., Losch, M., Makshtas, A., Mills, B., Nurmi, P., Perovich, D., Reid, P., Renfrew, I. A., Smith, G., Svensson, G., Tolstykh, M., and Yang, Q.: Advancing Polar Prediction Capabilities on Daily to Seasonal Time Scales, Bulletin of the American Meteorological Society, 97, 1631-1647, 10.1175/bams-d-14-00246.1, 2016.

Kaleschke, L., Tian-Kunze, X., Maaß, N., Mäkynen, M., and Drusch, M.: Sea ice thickness retrieval from SMOS brightness temperatures during the Arctic freeze-up period, Geophysical Research Letters, 39, 10.1029/2012GL050916, 2012.

Kobayashi, S., Ota, Y., Harada, Y., Ebita, A., Moriya, M., Onoda, H., Onogi, K., Kamahori, H., Kobayashi, C., Endo, H., Miyaoka, K., and Takahashi, K.: The JRA-55 Reanalysis: General Specifications and Basic Characteristics, Journal of the Meteorological Society of Japan. Ser. II, 93, 5-48, 10.2151/jmsj.2015-001, 2015.

Large, W. G., Mcwilliams, J. C., and Doney, S. C.: Oceanic vertical mixing: A review and a model with a nonlocal boundary layer parameterization, Reviews of Geophysics, 32, 363-403, 1994.

Laxon, S. W., Giles, K. A., Ridout, A. L., Wingham, D. J., Willatt, R., Cullen, R., Kwok, R., Schweiger, A., Zhang, J., Haas, C., Hendricks, S., Krishfield, R., Kurtz, N., Farrell, S., and Davidson, M.: CryoSat-2 estimates of Arctic sea ice thickness and volume, Geophysical Research Letters, 40, 732-737, 10.1002/grl.50193, 2013.

Liang, X., and Losch, M.: On the Effects of Increased Vertical Mixing on the Arctic Ocean and Sea Ice, Journal of Geophysical Research: Oceans, 123, 9266-9282, 10.1029/2018jc014303, 2018.

Liang, X., Losch, M., Nerger, L., Mu, L., Yang, Q., and Liu, C.: Using Sea Surface Temperature Observations to Constrain Upper Ocean Properties in an Arctic Sea Ice-Ocean Data Assimilation System, Journal of Geophysical Research: Oceans, 124, 4727-4743, 10.1029/2019jc015073, 2019.

Liang, X., ZHAO, F., Li, C., ZHANG, L., and LI, B.: Evaluation of ArcIOPS sea ice forecasting products during the ninth CHINARE-Arctic in summer 2018, Advances in Polar ence, v.31;No.78, 19-30, 2020.

Liu, L., Yang, G., Wang, B., Zhang, C., Li, R., Zhang, Z., Ji, Y., and Wang, L.: C-Coupler1: a Chinese community coupler for Earth system modeling, Geosci. Model Dev., 7, 2281-2302, 10.5194/gmd-7-2281-2014, 2014.

Liu, L., Zhang, C., Li, R., Wang, B., and Yang, G.: C-Coupler2: a flexible and user-friendly community coupler for model coupling and nesting, Geosci. Model Dev., 11, 3557-3586, 10.5194/gmd-11-3557-2018, 2018.

Locarnini, R. A., Mishonov, A., Antonov, J., Boyer, T., Garcia, H., and Levitus, S.: World Ocean Atlas 2005 Volume 1: Temperature NOAA Atlas NESDIS, 61, 2006.

Losch, M., Menemenlis, D., Campin, J.-M., Heimbach, P., and Hill, C.: On the formulation of sea-ice models. Part 1: Effects of different solver implementations and parameterizations, Ocean Modelling, 33, 129-144, https://doi.org/10.1016/j.ocemod.2009.12.008, 2010.

Lynch, A. H., Chapman, W. L., Walsh, J. E., and Weller, G.: Development of a Regional Climate Model of the Western Arctic, Journal of Climate, 8, 1555-1570, 10.1175/1520-0442(1995)008<1555:doarcm>2.0.co;2, 1995.

Marshall, J., Hill, C., Perelman, L., and Adcroft, A.: Hydrostatic, quasi-hydrostatic, and nonhydrostatic ocean modeling, Journal of Geophysical Research: Oceans, 102, 5733-5752, 10.1029/96jc02776, 1997.

Maslowski, W., Clement Kinney, J., Higgins, M., and Roberts, A.: The Future of Arctic Sea Ice, Annual Review of Earth and Planetary Sciences, 40, 625-654, 10.1146/annurev-earth-042711-105345, 2012.

Melling, H., and Riedel, D. A.: The underside topography of sea ice over the continental shelf of the Beaufort Sea in the winter of 1990, Journal of Geophysical Research: Oceans, 100, 13641-13653, 10.1029/95JC00309, 1995.

Menemenlis, D., J. M. Campin, P. Heimbach, C. Hill, T. Lee, A. Nguyen, M. Schodlok, and Zhang, H.: ECCO2: High resolution global ocean and sea ice data synthesis, Mercator Ocean Q. Newsl., 31, 13-21, 2008.

Neelin, J. D., Latif, M., and Jin, F.: Dynamics of Coupled Ocean-Atmosphere Models: The Tropical Problem, Annual Review of Fluid Mechanics, 26, 617-659, 10.1146/annurev.fl.26.010194.003153, 1994.

Nguyen, A. T., Menemenlis, D., and Kwok, R.: Arctic ice-ocean simulation with optimized model parameters: Approach and assessment, Journal of Geophysical Research: Oceans, 116, 10.1029/2010JC006573, 2011.

Pellerin, P., Ritchie, H., Saucier, F. J., Roy, F., Desjardins, S., Valin, M., and Lee, V.: Impact of a Two-Way Coupling between an Atmospheric and an Ocean-Ice Model over the Gulf of St. Lawrence, Monthly Weather Review, 132, 1379-1398, 10.1175/1520-0493(2004)132<1379:ioatcb>2.0.co;2, 2004.

Posey, P. G., Metzger, E. J., Wallcraft, A. J., Hebert, D. A., Allard, R. A., Smedstad, O. M., Phelps, M. W., Fetterer, F., Stewart, J. S., Meier, W. N., and Helfrich, S. R.: Improving Arctic sea ice edge forecasts by assimilating high horizontal resolution sea ice concentration data into the US Navy's ice forecast systems, The Cryosphere, 9, 1735-1745, 10.5194/tc-9-1735-2015, 2015.

Proshutinsky, A., Yang, J., Krishfield, R., Gerdes, R., Karcher, M., Kauker, F., Koeberle, C., Hakkinen, S., Hibler, W., Holland, D., Maqueda, M., Holloway, G., Hunke, E., Maslowski, W., Steele, M., and Zhang, J.: Arctic ocean study: Synthesis of model results and observations, Eos, Transactions American Geophysical Union, 86, 368-371, 10.1029/2005EO400003, 2005.

Ricker, R., Hendricks, S., Helm, V., Skourup, H., and Davidson, M.: Sensitivity of CryoSat-2 Arctic sea-ice freeboard and thickness on radar-waveform interpretation, The Cryosphere, 8, 1607-1622, 10.5194/tc-8-1607-2014, 2014.

Ricker, R., Hendricks, S., Kaleschke, L., Tian-Kunze, X., King, J., and Haas, C.: A weekly Arctic sea-ice thickness data record from merged CryoSat-2 and SMOS satellite data, The Cryosphere, 11, 1607-1623, 10.5194/tc-11-1607-2017, 2017.

Rinke, A., Lynch, A. H., and Dethloff, K.: Intercomparison of Arctic regional climate simulations: Case studies of January and June 1990, Journal of Geophysical Research: Atmospheres, 105, 29669-29683, 10.1029/2000jd900325, 2000.

Saha, S., Moorthi, S., Pan, H.-L., Wu, X., Wang, J., Nadiga, S., Tripp, P., Kistler, R., Woollen, J., Behringer, D., Liu, H., Stokes, D., Grumbine, R., Gayno, G., Wang, J., Hou, Y.-T., Chuang, H.-y., Juang, H.-M. H., Sela, J., Iredell, M., Treadon, R., Kleist, D., Delst, P. V., Keyser, D., Derber, J., Ek, M., Meng, J., Wei, H., Yang, R., Lord, S., Dool, H. v. d., Kumar, A., Wang, W., Long, C., Chelliah, M., Xue, Y., Huang, B., Schemm, J.-K., Ebisuzaki, W., Lin, R., Xie, P., Chen, M., Zhou, S., Higgins, W., Zou, C.-Z., Liu, Q., Chen, Y., Han, Y., Cucurull, L., Reynolds, R. W., Rutledge, G., and Goldberg, M.: The NCEP Climate Forecast System Reanalysis, Bulletin of the American Meteorological Society, 91, 1015-1058, 10.1175/2010bams3001.1, 2010.

Schrum, C., Hübner, U., Jacob, D., and Podzun, R.: A coupled atmosphere/ice/ocean model for the North Sea and the Baltic Sea, Climate Dynamics, 21, 131-151, 10.1007/s00382-003-0322-8, 2003.

Semtner, A. J.: A Model for the Thermodynamic Growth of Sea Ice in Numerical Investigations of Climate, Journal of Physical Oceanography, 6, 379-389, 10.1175/1520-0485(1976)006<0379:amfttg>2.0.co;2, 1976.

Shu, Q., Song, Z., and Qiao, F.: Assessment of sea ice simulations in the CMIP5 models, The Cryosphere, 9, 399-409, 10.5194/tc-9-399-2015, 2015.

Simmonds, I., and Rudeva, I.: The great Arctic cyclone of August 2012, Geophysical Research Letters, 39, 10.1029/2012gl054259, 2012.

Skachko, S., Buehner, M., Laroche, S., Lapalme, E., Smith, G., Roy, F., Surcel-Colan, D., Bélanger, J. M., and Garand, L.: Weakly coupled atmosphere–ocean data assimilation in the Canadian global prediction system (v1), Geosci. Model Dev., 12, 5097-5112, 10.5194/gmd-12-5097-2019, 2019.

Skamarock, W. C., Klemp, J. B., Dudhia, J., Gill, D. O., Barker, D., and Duda, M. G.: A Description of the Advanced Research WRF Version 3 (No. NCAR/TN-475+STR), University Corporation for Atmospheric Research, 2008.

Smith, G. C., Roy, F., Mann, P., Dupont, F., Brasnett, B., Lemieux, J.-F., Laroche, S., and Bélair, S.: A new atmospheric dataset for forcing ice–ocean models: Evaluation of reforecasts using the Canadian global deterministic prediction system, Quarterly Journal of the Royal Meteorological Society, 140, 881-894, 10.1002/qj.2194, 2014.

Smith, G. C., Roy, F., Reszka, M., Surcel Colan, D., He, Z., Deacu, D., Belanger, J.-M., Skachko, S., Liu, Y., Dupont, F., Lemieux, J.-F., Beaudoin, C., Tranchant, B., Drévillon, M., Garric, G., Testut, C.-E., Lellouche, J.-M., Pellerin, P., Ritchie, H., Lu, Y., Davidson, F., Buehner, M., Caya, A., and Lajoie, M.: Sea ice forecast verification in the Canadian Global Ice Ocean Prediction System, Quarterly Journal of the Royal Meteorological Society, 142, 659-671, 10.1002/qj.2555, 2016.

Smith, G. C., Bélanger, J.-M., Roy, F., Pellerin, P., Ritchie, H., Onu, K., Roch, M., Zadra, A., Colan, D. S., Winter, B., Fontecilla, J.-S., and Deacu, D.: Impact of Coupling with an Ice–Ocean Model on Global Medium-Range NWP Forecast Skill, Monthly Weather Review, 146, 1157-1180, 10.1175/MWR-D-17-0157.1, 2018.

Stroeve, J. C., Kattsov, V., Barrett, A., Serreze, M., Pavlova, T., Holland, M., and Meier, W. N.: Trends in Arctic sea ice extent from CMIP5, CMIP3 and observations, Geophysical Research Letters, 39, 10.1029/2012gl052676, 2012.

Sun, R., Subramanian, A. C., Miller, A. J., Mazloff, M. R., Hoteit, I., and Cornuelle, B. D.: SKRIPS v1.0: a regional coupled ocean–atmosphere modeling framework (MITgcm–WRF) using ESMF/NUOPC, description and preliminary results for the Red Sea, Geosci. Model Dev., 12, 4221-4244, 10.5194/gmd-12-4221-2019, 2019.

Tian-Kunze, X., Kaleschke, L., Maaß, N., Mäkynen, M., Serra, N., Drusch, M., and Krumpen, T.: SMOS-derived thin sea ice thickness: algorithm baseline, product specifications and initial verification, The Cryosphere, 8, 997-1018, 10.5194/tc-8-997-2014, 2014.

Van Pham, T., Brauch, J., Dieterich, C., Frueh, B., and Ahrens, B.: New coupled atmosphere-ocean-ice system COSMO-CLM/NEMO: assessing air temperature sensitivity over the North and Baltic Seas, Oceanologia, 56, 167-189, https://doi.org/10.5697/oc.56-2.167, 2014.

Walters, D. N., Best, M. J., Bushell, A. C., Copsey, D., Edwards, J. M., Falloon, P. D., Harris, C. M., Lock, A. P., Manners, J. C., Morcrette, C. J., Roberts, M. J., Stratton, R. A., Webster, S., Wilkinson, J. M., Willett, M. R., Boutle, I. A., Earnshaw, P. D., Hill, P. G., MacLachlan, C., Martin, G. M., Moufouma-Okia, W., Palmer, M. D., Petch, J. C., Rooney, G. G., Scaife, A. A., and Williams, K. D.: The Met Office Unified Model Global Atmosphere 3.0/3.1 and JULES Global Land 3.0/3.1 configurations, Geosci. Model Dev., 4, 919-941, 10.5194/gmd-4-919-2011, 2011.

Williams, K. D., Copsey, D., Blockley, E. W., Bodas-Salcedo, A., Calvert, D., Comer, R., Davis, P., Graham, T., Hewitt, H. T., Hill, R., Hyder, P., Ineson, S., Johns, T. C., Keen, A. B., Lee, R. W., Megann, A., Milton, S. F., Rae, J. G. L., Roberts, M. J., Scaife, A. A., Schiemann, R., Storkey, D., Thorpe, L., Watterson, I. G., Walters, D. N., West, A., Wood, R. A., Woollings, T., and Xavier, P. K.: The Met Office Global Coupled Model 3.0 and 3.1 (GC3.0 and GC3.1) Configurations, Journal of Advances in Modeling Earth Systems, 10, 357-380, 10.1002/2017ms001115, 2018.

Wingham, D. J., Francis, C. R., Baker, S., Bouzinac, C., Brockley, D., Cullen, R., de Chateau-Thierry, P., Laxon, S. W., Mallow, U., Mavrocordatos, C., Phalippou, L., Ratier, G., Rey, L., Rostan, F., Viau, P., and Wallis, D. W.: CryoSat: A mission to determine the fluctuations in Earth's land and marine ice fields, Advances in Space Research, 37, 841-871, https://doi.org/10.1016/j.asr.2005.07.027, 2006.

Yang, Y., Qiao, F., Zhao, W., Y., T., and Yuan, Y.: MASNUM ocean wave numerical model in spherical coordinates and its application, Acta Oceanol. Sin., 27, 1-7, 2005.

Zhang, J., and Rothrock, D. A.: Modeling Global Sea Ice with a Thickness and Enthalpy Distribution Model in Generalized Curvilinear Coordinates, Monthly Weather Review, 131, 845-861, 10.1175/1520-0493(2003)131<0845:mgsiwa>2.0.co;2, 2003.

Zhao, B., Qiao, F., Cavaleri, L., Wang, G., Bertotti, L., and Liu, L.: Sensitivity of typhoon modeling to surface waves and rainfall, Journal of Geophysical Research: Oceans, 122, 1702-1723, 10.1002/2016jc012262, 2017.

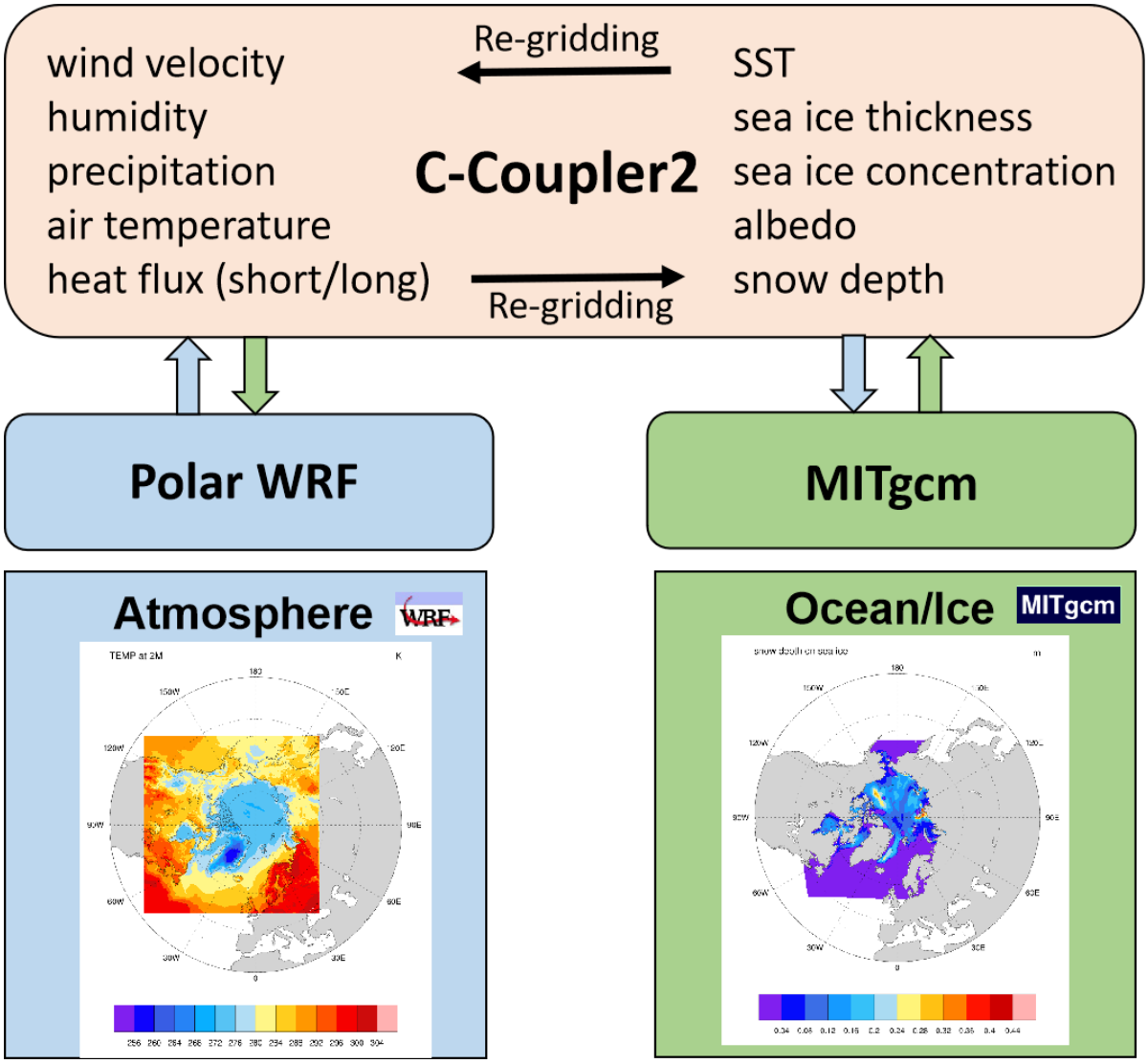

Figure 1: Coupling strategy of the Polar WRF-MITgcm coupled model system.

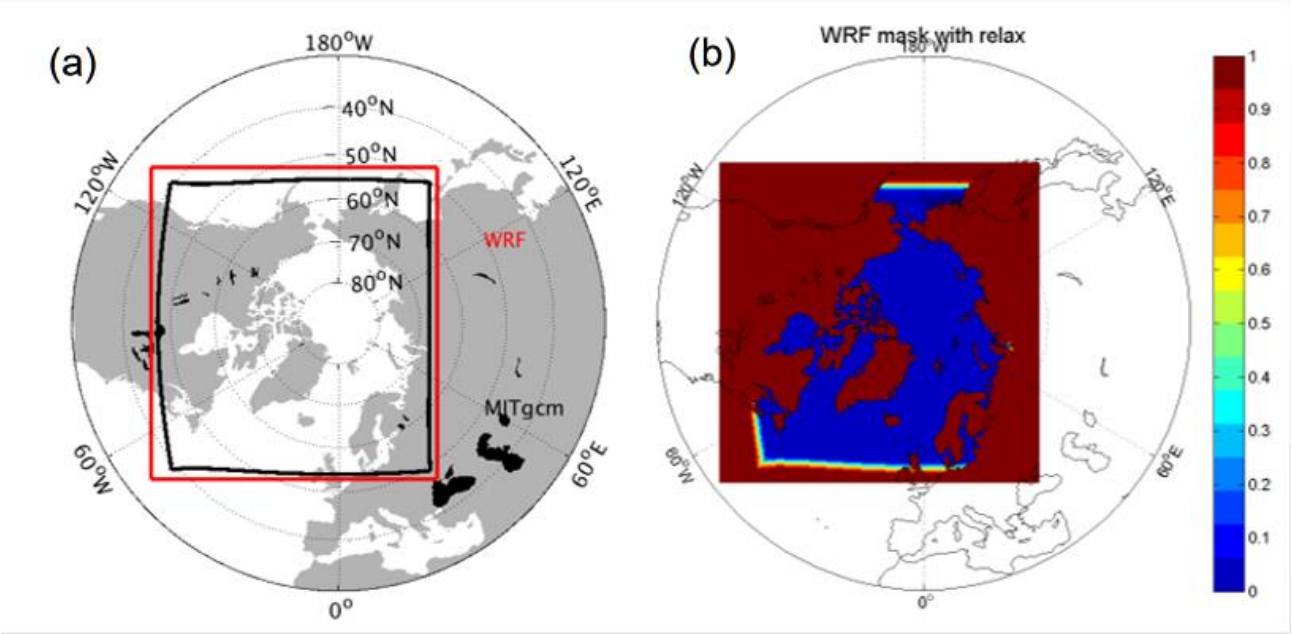

Figure 2: (a) Model domain of the MITgcm and the Polar WRF model. The red and black lines denote the boundaries of the Polar WRF and the MITgcm model, respectively. (b) Relaxation coefficient for the external forcing file of the Polar WRF bottom boundary conditions.

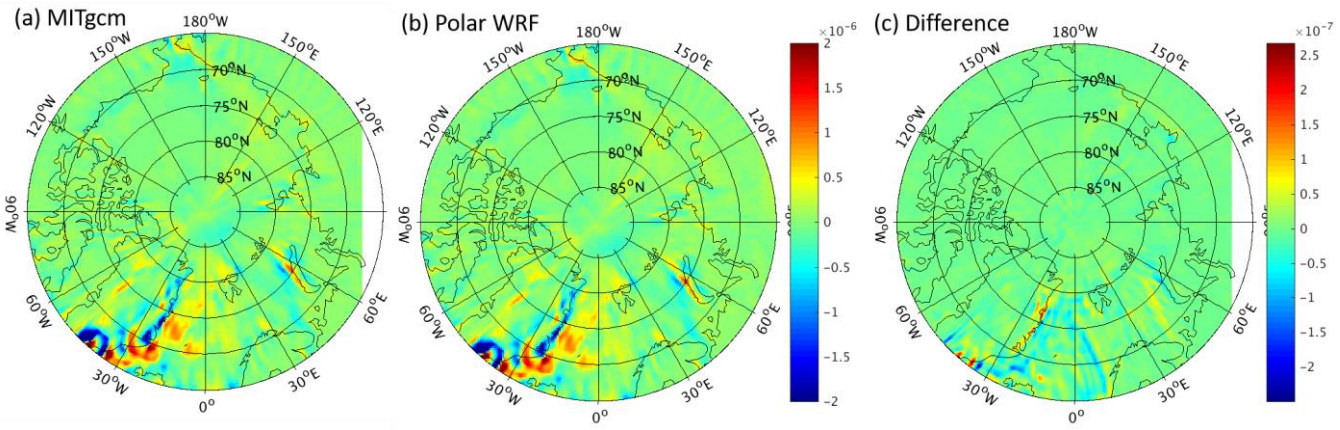

Figure 3: Wind stress curl (unit: Nm-2) derived from (a) the MITgcm output, (b) the Polar WRF output, and (c) their difference on March 1, 2012. The difference of wind stress curl between the Polar WRF and MITgcm is calculated by interpolating the Polar WRF output onto the MITgcm grid.

740

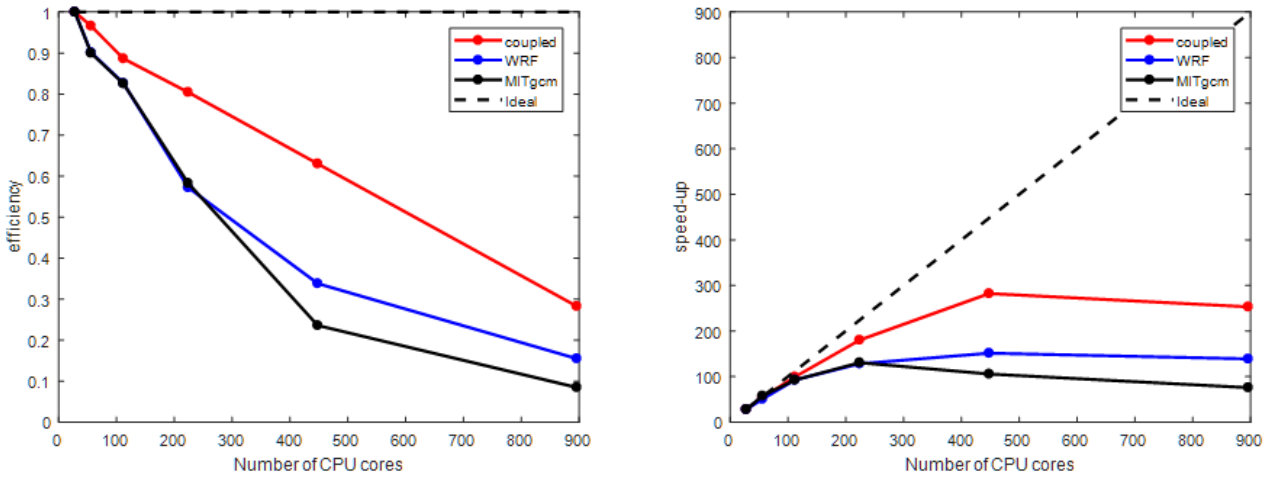

Figure 4: The parallel efficiency (left) and speed-up (right) test of the coupled model and the stand-alone component models, employing up to 896 CPU cores. The simulation using 28 CPU cores is regarded as the baseline case when computing the speed-up. The tests are performed on a Lenovo Blade Server system composed of 240 dual-socket compute nodes based on 14-core Intel Haswell processors.

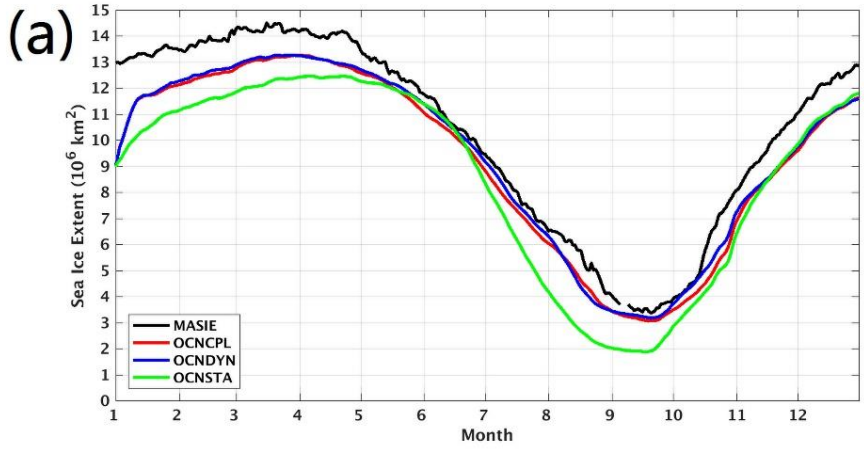
(a)
Sea Ice Extent (10^6 km^2)
Month
MASIE
OCNCPL
OCNDYN
OCNSTA

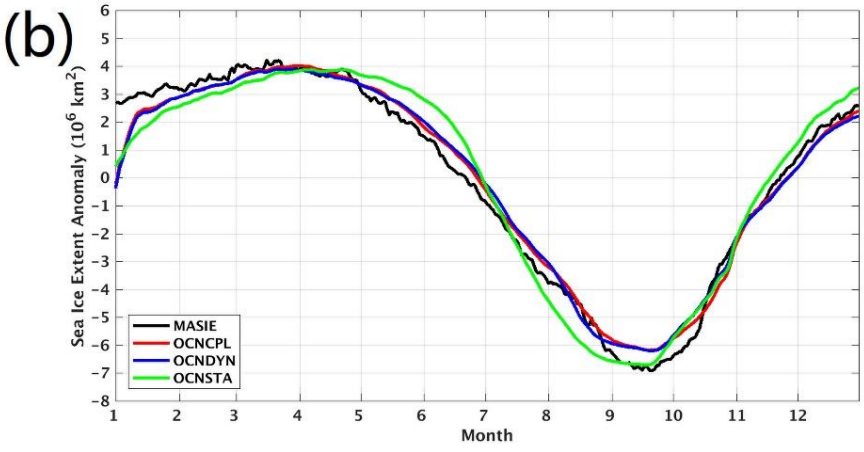
(b)
Sea Ice Extent Anomaly (10^6 km^2)
Month
MASIE
OCNCPL
OCNDYN
OCNSTA

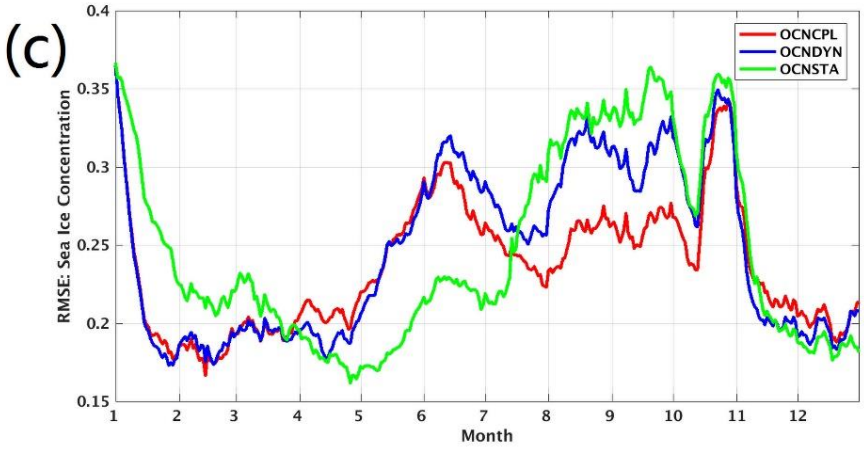
(c)
RMSE: Sea Ice Concentration
Month
OCNCPL
OCNDYN
OCNSTA

Figure 5~~Figure 45~~: Time series of (a) sea ice extent, (b) sea ice extent anomaly, and (c) root mean square error (RMSE) of modeled sea ice concentration with respect to the OSISAF observation in 2012. The black, red, green and blue lines in (a) denote sea ice extent of the MASIE observation, the OCNCPL run, the OCNSTA run and the OCNDYN run, respectively. The black, red, green and blue lines in (b) denote sea ice extent anomaly of the MASIE observation, the OCNCPL run, the OCNSTA run and the OCNDYN run, respectively. The red, green and blue lines in (c) denote the sea ice concentration RMSE of the OCNCPL run, the OCNSTA run and the OCNDYN run, respectively. MASIE = Multisensor Analyzed Sea Ice Extent; OSISAF = Ocean and Sea Ice Satellite Application Facility.

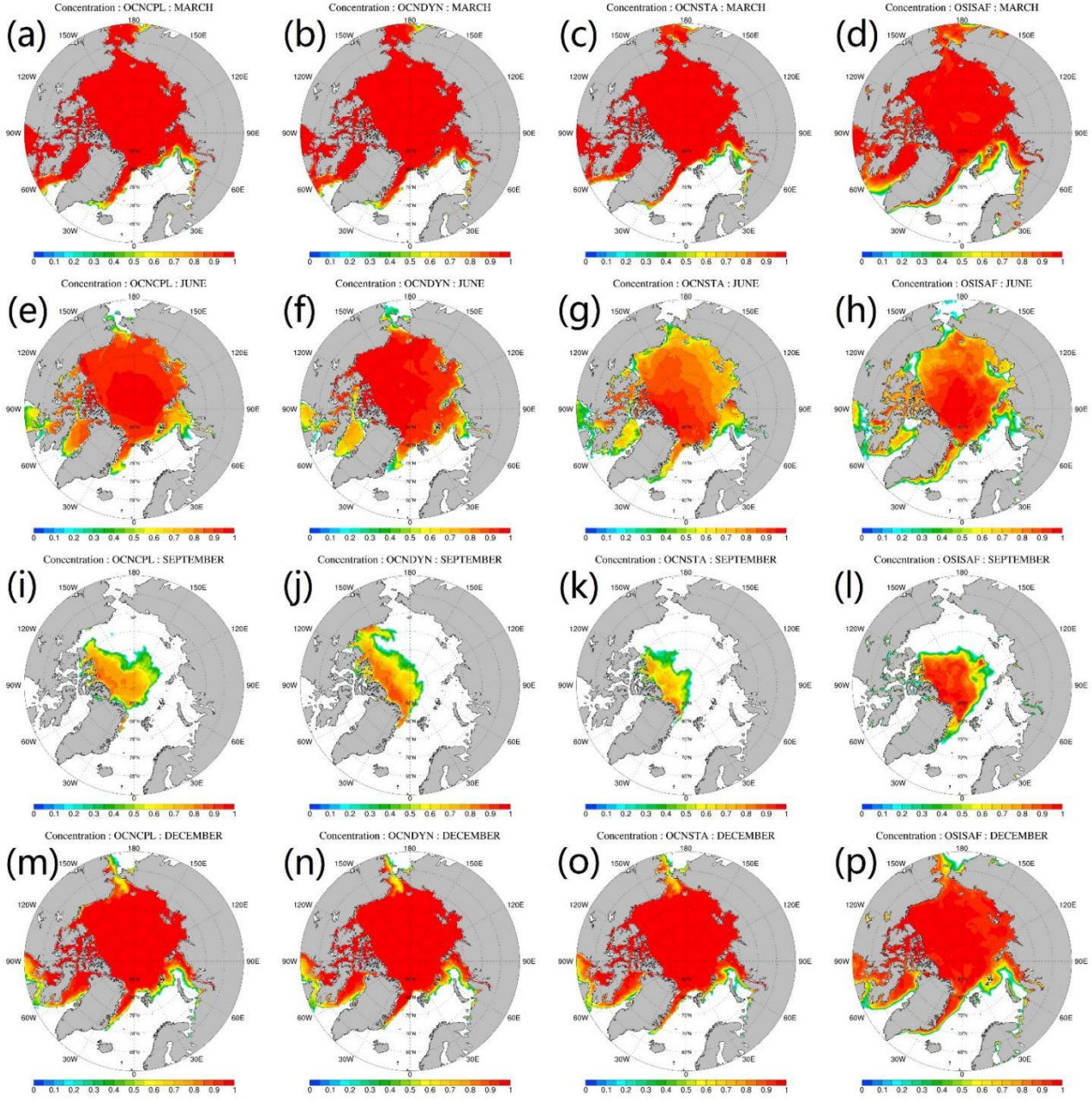

Figure 6~~Figure 56~~: Modeled and observed monthly mean sea ice concentration. ~~The~~ From top to bottom ~~, middle, and bottom~~ panels show the ~~July~~March, ~~August~~June, September and December~~September~~ sea ice concentration, respectively. ~~The~~From left to ~~, middle, and~~ right panels show sea ice concentration of the OCNCPL run, the OCNDYN run, the OCNSTA run and the OSISAF observations. OSISAF = Ocean and Sea Ice Satellite Application Facility.

765

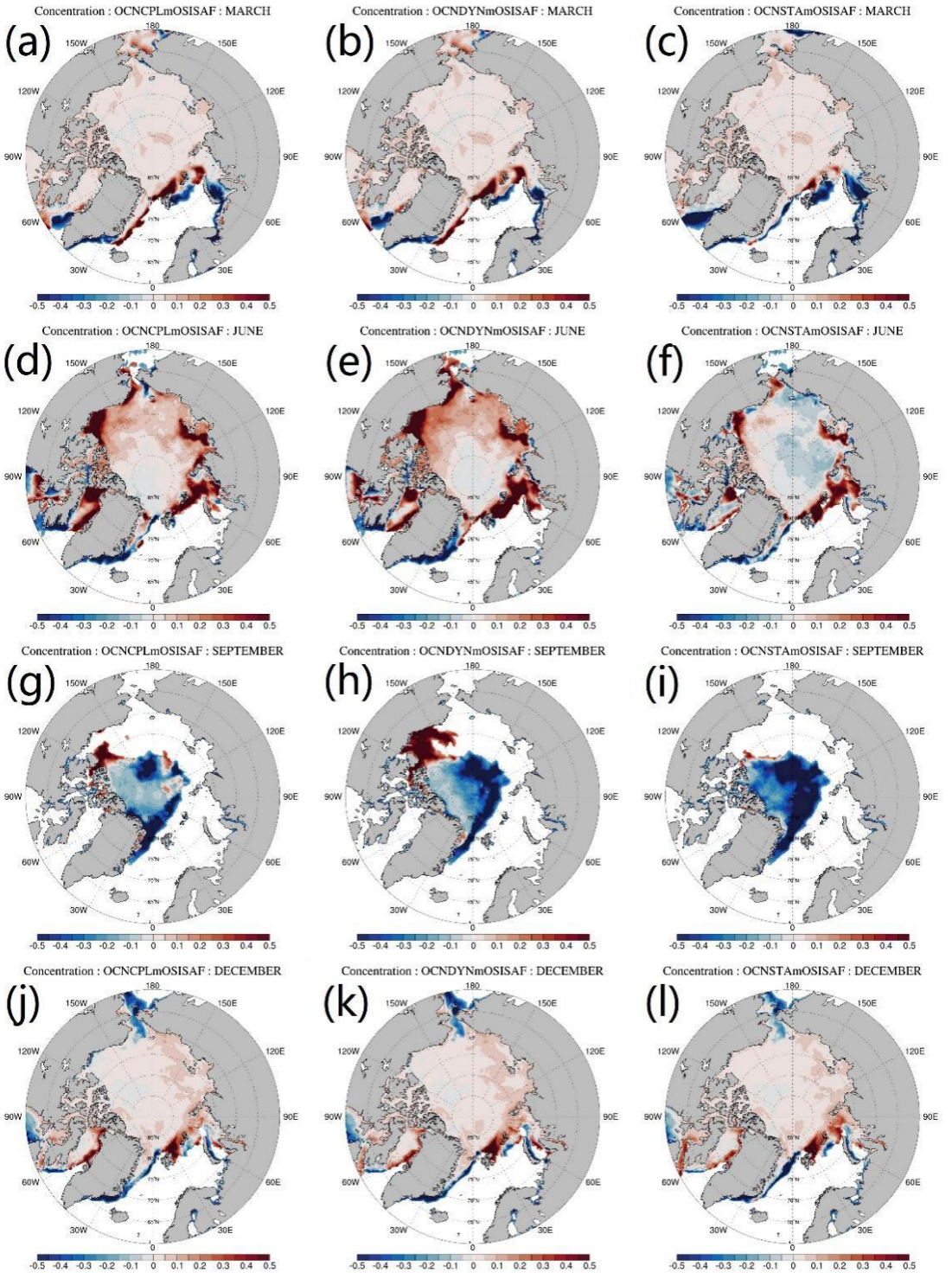
Concentration : OCNCPLmOSISAF : MARCH
(a)
Concentration : OCNDYNmOSISAF : MARCH
(b)
Concentration : OCNSTAmOSISAF : MARCH
(c)
Concentration : OCNCPLmOSISAF : JUNE
(d)
Concentration : OCNDYNmOSISAF : JUNE
(e)
Concentration : OCNSTAmOSISAF : JUNE
(f)
Concentration : OCNCPLmOSISAF : SEPTEMBER
(g)
Concentration : OCNDYNmOSISAF : SEPTEMBER
(h)
Concentration : OCNSTAmOSISAF : SEPTEMBER
(i)
Concentration : OCNCPLmOSISAF : DECEMBER
(j)
Concentration : OCNDYNmOSISAF : DECEMBER
(k)
Concentration : OCNSTAmOSISAF : DECEMBER
(l)
180
150W
150E
120W
120E
90W
90E
60W
60E
30W
30E
0
-0.5 -0.4 -0.3 -0.2 -0.1 0 0.1 0.2 0.3 0.4 0.5

Figure 7: Deviation between the modeled and observed monthly mean sea ice concentration. From top to bottom panels show the March, June, September and December sea ice concentration deviation respect to the OSISAF observations, respectively. The left, middle, and right panels show results of the OCNCPL run, the OCNDYN run, and the OCNSTA run. OSISAF = Ocean and Sea Ice Satellite Application Facility.

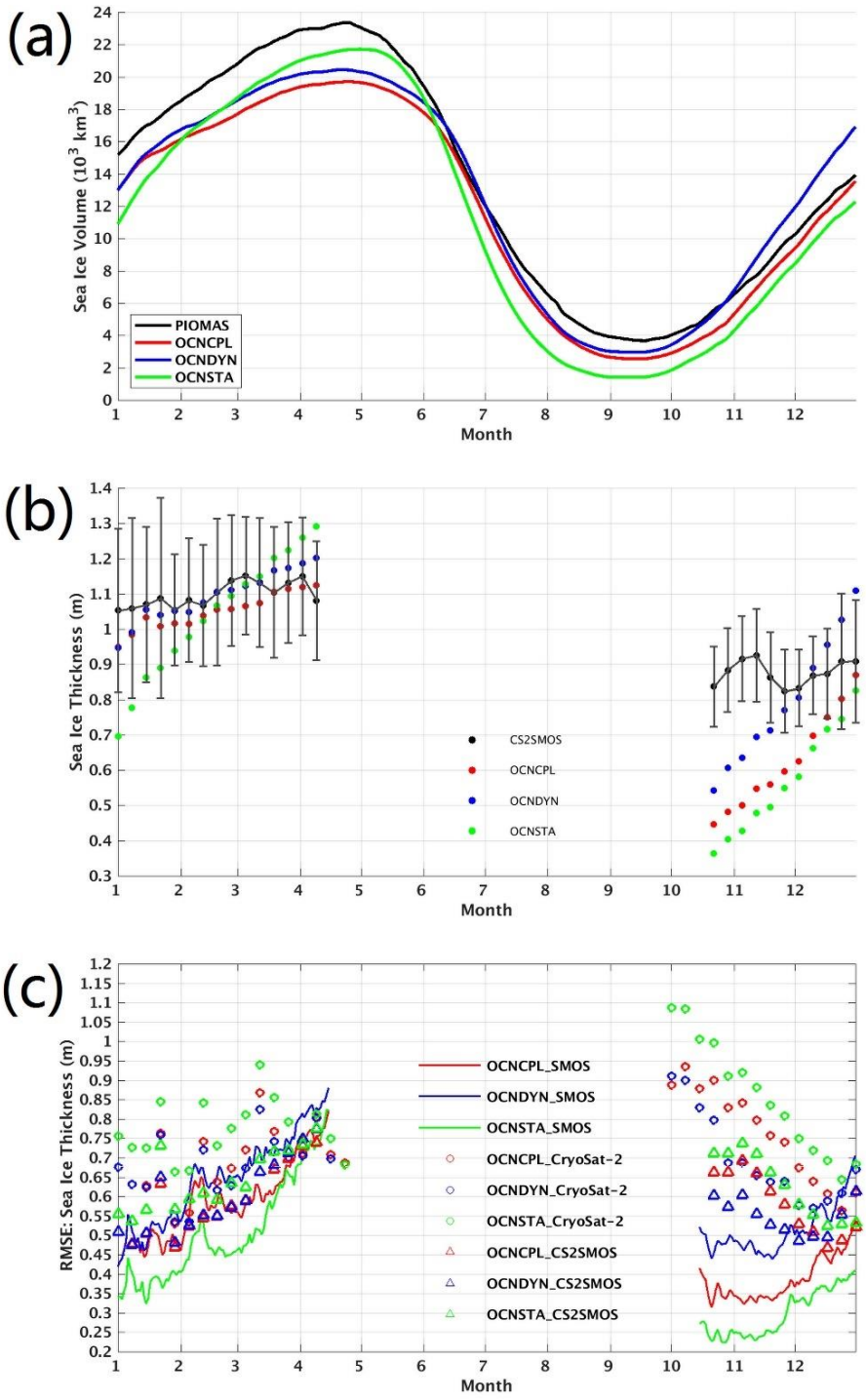

775 Figure 8: Time series of (a) total sea ice volume, (b) spatial mean sea ice thickness, and (c) the RMSE of sea ice thickness with respect to the satellite-retrieved observations in 2012. The black, red, green and blue lines in (a) denote total sea ice

volume of the PIOMAS data, the OCNCPL run, the OCNSTA run and ~~and~~ the OCNDYN run ~~and the OCNSTA run~~, respectively. The black, red, green and blue dots in (b) denote sea ice thickness of the CS2SMOS observations, the OCNCPL run, ~~the OCNDYN run and~~ the OCNSTA run and the OCNDYN run ~~and the OCNDYN run~~, respectively. The black bar in (b) represents the observational uncertainties of the CS2SMOS data. The red, green and blue masks in (c) denote sea ice thickness RMSE of the OCNCPL run, the OCNSTA run and ~~and~~ the OCNDYN run ~~and the OCNSTA run~~ with respect to the SMOS observations in thin ice (< 1 m) region (line), the Cryosat-2 observations (circle), the CS2SMOS observations (triangle), respectively. Model grid points without available observations are not taken into the sea ice thickness RMSE calculation. PIOMAS = Pan-Arctic Ice Ocean Modeling and Assimilation System; SMOS = Soil Moisture Ocean Salinity.

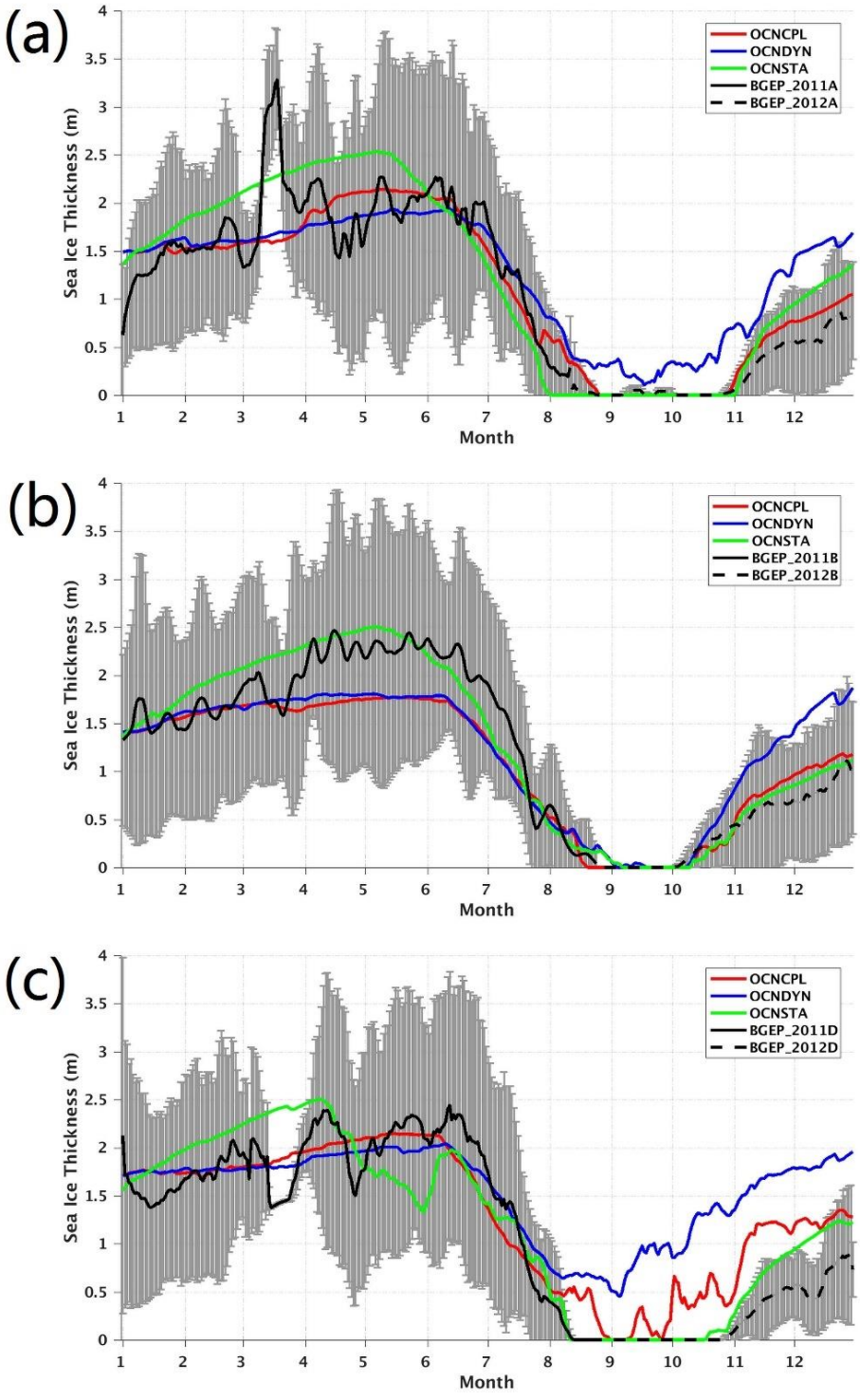
(a)
OCNCPL
OCNDYN
OCNSTA
BGEP_2011A
BGEP_2012A
Sea Ice Thickness (m)
Month
(b)
OCNCPL
OCNDYN
OCNSTA
BGEP_2011B
BGEP_2012B
Sea Ice Thickness (m)
Month
(c)
OCNCPL
OCNDYN
OCNSTA
BGEP_2011D
BGEP_2012D
Sea Ice Thickness (m)
Month

Figure 9: Time series of sea ice thickness at three positions: (a) (75 °N, 150 °W), (b) (78 °N, 150 °W), and (c) (74 °N, 140 °W). The red, ~~and~~ blue and green lines denote sea ice thickness of the OCNCPL run, ~~and~~ the OCNDYN run and the OCNSTA run, respectively. The black solid and dashed lines denote sea ice thickness observations of the BGEP ULSs, which were deployed in the summers of 2011 and 2012. The black lines of the BGEP ULS observations have been smoothed with the gray bar representing the observational uncertainties. BGEP = Beaufort Gyre Exploration Project; ULS = upward-looking sonar.

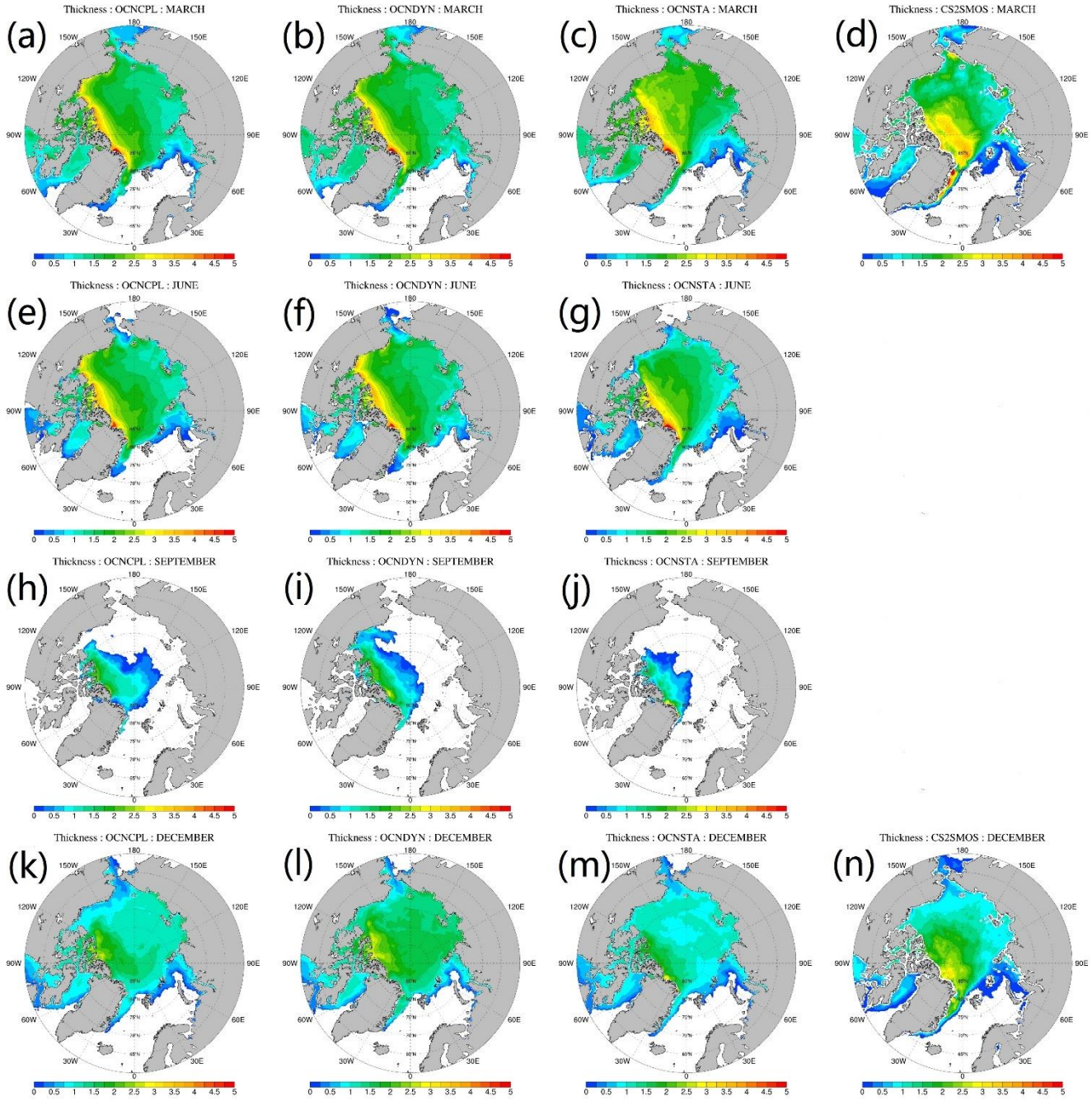

Figure 10**:** Monthly mean sea ice thickness. ~~The top, middle, and bottom~~ From top to bottom panels show the March, June, September, and December sea ice thickness, respectively. **From**~~The~~ left~~, middle, and~~ **to** right panels show sea ice thickness of the OCNCPL run, the OCNDYN run, the OCNSTA run and **the** CS2SMOS **data**~~the deviation between them~~**.**

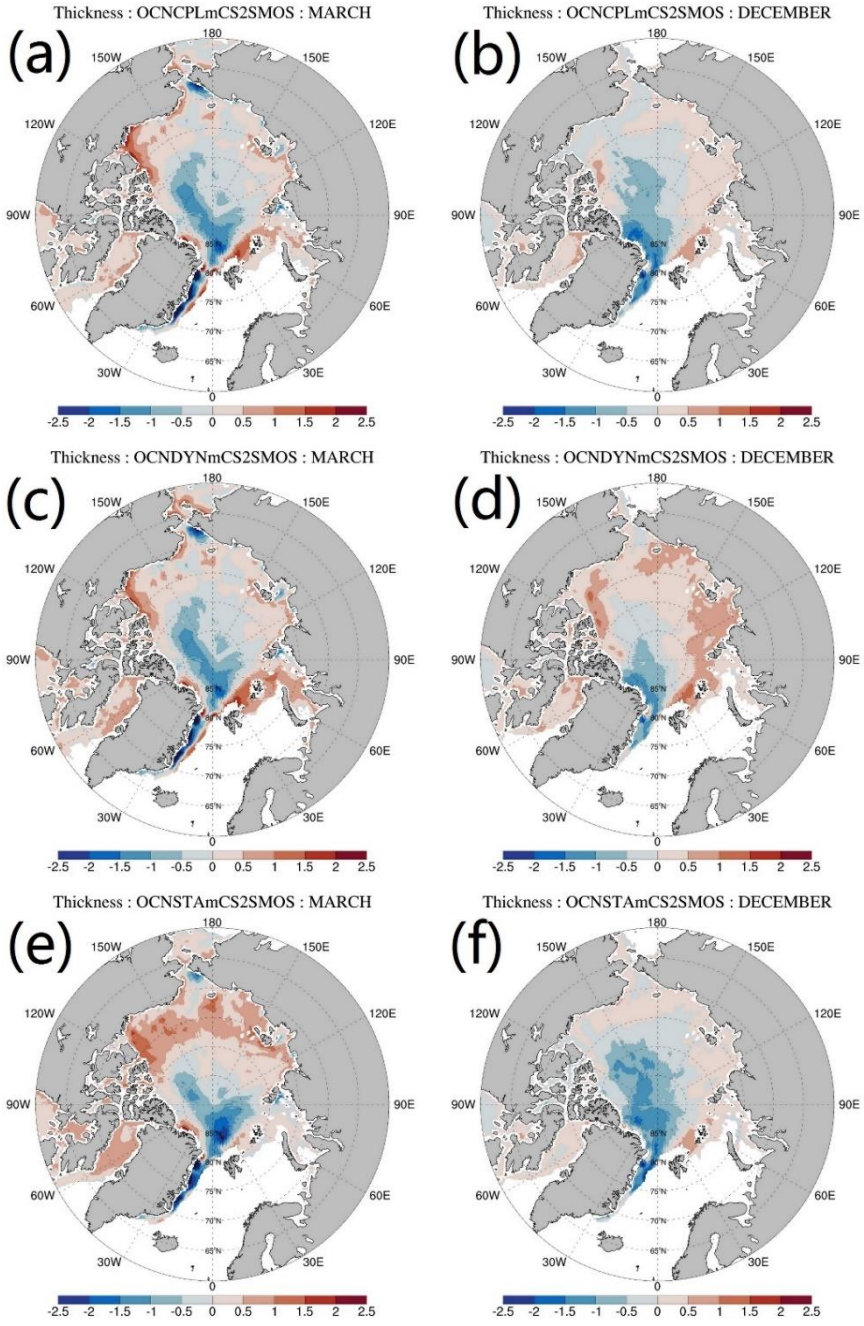

Figure 11: Deviation of the modeled monthly mean sea ice thickness and the CS2SMOS data. The top, middle, and bottom panels show sea ice thickness deviation of the OCNCPL run, the OCNDYN run and the OCNSTA run, respectively. The left and right panels show results in March and December.

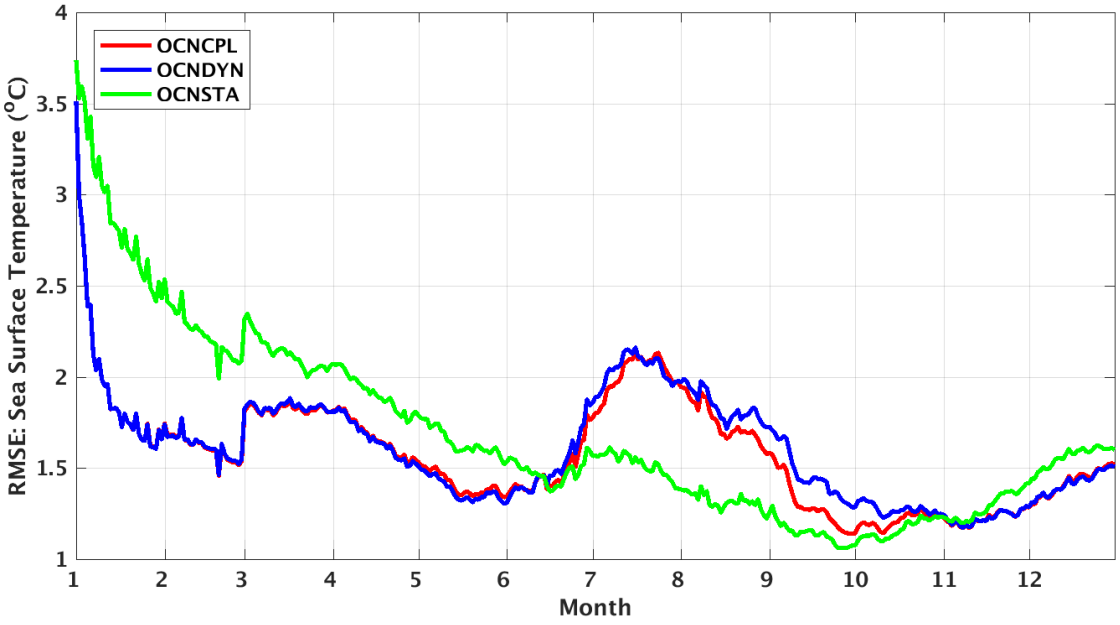

Figure 12: Time series of the RMSE of modeled SST with respect to the GMPE observations in ~~summer of~~ 2012. The red, ~~and~~ blue and green lines denote the SST RMSE of the OCNCPL run, ~~and~~ the OCNDYN run and the OCNSTA run, respectively. GMPE = Group for High-Resolution Sea Surface Temperature Multi-Product Ensemble.

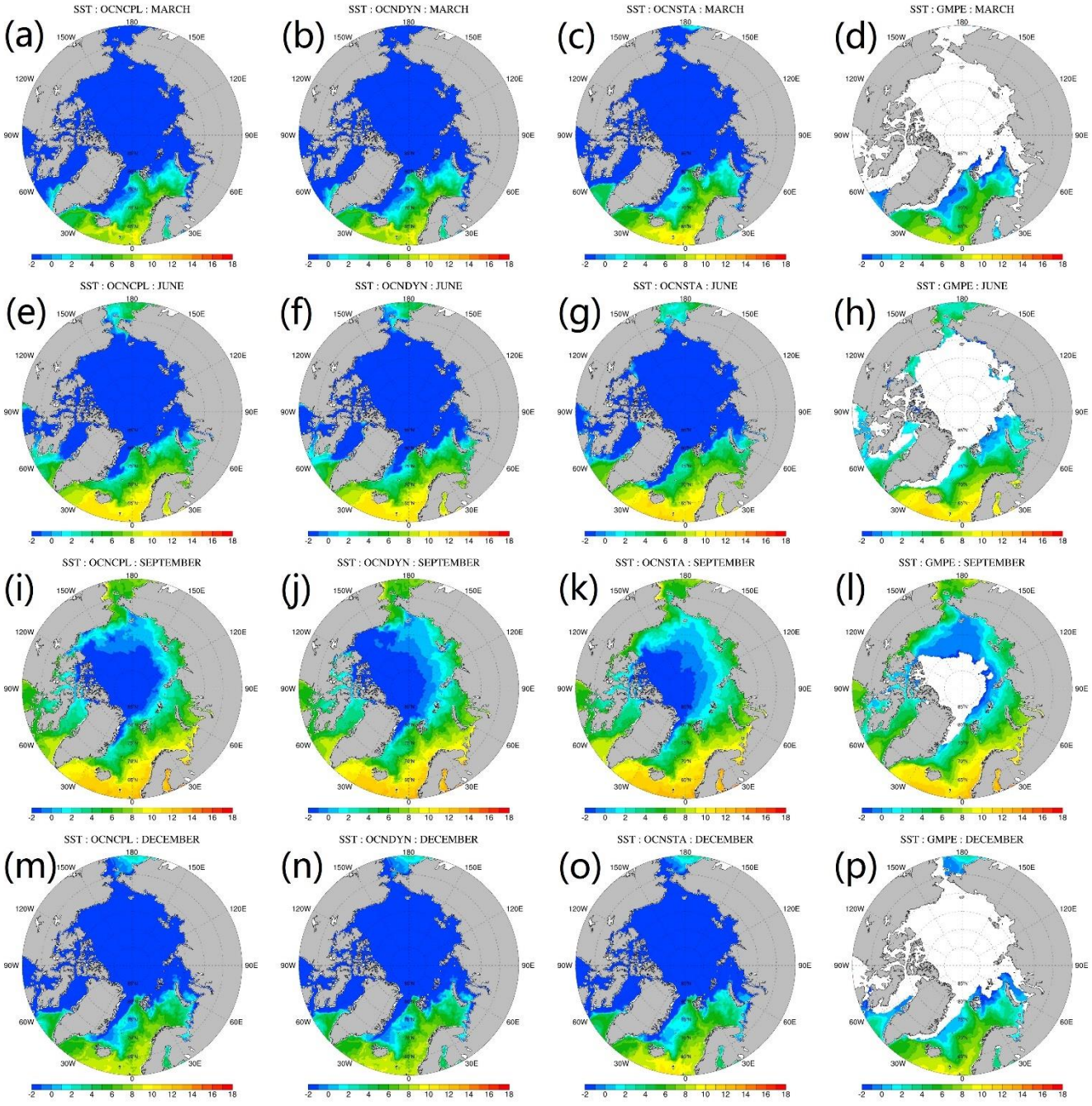

Figure 13: Modeled and observed monthly mean SST. ~~Rows 1 to 4~~From top to bottom panels~~3~~ show the March, June, September and December~~July, August, and September~~ SST, respectively. From left to right panels~~Columns 1 to 4~~ show the SST of the OCNCPL run, the OCNDYN run, the OCNSTA run and the GMPE observations, ~~the OCNCPL run, the~~

~~OCNDYN run, and the deviation between the OCNCPL and OCNDYN runs,~~ respectively. GMPE = Group for High-Resolution Sea Surface Temperature Multi-Product Ensemble.

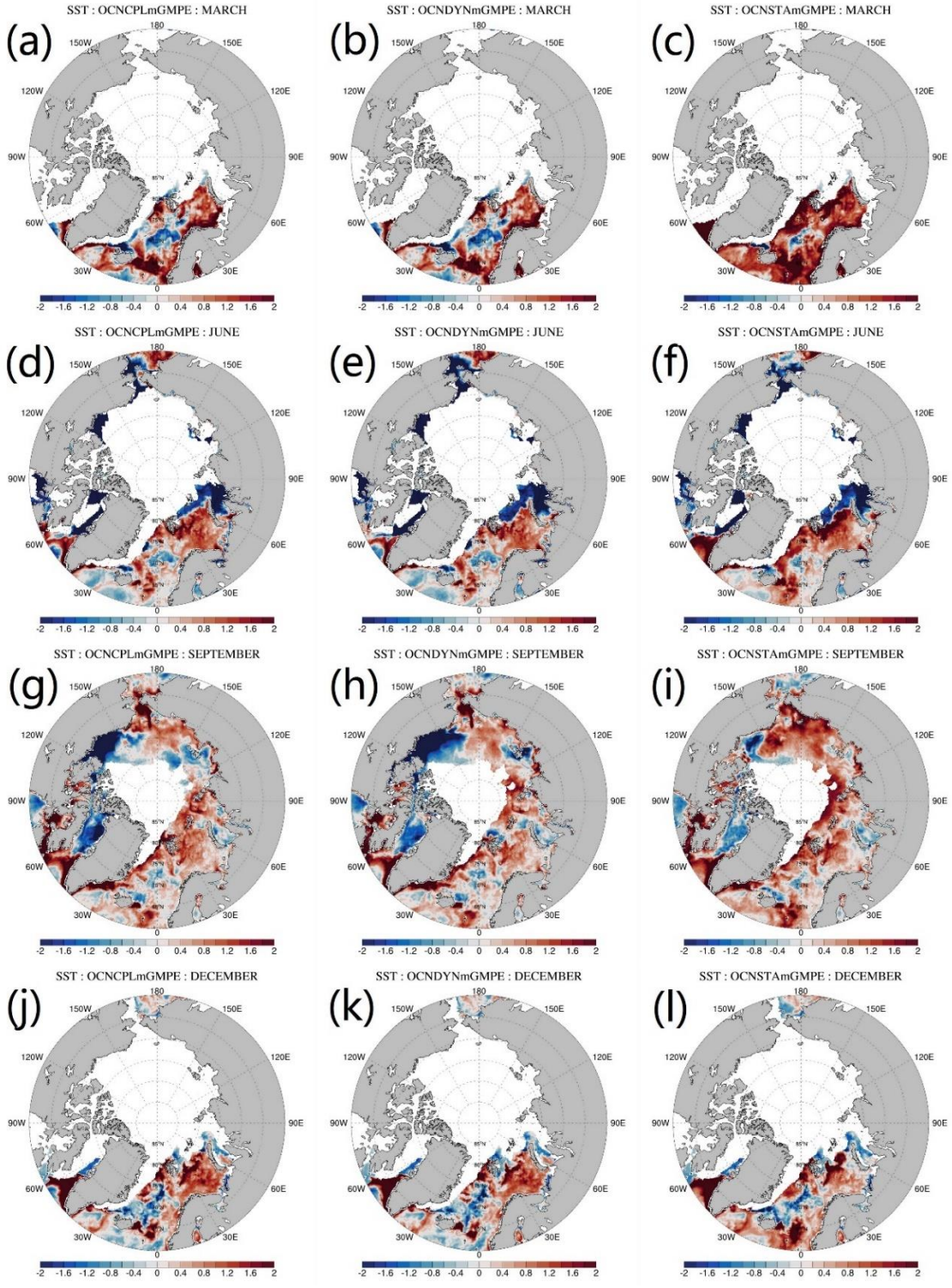
SST : OCNCPLmGMPE : MARCH
(a)
SST : OCNDYNmGMPE : MARCH
(b)
SST : OCNSTAmGMPE : MARCH
(c)
SST : OCNCPLmGMPE : JUNE
(d)
SST : OCNDYNmGMPE : JUNE
(e)
SST : OCNSTAmGMPE : JUNE
(f)
SST : OCNCPLmGMPE : SEPTEMBER
(g)
SST : OCNDYNmGMPE : SEPTEMBER
(h)
SST : OCNSTAmGMPE : SEPTEMBER
(i)
SST : OCNCPLmGMPE : DECEMBER
(j)
SST : OCNDYNmGMPE : DECEMBER
(k)
SST : OCNSTAmGMPE : DECEMBER
(l)
180
150W
150E
120W
120E
90W
90E
60W
60E
30W
30E
0
85°N
-2 -1.6 -1.2 -0.8 -0.4 0 0.4 0.8 1.2 1.6 2

Figure 14: Deviation of the modeled ~~and observed~~ monthly mean SST ~~compared with~~and the GMPE SST data. ~~Rows 1 to 4~~From top to bottom panels show the March, June, September and December SST deviation, respectively. From left to right panels~~Columns 1 to 4~~ show the SST of the OCNCPL run, the OCNDYN run and the OCNSTA run, respectively. GMPE = Group for High-Resolution Sea Surface Temperature Multi-Product Ensemble.

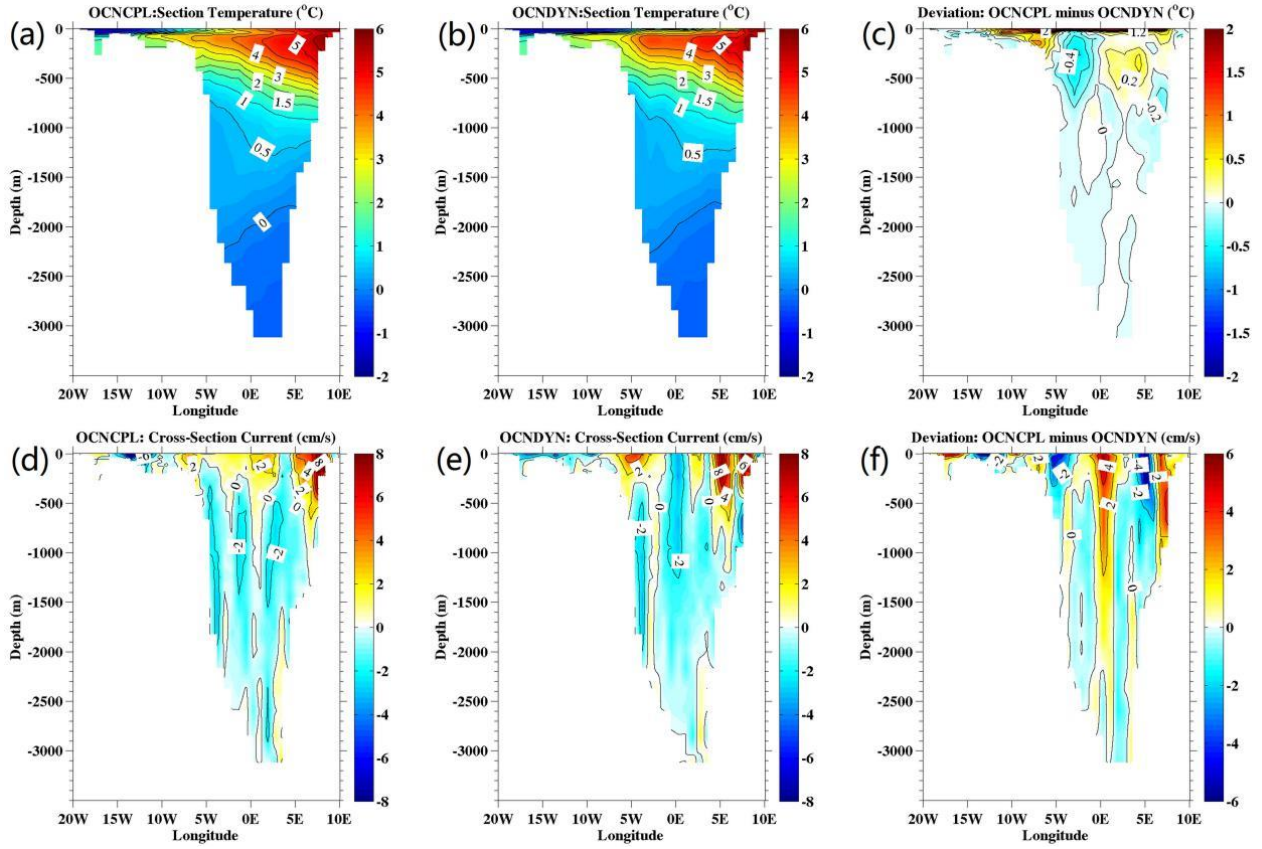

Figure 15: July-August-September mean ocean temperature and meridional velocity section along 78 °N in Fram Strait. The top and bottom panels show the ocean temperature and meridional velocity, respectively. The left, middle, and right panels show the OCNCPL run, the OCNDYN run, and the deviation between them, respectively.

Table 1: Comparison of CPU time spent on coupled and stand-alone runs. The CPU time spent on two stand-alone simulations are presented to show the difference between coupled and stand-alone simulations. 'total_cpu_number' denotes the requested CPUs, 'total_run_time' denotes the total CPU elapsed time. 'wrf_interface', 'wrf_integration', 'mitgcm_interface' and 'mitgcm_integration' denote the CPU elapsed time used for coupling interface by the WRF, numerical integration by the WRF, coupling interface by the MITgcm, and numerical integration by the MITgcm, respectively. 'wrf_time_alone' denotes the CPU elapsed time of the stand-alone WRF runs. 'mitgcm_time_alone' denotes the CPU elapsed time of the stand-alone MITgcm runs. Each run is integrated for 7 model days.

total_cpu_number	cpu_number_on_each_component_model	total_run_time (unit: s)	wrf_interface (unit: s)	mitgcm_interface (unit: s)	wrf_integration (unit: s)	wrf_time_alone (unit: s)	mitgcm_integration (unit: s)	mitgcm_time_alone (unit: s)
28	14	12840	4.8	12131	12835.2	/	709	/
56	28	12000	4.74	11196	11995.26	7140	804	317
112	56	10440	5.16	6477	10434.84	3960	3963	154
224	112	3780	5.26	3550	3774.74	2160	230	96
448	224	2460	5.21	2116	2454.79	1560	344	68
896	448	1380	358	48	1022	1320	1332	84

~~Table 1~~Table 2: Monthly mean northward cross-section velocity (cm/s) and temperature (°C) averaged between 5°E and 8°40'E at 78°50'N in Fram Strait. A1 represents algorithm 1 that values are calculated from sea water with potential temperature higher than 1°C. A2 represents algorithm 2 that values are calculated from sea water with potential temperature higher than -0.1°C. A3 represents algorithm 3 that values are calculated from sea water with depth shallower than 700 m. The observations are averaged between 1998 and 2003. WSCOBS = West Spitsbergen Current Observation.

		July		August		September	
		V_{mean}	T_{mean}	V_{mean}	T_{mean}	V_{mean}	T_{mean}
A1: (T>1°C)	OCNCPL	3.94	3.56	4.03	3.66	4.03	4.02
	OCNDYN	3.22	3.69	2.93	3.79	2.27	3.91
	WSCOBS	6.26	2.76	6.98	2.90	7.36	3.02
A2: (T>-0.1°C)	OCNCPL	3.53	2.30	3.32	2.35	3.24	2.54
	OCNDYN	2.63	2.58	2.38	2.69	1.98	2.66
	WSCOBS	5.82	2.35	6.39	2.44	6.69	2.51
A3: (0-700 m)	OCNCPL	4.21	3.97	4.33	4.03	4.16	4.53
	OCNDYN	3.87	4.36	3.53	4.54	2.55	4.65
	WSCOBS	6.09	2.61	6.67	2.72	7.04	2.83